NASA CR-72995

AN EVALUATION OF A HUBLESS INDUCER AND A FULL FLOW HYDRAULIC TURBINE DRIVEN INDUCER BOOST PUMP

by

B. K. Lindley and A. R. Martinson

Aerojet Liquid Rocket Company
Sacramento, California 95812

prepared for

NATIONAL AERONAUTICS AND SPACE ADMINISTRATION

NASA Lewis Research Center
Contract NAS 3-11218
W. A. Rostafinski, Project Manager

NOTICE

This report was prepared as an account of Government-sponsored work. Neither the United States, nor the National Aeronautics and Space Administration (NASA), nor any person acting on behalf of NASA:

A.) Makes any warranty or representation, expressed or implied, with respect to the accuracy, completeness, or usefulness of the information contained in this report, or that the use of any information, apparatus, method, or process disclosed in this report may not infringe privately-owned rights; or

B.) Assumes any liabilities with respect to the use of, or for damages resulting from the use of, any information, apparatus, method or process disclosed in this report.

As used above, "person acting on behalf of NASA" includes any employee or contractor of NASA, or employee of such contractor, to the extent that such employee or contractor of NASA or employee of such contractor prepares, disseminates, or provides access to any information pursuant to his employment or contract with NASA, or his employment with such contractor.

1. Report No.	2. Government Accession No.	3. Recipient's Catalog No.
NASA CR-72995		

4. Title and Subtitle	5. Report Date
AN EVALUATION OF A HUBLESS INDUCER AND A FULL FLOW HYDRAULIC TURBINE DRIVEN INDUCER BOOST PUMP	October 1971
	6. Performing Organization Code 11218-F
7. Author(s) B. K. Lindley and A. R. Martinson	8. Performing Organization Report No.
	10. Work Unit No.
9. Performing Organization Name and Address Aerojet Liquid Rocket Company P.O. Box 13222 Sacramento, California 95813	11. Contract or Grant No. NAS3-11218
	13. Type of Report and Period Covered Contractor Report
12. Sponsoring Agency Name and Address National Aeronautics and Space Administration Lewis Research Center Cleveland, Ohio	14. Sponsoring Agency Code

15. Supplementary Notes

Project Manager, W. A. Rostafinski, Liquid Rocket Technology Branch, NASA Lewis Research Center, Cleveland, Ohio

16. Abstract

A study to investigate the characteristics of a hubless converging inducer was initiated in April 1968, redirected in September 1969, and completed in June 1971. The purpose of the study was to compare the performance of several configurations of hubless inducers with a hydrodynamically similar conventional inducer and to demonstrate the performance of a full flow hydraulic turbine driven inducer boost pump using these inducers. A boost pump of this type consists of a low speed inducer connected to a hydraulic turbine with a high speed rotor located in between. All the flow passes through the inducer, rotor, and hydraulic turbine, then into the main pump. The rotor, which is attached to the main pump shaft, provides the input power to drive the hydraulic turbine which, in turn, drives the inducer. The inducer, rotating at a lower speed, develops the necessary head to prevent rotor cavitation. The rotor speed is consistent with present main engine liquid hydrogen pump designs and the overall boost pump head rise is sufficient to provide adequate main pump suction head. This system would have the potential for operating at lower liquid hydrogen tank pressures.

17. Key Words (Suggested by Author(s))	18. Distribution Statement
Inducers Hubless Converging Inducer Boost Pumps	Unclassified - unlimited

19. Security Classif. (of this report)	20. Security Classif. (of this page)	21. No. of Pages	22. Price*
Unclassified	Unclassified		

ABSTRACT

A study to investigate the characteristics of a hubless converging inducer was initiated in April 1968, redirected in September 1969, and completed in June 1971. The purpose of the study was to compare the performance of several configurations of hubless inducers with a hydrodynamically similar conventional inducer and to demonstrate the performance of a full flow hydraulic turbine driven inducer boost pump using these inducers. A boost pump of this type consists of an inducer connected to a hydraulic turbine with a high speed rotor located in between. All the flow passes through the inducer, rotor, and hydraulic turbine, then into the main pump. The rotor, which is attached to the main pump shaft, provides the input power to drive the hydraulic turbine which, in turn, drives the inducer. The inducer, rotating at a lower speed, develops the necessary head to prevent rotor cavitation. The rotor speed is consistent with present main engine liquid hydrogen pump designs and the overall boost pump head rise is sufficient to provide adequate main pump suction head. This system would have the potential for operating at lower liquid hydrogen tank pressures.

TABLE OF CONTENTS

Table of Contents (cont.)

FIGURE LIST

Figure List (cont.)

Figure List (cont.)

Figure List (cont.)

TABLE LIST

I. SUMMARY

Pump cavitation in high speed turbomachinery is a major design consideration. Cavitation can be controlled by high suction performance inducers and/or by a boost pump located upstream of the main pump.

A hubless inducer was designed and tested and the performance compared to that of a similar conventional inducer. The suction performance of the hubless inducer was not significantly better than that of the conventional inducer after accounting for the larger inlet tip blade angle. Per established theory, inducers with larger inlet tip blade angles will have higher suction performance. The hubless inducer concept does, however, allow inducers with larger blade angles to be manufactured. Hubless inducers can best be used when the available drive power is at the outer shroud.

The full flow hydraulic turbine drive boost pump shows potential for use with high speed pumps. It has the ability to start very quickly and maintain an almost constant speed ratio over the entire flow speed range. The performance limiting component was the high speed rotor, which cavitated more than was expected. The rotor configuration is limited by overall boost pump requirements, but there are several possible design approaches to reduce rotor cavitation. During preliminary design selection of a pumping system, a boost pump of this type should be considered, if any of the following criteria must be met:

1. Fast starts
2. No additional gears
3. No recirculating flow
4. Comparable high efficiency
5. Constant speed ratio

II. INTRODUCTION

There are two major requisites to the high efficiency that will be required for pumping systems for future rocket engines: (1) high pump shaft speed to reduce turbopump weight, and (2) a low operating pump suction pressure to reduce propellant tank weights. In the design of a pump these two requirements have a direct effect on each other. That is, the lower the pump suction pressure, the lower the shaft speed must be to avoid cavitation and, conversely, the higher the pump speed, the higher the suction pressure must be to avoid cavitation. There are two ways that this design problem can be eliminated. The first is to develop high speed pump inducers that can operate at low inlet suction pressures. The second is to provide the main high speed pump with higher pressure delivered from a boost pump. Several boost pump concepts available to accomplish this objective are described in Ref 1.

The purpose of the work performed under this contract was to compare the performance of a hubless inducer with that of a conventional inducer in both cavitating and non-cavitating steady-state operation. Both inducers were then tested in a full-flow, hydraulic-turbine-driven inducer boost pump to demonstrate the performance of this concept for advanced boost pump application.

The hubless inducer concept is shown in Figure 1 and was first reported in Ref 2. Figure 1 also shows a conventional inducer for direct comparison. The full-flow, hydraulic-turbine-driven inducer boost pump concept is shown in Figure 2 and a working model was first reported in Ref 3. The inducer (hubless or conventional) is driven by a hydraulic turbine, the power being supplied through a rotor connected to the main pump shaft. The rotor is mounted between the inducer and turbine with all the delivered flow passing through each of the three units, then into the main pump. The inducer-turbine speed is approximately 1/2 to 1/3 that of the rotor, which results in a pumping system that can operate at low suction pressure and high main pump speed, satisfying both the design requirements.

The engineering drawings of the rotating components are presented as Appendix C and are referenced to their corresponding figures in the text.

Program tasks were as follows:

Original Work Program

Task I: Hydrodynamic Design, Mechanism Layout, and Fabrication of a Hubless Inducer;

Task II: Inducer Test to Determine Performance Characteristics.

The original work plan was terminated and the contract redirected during Task II because the original design specification resulted in inducer and rotor designs that were beyond the state-of-the-art. The revision in the work plan eliminated testing in liquid hydrogen and all subsequent testing was conducted in water, although the hardware was designed for hydrogen operation and could be tested in hydrogen with slight modifications.

Revised Work Program

Task III: Design, Fabrication and Test of a Conventional Inducer

Task IV: Design, Fabrication and Test of a Hubless Inducer

Task V: Design, Fabrication and Transient Test of a Hydraulic-Turbine-Driven Inducer Boost Pump

Task VI: Comparative Performance Evaluation and Final Report

The revised design specifications for the boost pump operating in liquid hydrogen are:

Flow rate	4900 gpm (0.309 m^3/s)
Boost pump head rise	2000 ft (610 m)
Main pump (rotor) shaft speed	30,000 rpm (3142 rad/sec)
Boost pump net positive suction head	25 ft (7.6 m)

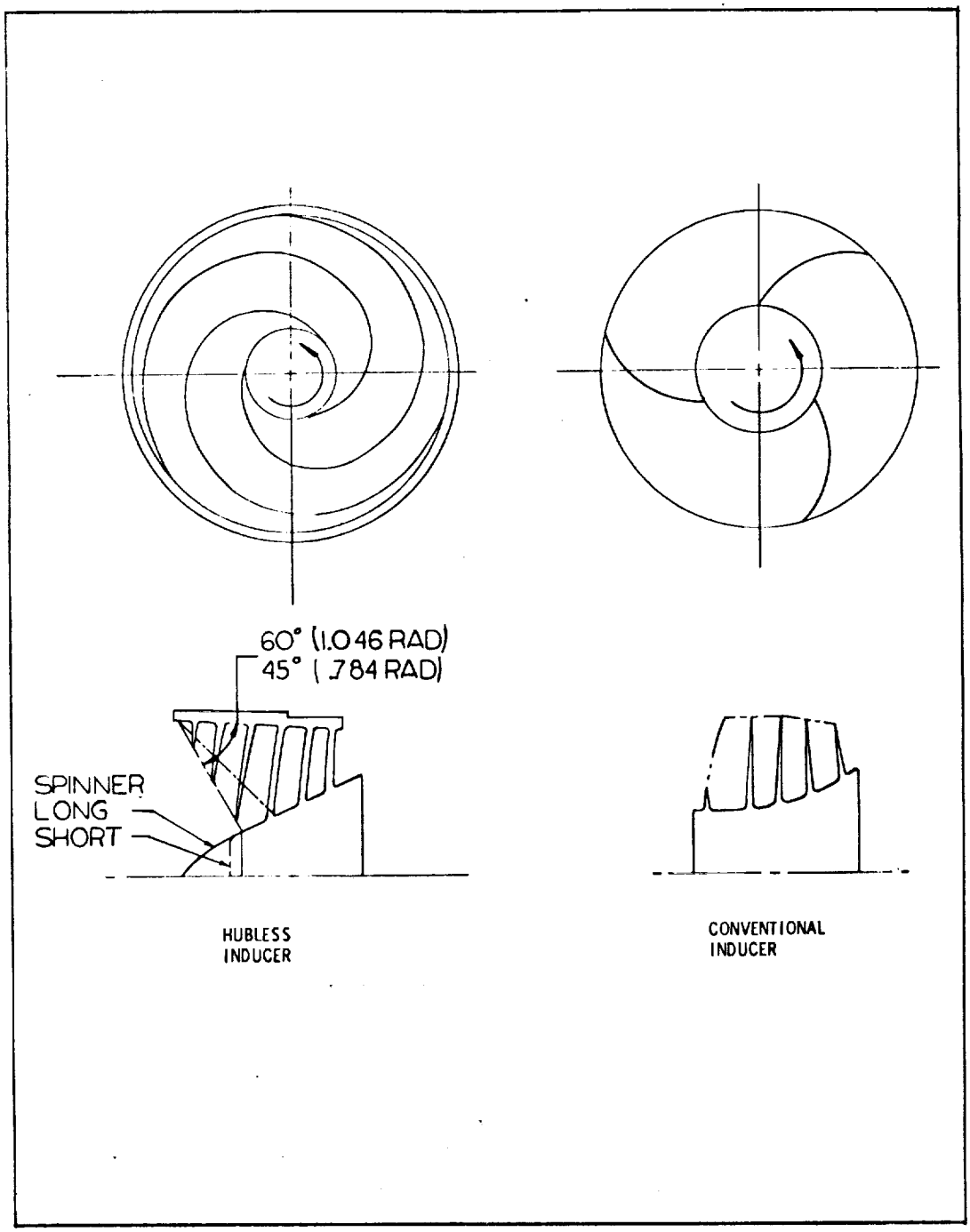

Figure 1. - Inducer Comparison, Hubless to Conventional

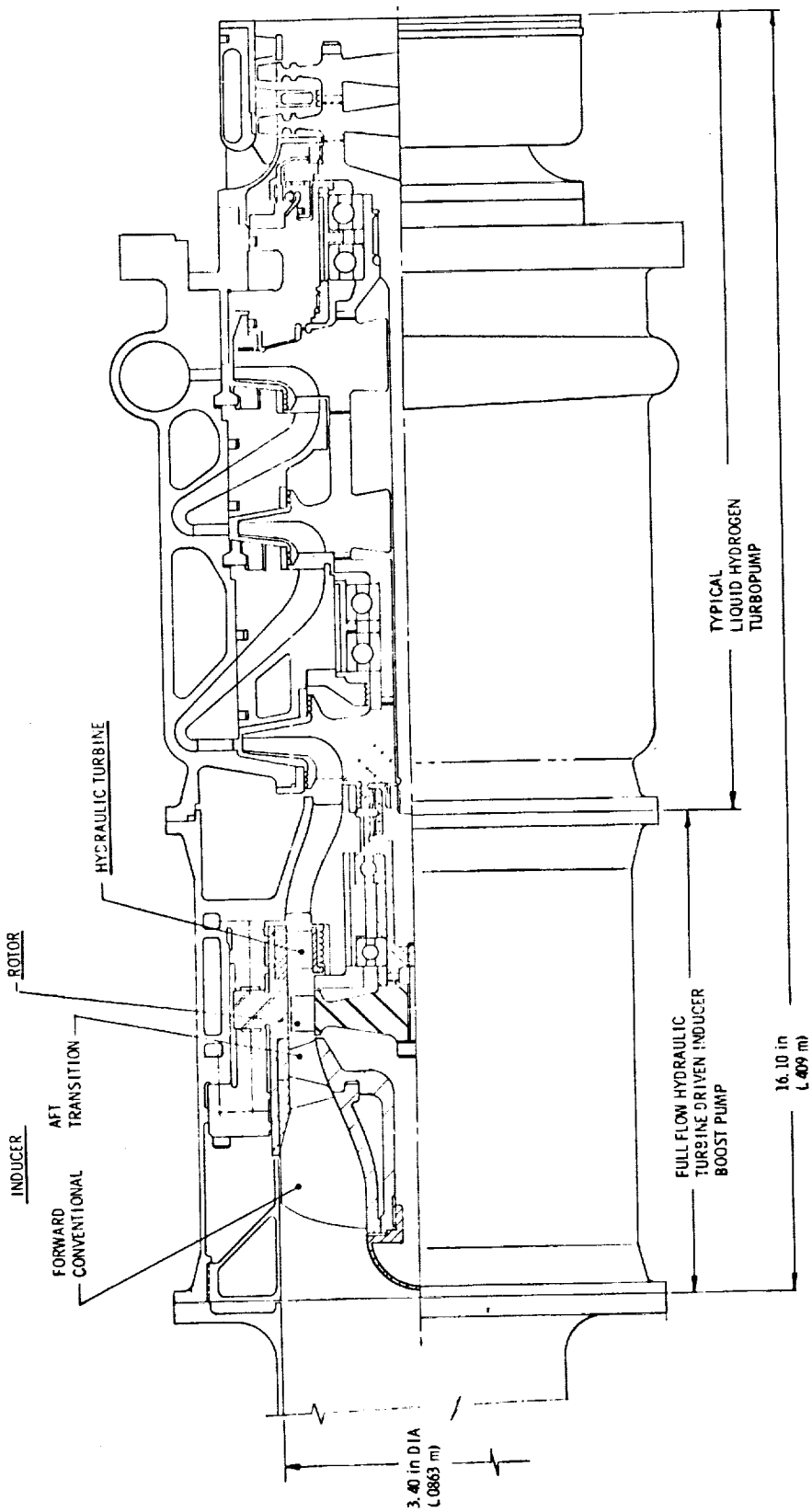

Full Flow Hydraulic Turbine Driven Inducer Boost Pump
and a Typical Hydrogen Main Pump

Figure 2

III. PARAMETRIC ANALYSIS

In order to determine the requirements of the inducers, rotor, and hydraulic turbine, a parametric analysis was conducted. This analysis set the overall requirements of the boost pump, as well as the individual requirements of each element of the boost pump. A survey was conducted of present and future pumping systems that require a boost pump. From this survey, it was possible to establish limits on main pump speed, flow, and operating net positive suction pressure.

A. DESIGN POINT SPECIFICATION

The design point specifications set the overall boost pump operating conditions. These specifications were determined after the contract revision and were used with the NASA project concurrence.

1. Flow and NPSH

The flow rate of 4900 gpm (0.309 m^3/s) was selected from the original RFP which gave limits of 4900 (0.309) to 11,000 (0.694) gpm (m^3/s). The 4900 gpm (0.309 m^3/s) flow rate, when scaled to water, best fit the ALRC low head test flow loop. High flow rates would require higher head rise designs in order to 'pump' the flow loop.

The contractually specified NPSH of 25 ft (7.6 m) in hydrogen was used with an additional 80 ft (24.4 m) for thermodynamic head. This amount of thermodynamic head was used in designing the M-1 engine fuel pump (Ref 4) and is a conservative estimate compared to the value used on current hydrogen pump designs.

2. Main Pump Shaft Speed

There were four liquid hydrogen engine systems in which extensive studies have been made to determine the design requirement of the main pumps. In each of these the main pump speed was set at approximately 30,000 rpm (3142 rad/s). The speed-limiting parameters were bearing load/critical speed or blade stresses in either the pump or the turbine. All of the pumping systems used some type of boost pump to preclude main pump cavitation.

3. Overall Head Rise

The overall head rise required of the boost pump can be determined from the flow, speed, and operating suction specific speed of the main pump. Figure 3 shows the required boost pump head rise for a centrifugal main pump with an inducer and without an inducer. It was assumed that, with an inducer, the main pump could be designed to operate at 20,000 (7.3) suction specific speed and without an inducer at 7,000 (2.55) suction specific speed. Main pumps within this specific speed range can be designed with present technology. In either case, 2,000 ft (630 m) boost pump head rise will allow for considerable variance in the specified main pump flow and/or speed.

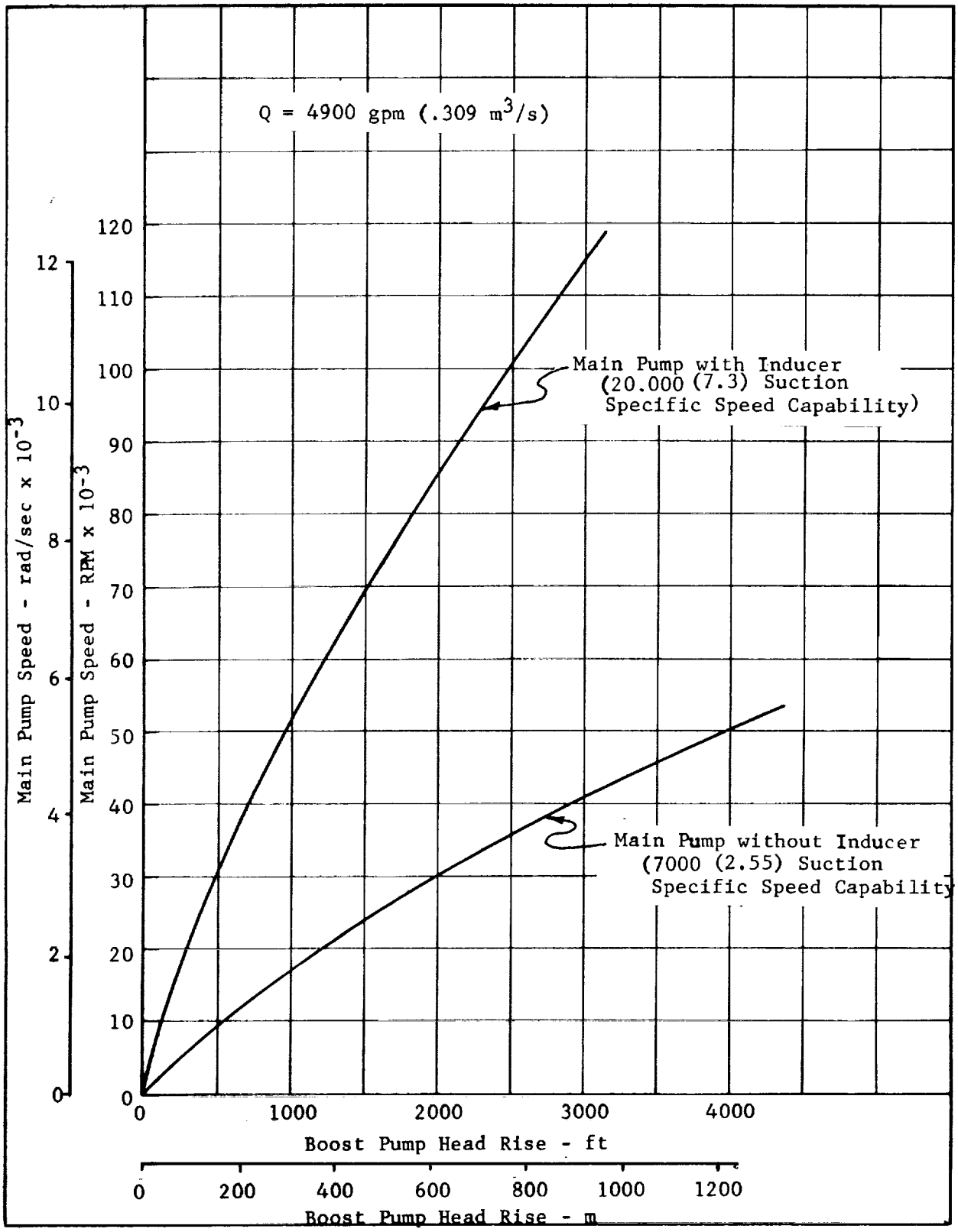

Figure 3. - Main Pump Speed vs. Boost Pump Head Rise

B. ROTOR CAVITATION

The boost pump rotor has two major design criteria: they are blade loading and blade cavitation. The blade loading was considered to be within normal design practice as outlined in Ref 5. The cavitation criteria of high setting angle, axial flow blading, however, has only recently been evaluated. Cavitation numbers for stationary cascade, high setting angle blades are given in Ref 6, but data for this type of blade under rotation and with inlet prewhirl were not available.

1. Cavitation Model

To evaluate the design parameters which influence rotor cavitation, an analytical model was developed. This model defines the available rotor cavitation constant as the dependent parameter. Cavitation constant (K) has long been used to evaluate cavitation performance and is defined as follows:

$$K = \frac{\tau - \Phi^2 - \psi_1^{*2}}{(1 - \psi_1^*)^2 + \Phi^2} \tag{1}$$

The inlet NPSH of the rotor will be equal to the actual head rise of the inducer if it is assumed that the NPSH of the inducer equals the increase in fluid vapor head due to heating within the inducer. It is also assumed that there will be no contour change between the inducer exit and rotor inlet. (A similar, valid expression can, however, be derived with contour changes.)

$$NPSH_R = \Delta H_I = \frac{\psi_I U_I^2}{g}$$

$$\tau_R = \frac{\Delta H_I}{U_R^2} \times 2g$$

$$\tau_R = \frac{\psi_I U_I^2}{g\, U_R^2} \times 2g$$

$$\tau_R = \frac{2\,\psi_I}{SR^2} \tag{2}$$

The inlet prewhirl of the rotor (ψ^*_{R1}) may be written in terms of the inducer head coefficient.

$$V_{\Theta R1} = V_{\Theta I2} = \frac{\psi_I U_I}{\eta_I}$$

$$\psi^*_{R1} = \frac{V_{\Theta R1}}{U_R} = \frac{\psi_I U_I}{U_R \eta_I}$$

$$\psi^*_{R1} = \frac{\psi_I}{SR\ \eta_I} \qquad (3)$$

The available inlet rotor cavitation number can then be written in terms of the inducer actual head coefficient by substituting Equations (2) and (3) into (1).

$$K = \frac{\frac{2\ \psi_I}{SR^2} - \Phi_R^2 - \frac{\psi_I^2}{SR^2 \eta_I^2}}{\left[1 - \frac{\psi_I}{SR\ \eta_I}\right]^2 + \Phi_R^2}$$

This available cavitation number is expressed graphically in Figures 4 through 8 as a function of speed ratio and inducer actual mean head coefficient. Also plotted on this figure are the D-3 flow loop head loss and the state-of-the-art in inducer design. Variations in the value of the fixed conditions are shown on these figures. Figure 4 best represents the conditions near the selected design. It can be seen that, for a given rotor blade cavitation number, high speed ratios can be obtained only with high head coefficient inducers. Designs to the left of the "inducer state-of-the-art" line would be considered conservative while those to the right represent involving greater risk designs. The inducer discharge flow coefficient varies along this line and is optimum at only one point, but there is a wide design range on flow coefficient.

The facility flow loop requirement (D-3A system) does not influence the design criteria, but any design tested at the D-3A test bay must lie above this limit in order to 'pump' the flow loop.

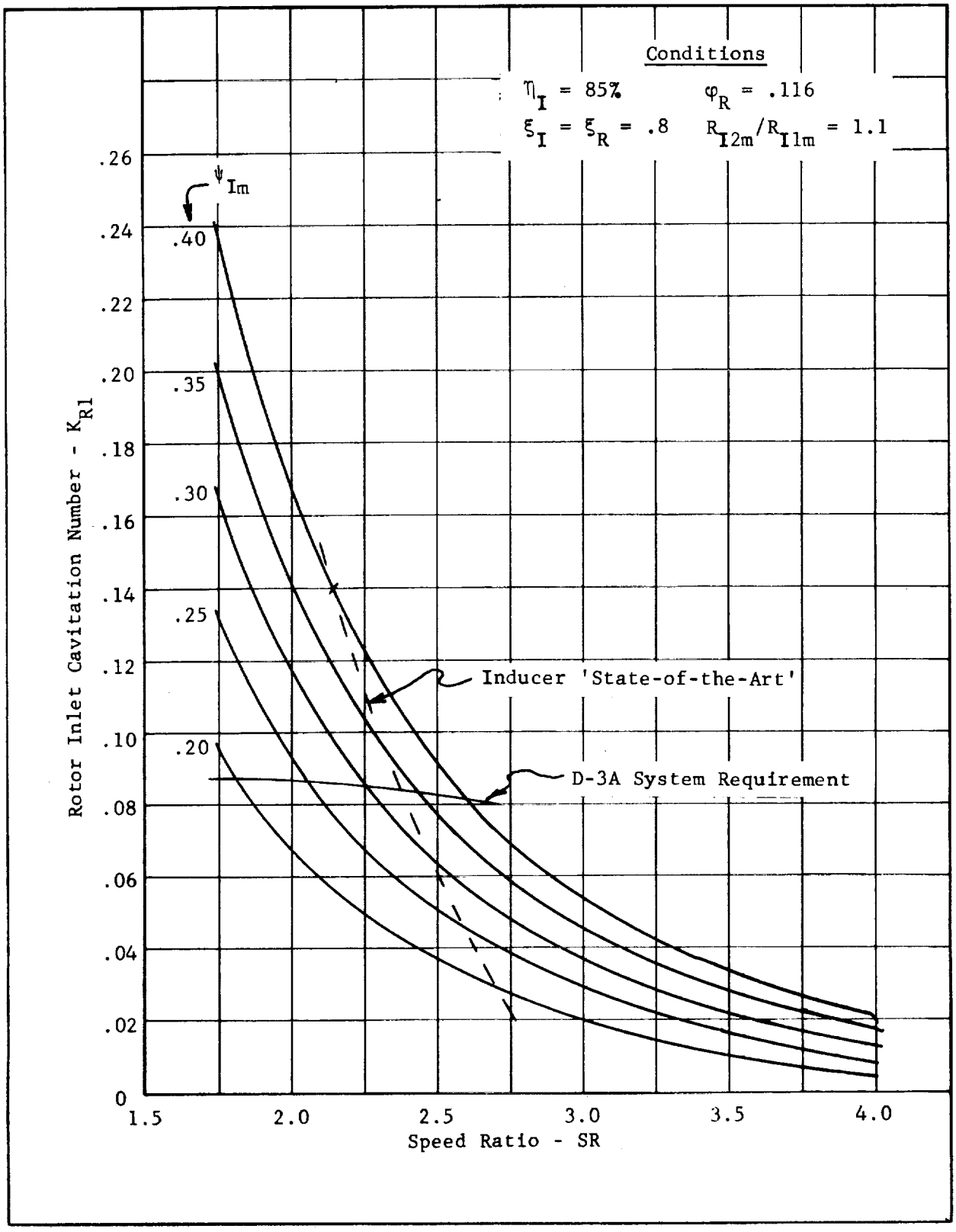

Figure 4. - Rotor Cavitation Number vs. Speed Ratio for ϕ_R=.116, ξ_R=.8, R_{I2m}/R_{I1m}=1.1

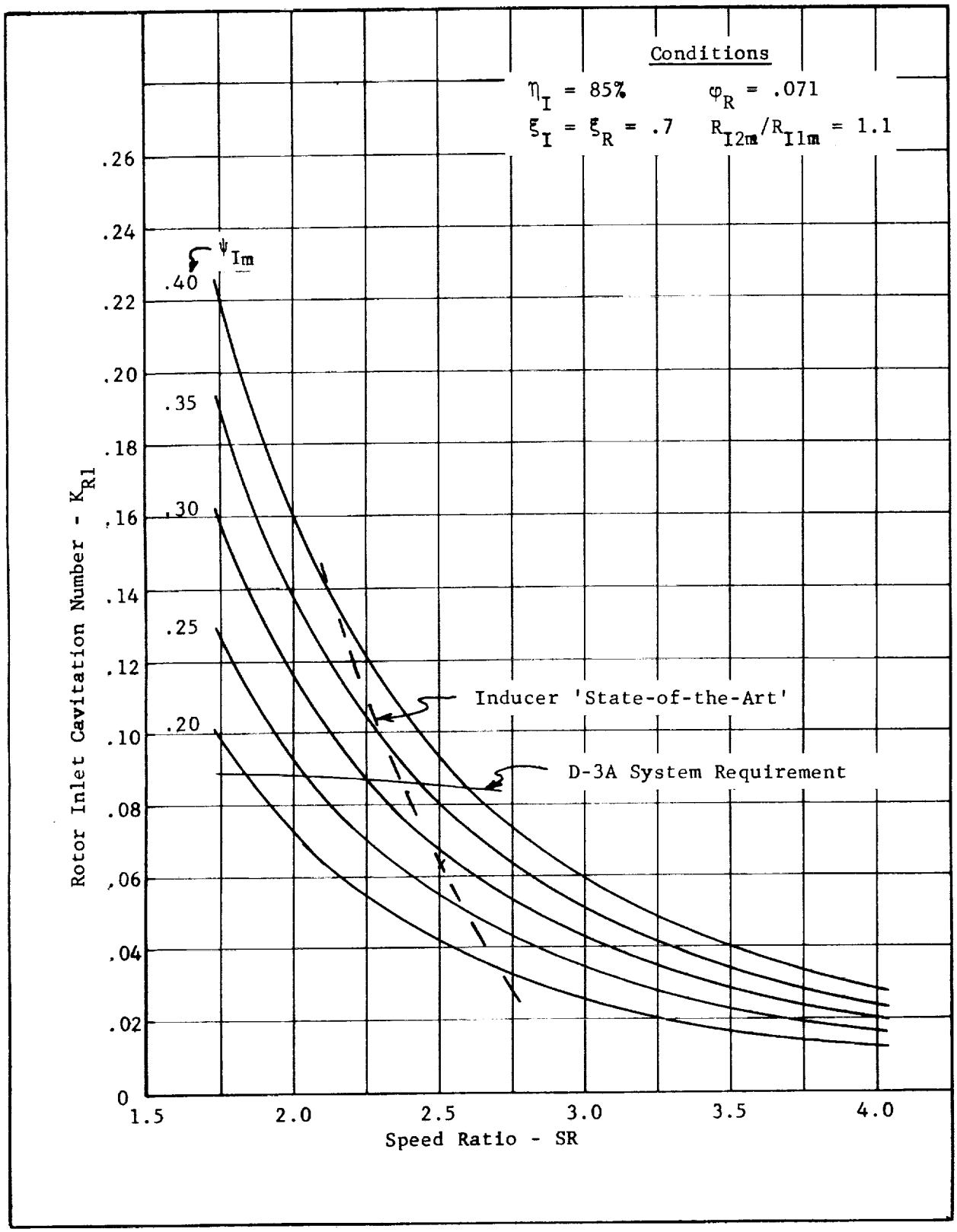

Figure 5. - Rotor Cavitation Number vs. Speed Ratio for ϕ_R=.071, ξ_R=.7, R_{I2m}/R_{I1m}=1.1

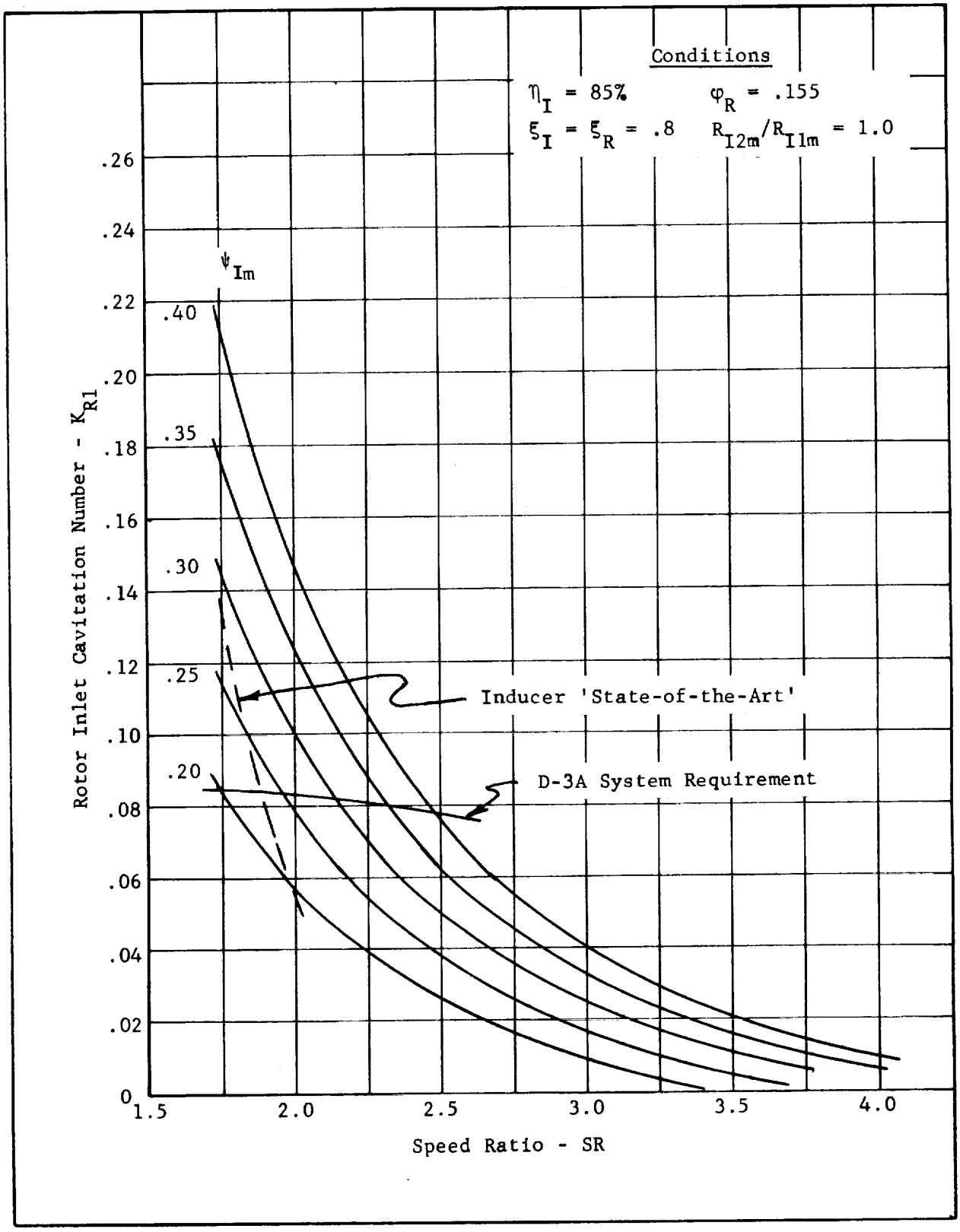

Figure 6. - Rotor Cavitation Number vs. Speed Ratio for ϕ_R=.155, ξ_R=.8, R_{I2m}/R_{I1m}=1.0

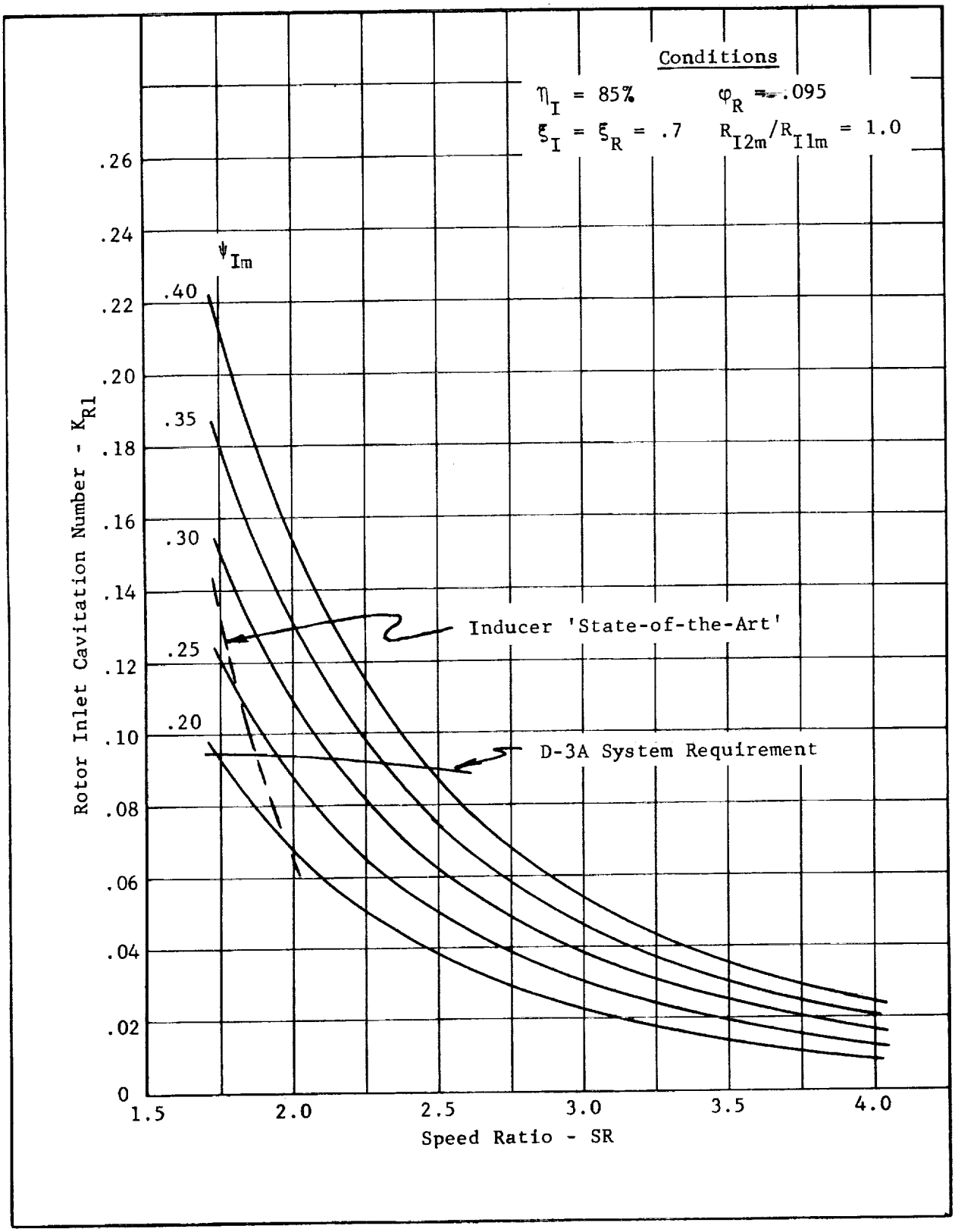

Figure 7. - Rotor Cavitation Number vs. Speed Ratio for ϕ_R=.095, ξ_R=.7, R_{I2m}/R_{I1m}=1.0

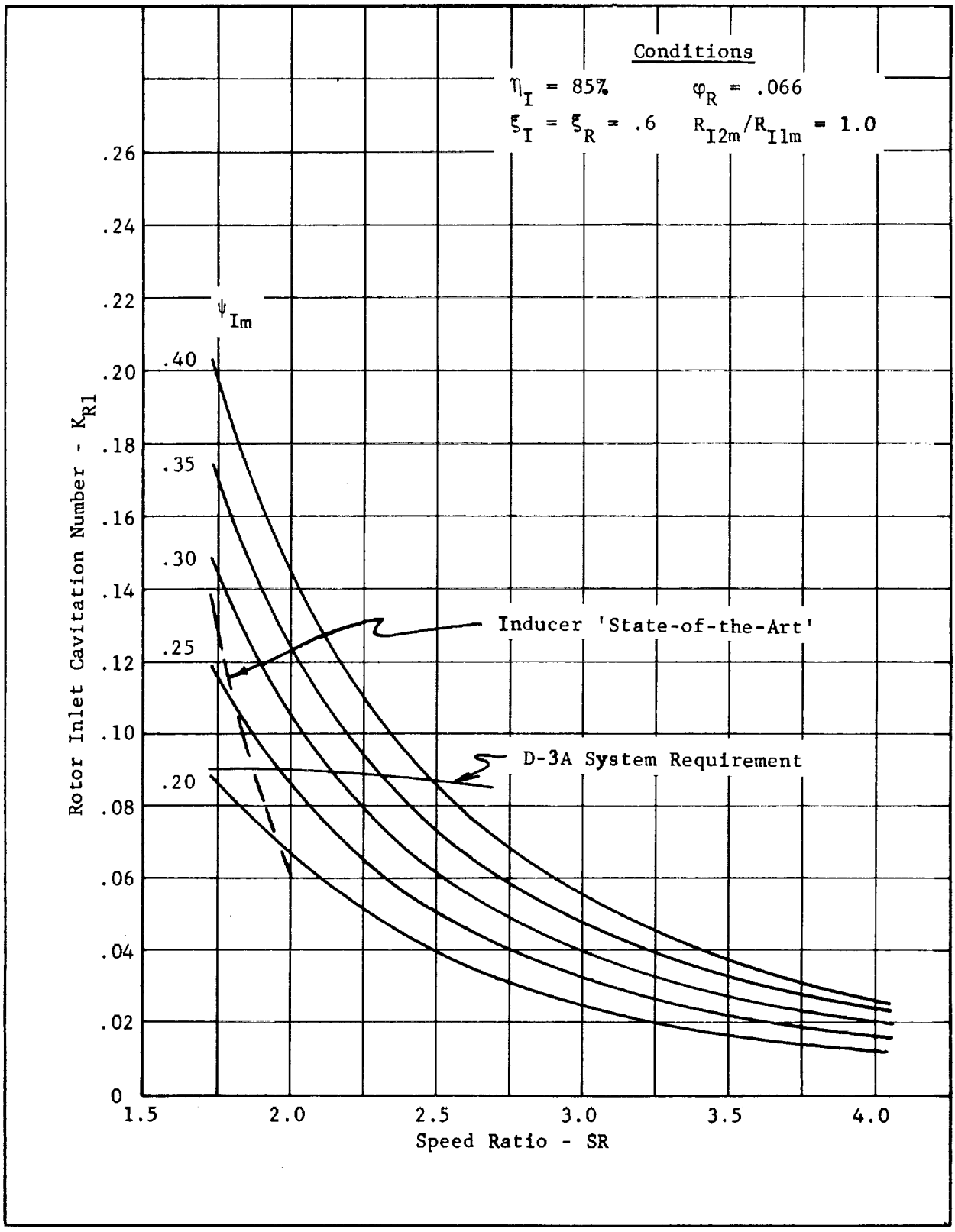

Figure 8. - Rotor Cavitation Number vs. Speed Ratio for ϕ_R=.066, ξ_R=.6, R_{I2m}/R_{I1m}=1.0

2. Available Cavitation Data

Figure 9 shows the required 3% head loss cavitation number of several axial flow blades (Ref 7 through Ref 12) at various flow coefficients. There is a considerable amount of "scatter" in these data and only one of the blade rows shown was tested with inlet fluid prewhirl. The two solid lines in this figure were taken from two-dimensional flow theory. The upper line represents an incidence to blade angle ratio of 0.425, which is typical of flat plate inducers. The lower line represents an incidence to blade angle ratio that is a function of actual design flow coefficient, as shown in Figure 10. Both of these "theoretical" lines are shown to indicate the relationship between cavitation number and flow coefficient at complete cavitation head breakdown. The cross-hatched data represents pumps produced and tested by ALRC.

The required cavitation number of the design rotor obtained from Figure 7 must be less than the available cavitation number selected from Figure 4 at the design conditions in order to ensure cavitation-free rotor operation.

The significance of these figures can best be illustrated by an example: Select an operating speed ratio of 2.14 at the conditions shown at the top of Figure 4. A reasonable value of the required cavitation number, from Figure 9 at the inlet flow coefficient of 0.116, is 0.1. From Figure 4 (at the selected speed ratio of 2.14) the inducer head coefficient must be 0.35 to produce an available cavitation number of (0.12) that is greater than the required cavitation number (0.1). This operating point will also satisfy the limits shown on Figure 4 (i.e., less than the 'inducer state-of-the-art', and will produce enough head to pump the D-3A system).

If a speed ratio of 2.75 had been selected, the limits of available cavitation number and minimum head to pump the flow loop could be satisfied only by an inducer which exceeded the inducer state-of-the-art.

The final condition that must be satisfied is the stable speed ratio criteria developed in Ref 3. This is shown graphically in Figure 11 where all designs up to approximately 2.5 would be stable. This criteria is considered conservative since it was developed from a theoretical model that does not consider actual losses to determine the slope of the torque-flow curve. Design speed ratios of 3 most likely could be used before instability occurs. The test data in the following sections will verify the torque stability characteristics of this concept.

C. WORK SPLIT AND ANNULAR GEOMETRY SELECTION

Based on the previously established design specifications and the cavitation model for the high speed rotor, a pitch or mean line one-dimensional work split analysis was made. The inducer - turbine speed, head, and flow coefficients were selected.

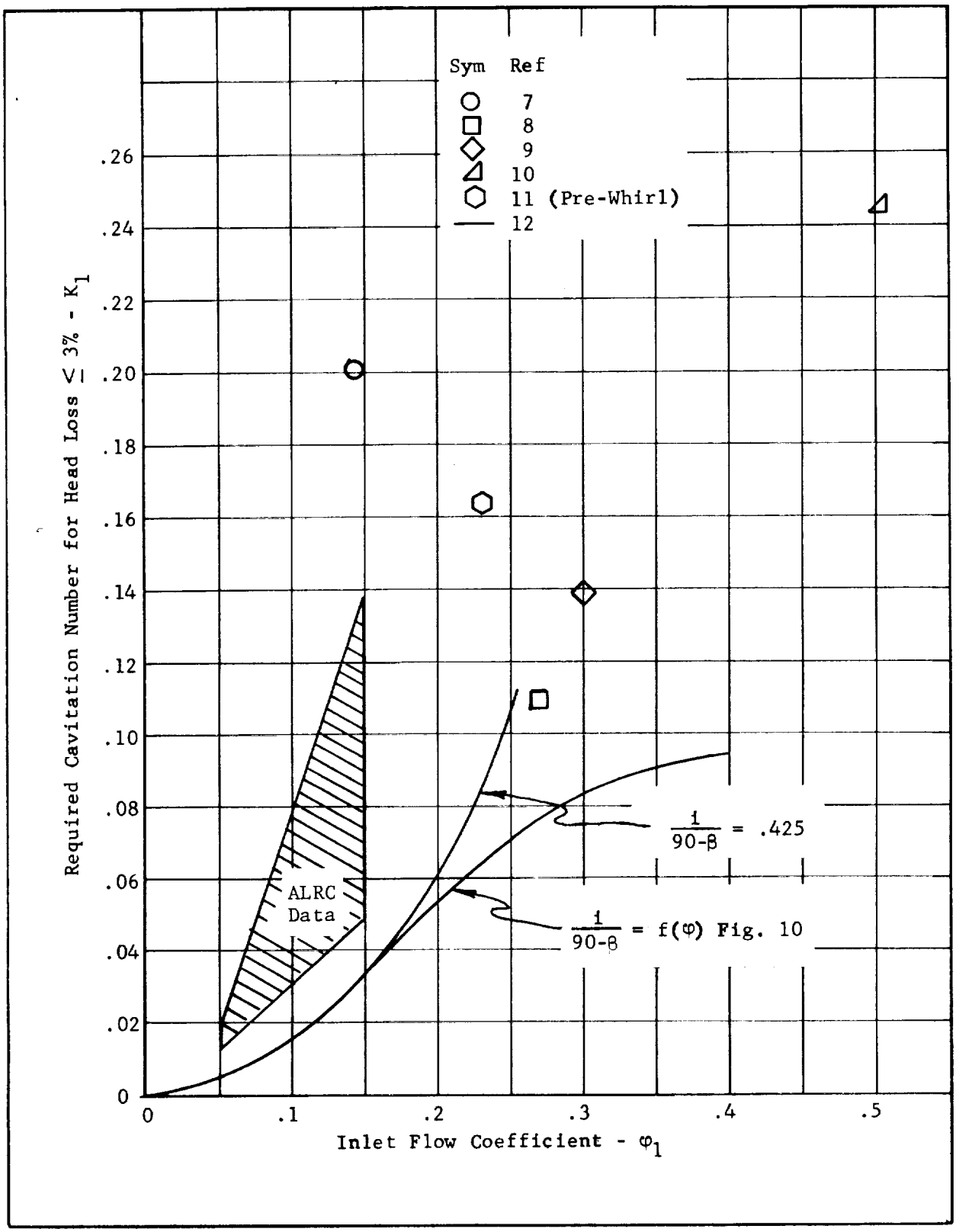

Figure 9. - Required Cavitation Number vs. Flow Coefficient for Various Rotors

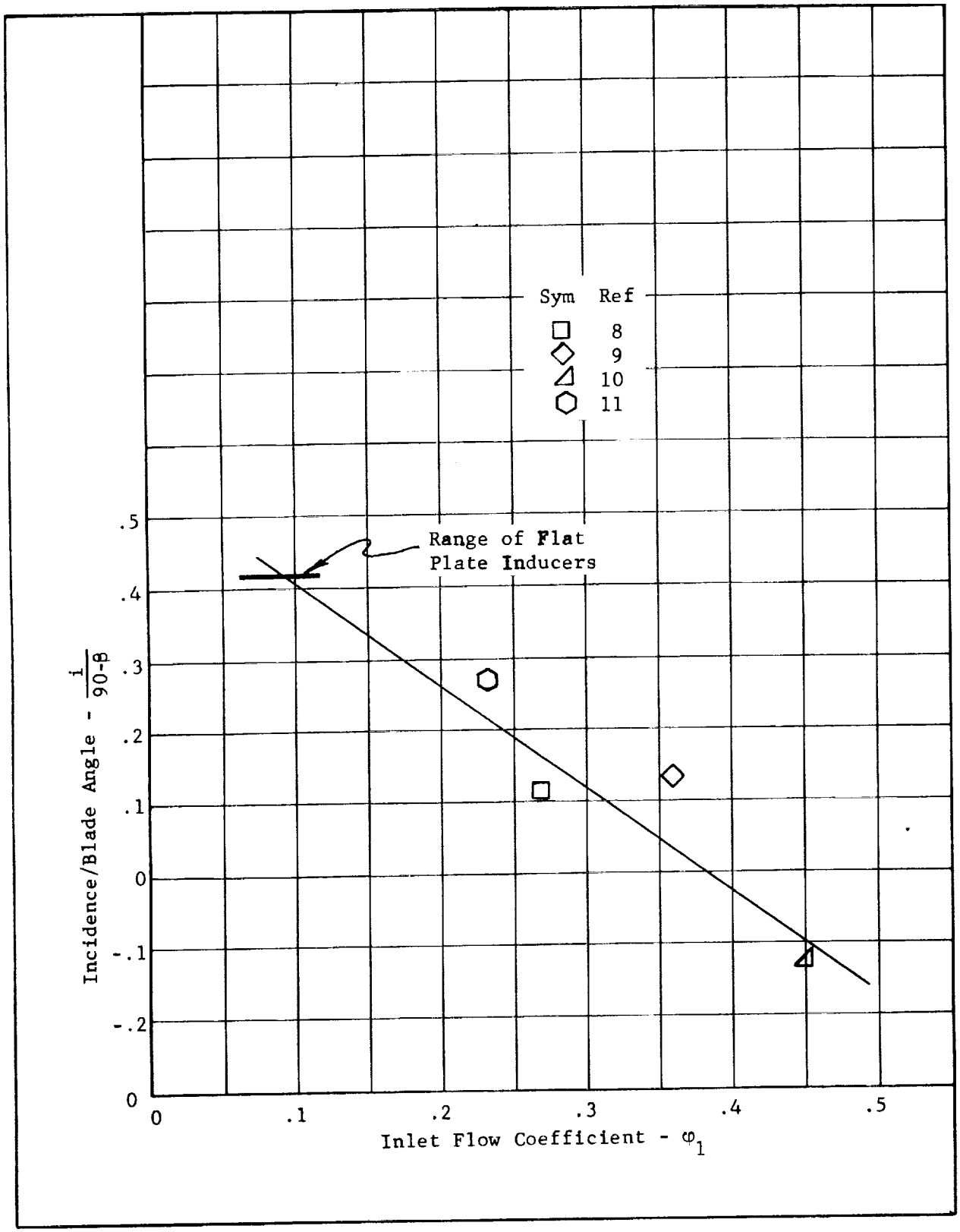

Figure 10. - Incidence to Blade Angle Ratio vs. Flow Coefficient for Various Rotors

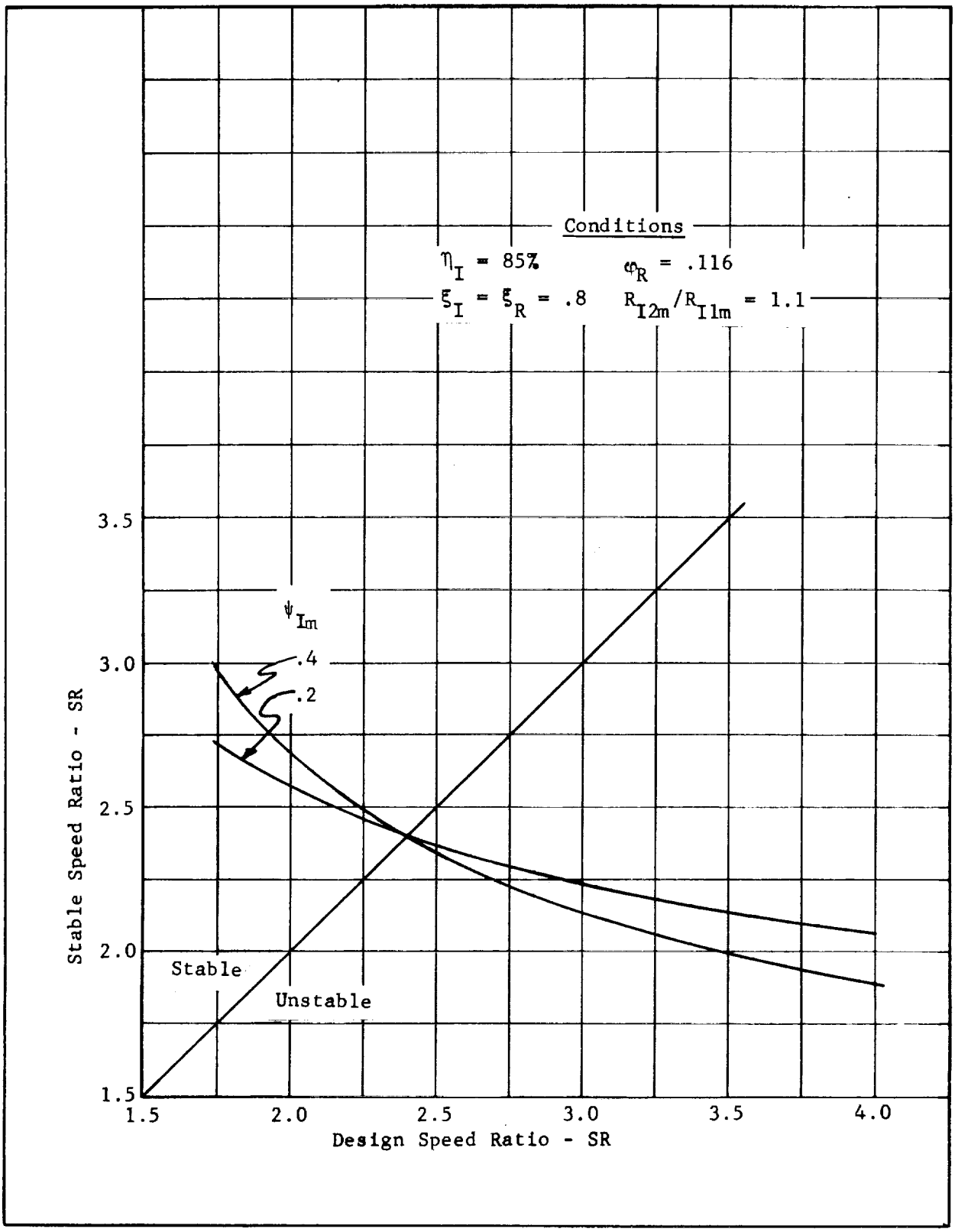

Figure 11· - Stable Speed Ratio vs. Design Speed Ratio

1. Inducer

The inducer speed was set to be consistent with the cavitation model of the high speed rotor. A speed ratio of 2.14 and an inducer discharge mean line head coe-ficient of approximately 0.35 were selected. This results in a speed of 14,000 rpm (1470 rad/s) and head rise of 1700 ft (518 m).

Since the inducer inlet geometry was fixed by the pump test fixture at a diameter of 7.72 in. (0.196 m), the inlet flow coefficient was 0.085 (0.071 for hubless). The following inducer parameters were set by the inducer work split analysis and are consistent with those of Ref 13.

	Conventional	Hubless
Inlet Tip Diameter	7.72 in (0.196 m)	7.72 in (0.196 m)
Inlet Hub Diameter	3.09 in (0.0784 m)	0
Discharge Tip Diameter	7.142 in (0.181 m)	7.142 in (0.181 m)
Discharge Hub Diameter	5.714 in (0.143 m)	5.714 in (0.143 m)
Inlet Tip Flow Coefficient	0.085	0.071
Discharge Tip Flow Coefficient	0.250	0.250
Discharge Mean Head Coefficient	0.288	0.288
Speed	14,000 rpm (1470 rad/s)	14,000 rpm (1470 rad/s)
Flow	4,900 gpm (0.309 m^3/s)	4,900 gpm (0.309 m^3/s)

2. Rotor

The rotor inlet and discharge flow annulus was maintained the same as the inducer discharge. The flow discharging for the inducer was assumed to have the same properties at the rotor inlet since there were no radii change. This annulus had previously been sized to prevent rotor cavitation and, therefore, only blade loading needed consideration. Figure 12 shows the one-dimensional rotor diffusion factor as a function of speed ratio and inducer head coefficient. Also shown is rotor mean head rise coefficient as a function of the same variable. At the selected operating point, the rotor diffuser factor will be 0.27 and the head rise coefficient 0.16. These values are consistant with those given in Ref 5. The design parameters based on the one-dimensional analysis for the high speed rotor are given below but were subject to change based on test results from the inducer.

Tip Diameter	7.142 in (0.181 m)
Hub Diameter	5.714 in (0.143 m)
Tip Flow Coefficient	0.117
Mean Head Coefficient Rise	0.16
Speed	30,000 rpm (3142 rad/s)
Flow	4,900 gpm (0.309 m^3/s)

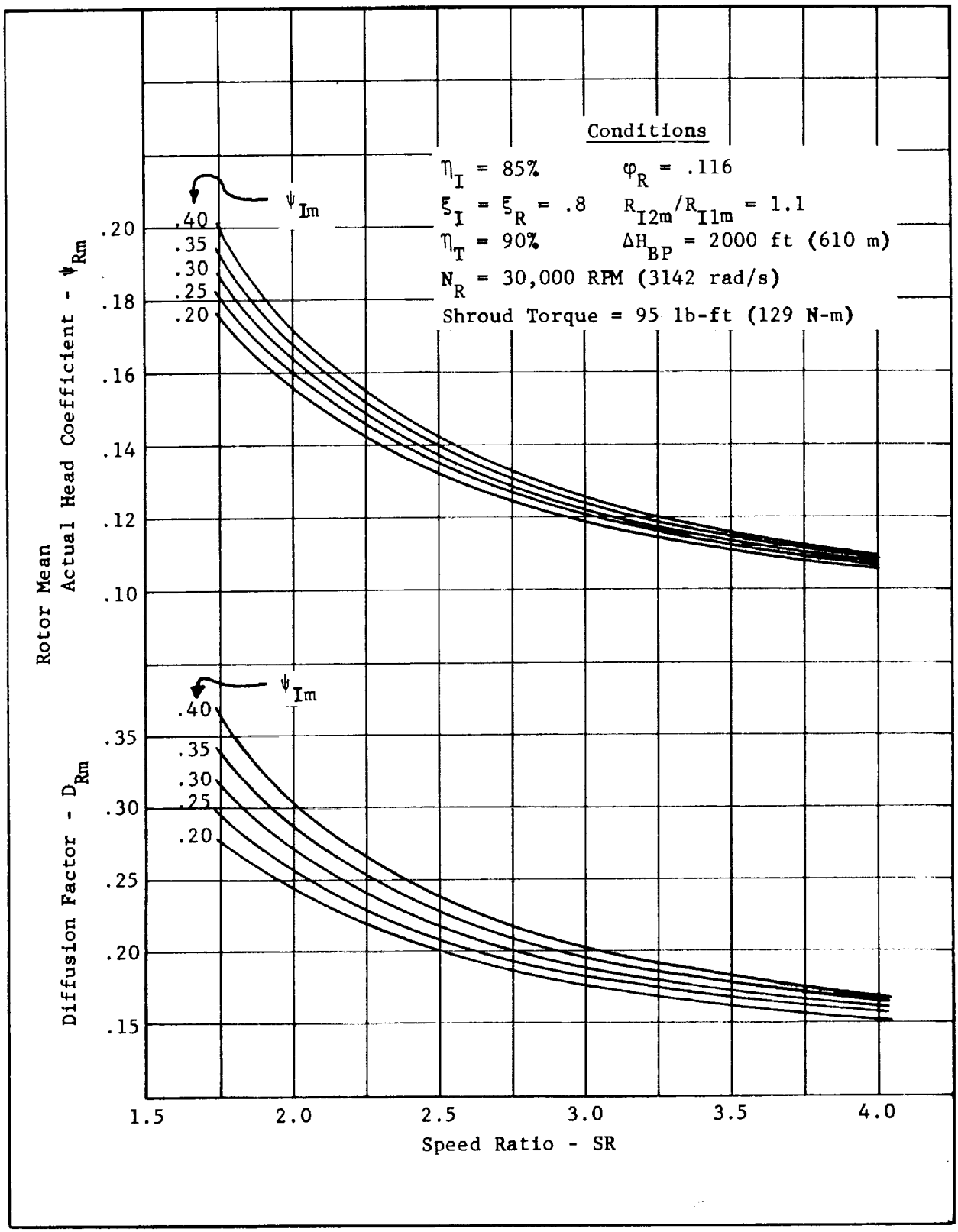

Figure 12. - Required Rotor Performance vs. Speed Ratio

3. Turbine

The hydraulic turbine must supply power to drive the inducer and shroud. Since the shroud consists of both the radial and axial hydrostatic bearings, the drag torque in water will be higher than if this system were tested in liquid hydrogen. For this reason, some modification to the turbine would be necessary in order to maintain a constant 2.14 speed ratio in liquid hydrogen. Again the flow annulus of the turbine was maintained the same as the rotor; this was done for ease in manufacturing of the turbine and adjacent components. On an actual pumping system the turbine discharge annulus would be designed to match the inlet of the downstream main pump. The design specifications for the turbine are as follows, again subject to change based on inducer testing.

Tip Diameter	7.142 in (0.181 m)
Hub Diameter	5.714 in (0.143 m)
Flow Coefficient	0.117
Head Coefficient Drop	0.75
Speed	14,000 rpm (1470 rad/s)
Flow	4,900 gpm (0.309 m^3/s)

IV. HYDRODYNAMIC DESIGN

With the nondimensional parameters of head and flow coefficient set from the parametric mean line analysis, a detailed hydrodynamic design was done on each of the blade rows, the end result of this design phase being blade coordinates for manufacturing. Since the resulting boost pump was a low head machine, the change in the hydrogen fluid properties was not considered. The nondimensional liquid hydrogen design data is therefore the same as the incompressible water test data.

A. INDUCER

An inducer head coefficient of 0.35 at the mean represents a moderately heavily loaded blade row. Since it was desirable to design for uniform discharge inducer flow and head, the inducer was divided into a tandem design with a separate forward and aft section. The aft section, or transition, would be exactly the same component for each inducer, hubless or conventional. This resulted in an inducer concept similar to that of Ref 14. The head rise in each section is approximately one-half of the total.

1. Forward Section

The forward section of the inducer provides the basic cavitation performance of the pumping machine.

a. Conventional Inducer

The design was consistant with a normal high suction performance inducer. It was decided to have a three-bladed inlet to minimize the blockage and still obtain the required solidity in a reasonable axial length. The inlet geometry to the inducer was based on the theory of Ref 12. The tip blade angle was calculated to be 81.5° by this method. All other radial blade angles satisfy the condition for a right helix. The leading edge radii of the vane from hub to tip were constant over the trim. A nominal value of 0.010 in (0.00025 m) was used for the radius of the leading edge. Sharpness is not only an aid to cavitation performance but also affects the discharge head, as shown in Ref 15. Figures 13 and 14 show the blade element design performance prediction for the conventional inducer; these predictions are based on simple radial equilibrium. The loss coefficient and the deviation angles were taken from Ref 14, 16, 17, and 18. The validity of this type of analysis is shown in Figure 15, where the calculated and measured parameters are shown for the design of Ref 19. The only inputs necessary for this analysis are the streamline blade deviation angles and loss coefficients. The discharge flow coefficient of the forward inducer section was increased to obtain a value midway between the inlet and transition discharge. In order to maintain the constantly increasing head, the blade angles were decreased along the mean streamline by the relationship $\psi = 1 - \frac{\phi}{\text{cotan } \beta}$. The blade thickness at the root was designed for minimum blockage, consistant with stress requirements. Stress levels were computed from 'worst case' conditions accounting for both fluid and centrifugal loading.

b. Hubless Inducer

In order to determine some design criteria for the inlet geometry of the hubless inducer, a computer program was developed which had four options for the type of flow which existed radially across the inducer inlet. The analysis obtained from this model, while qualitative, gave some insight to the flow conditions.

The four flow options in the inducer inlet were free vortex, forced vortex, power vortex, and zero angular fluid velocity. The flow within the inducer blade passage was assumed to follow the blade after the blade had reached a solidity of 1.0 along any given streamline. In all cases, it was also assumed that the total head within the inducer eye was equal to that of the free stream inlet pressure.

With these assumptions it was found that only the fourth type of flow field, zero angular velocity, could exist at the inducer inlet and support simple radial equilibrium. Secondly, it also became apparent that the smaller the inlet angle was the larger the inlet blade tip angle must be. This is caused by the limit in the rate of head increase, in the axial direction, generated by the blade above the free fluid. Large head increases along the tip streamline caused the flow to shift to the tip and the axial velocity of the free fluid to go to zero. Large inlet angles permit faster head increases along the streamlines within the blade.

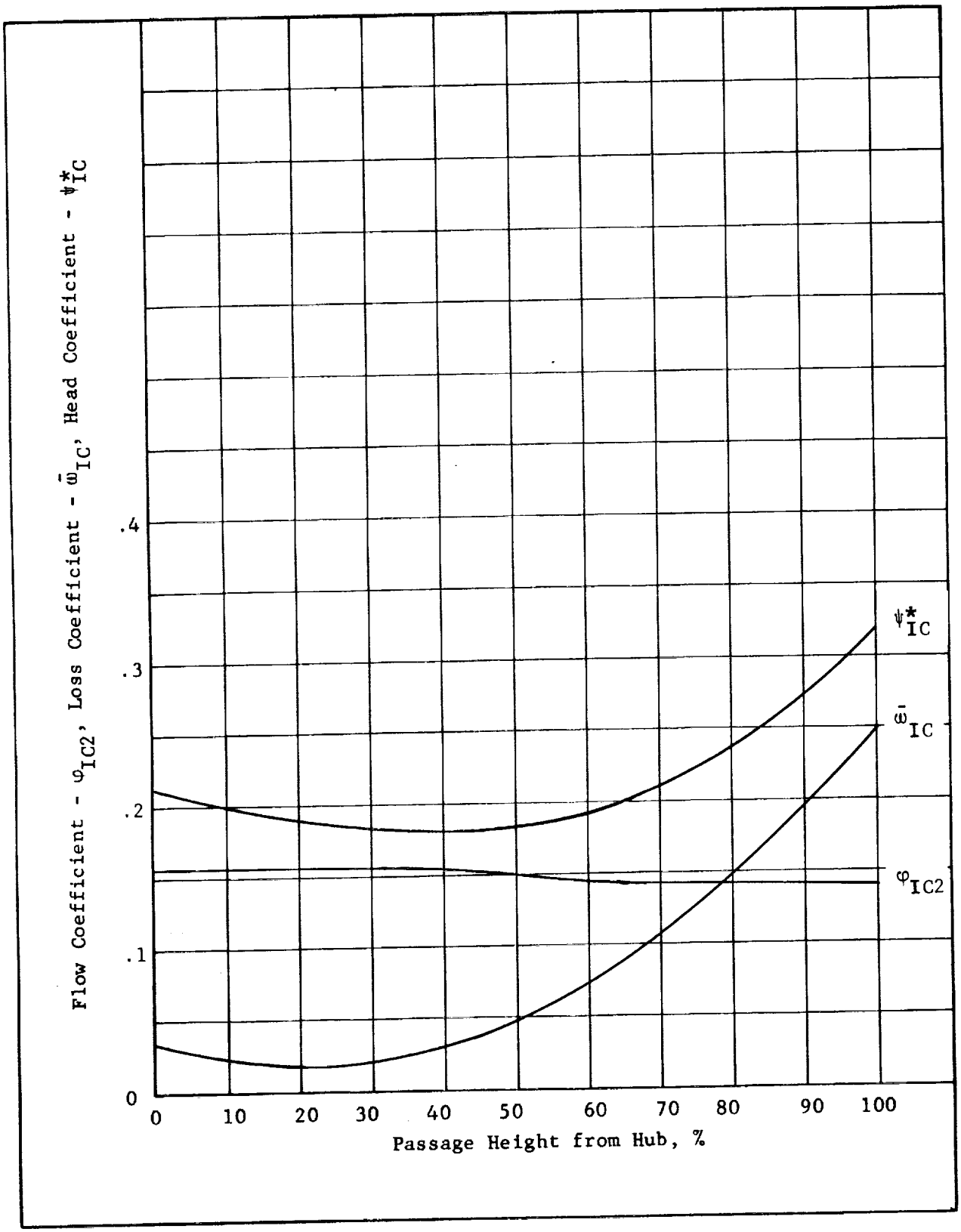

Figure 13. - Inducer Blade Performance vs. Passage Height

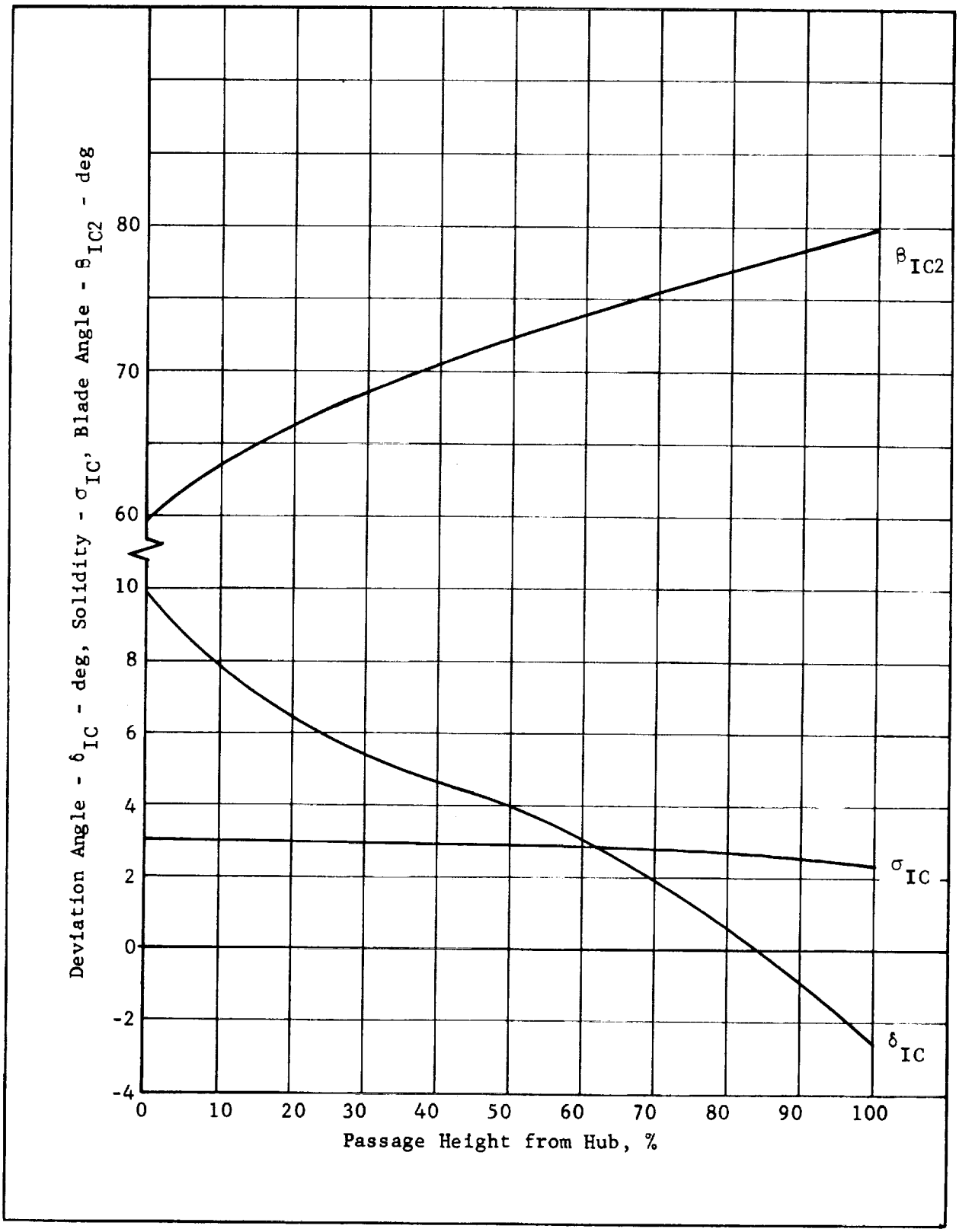

Figure 14. - Inducer Blade Geometry vs. Passage Height

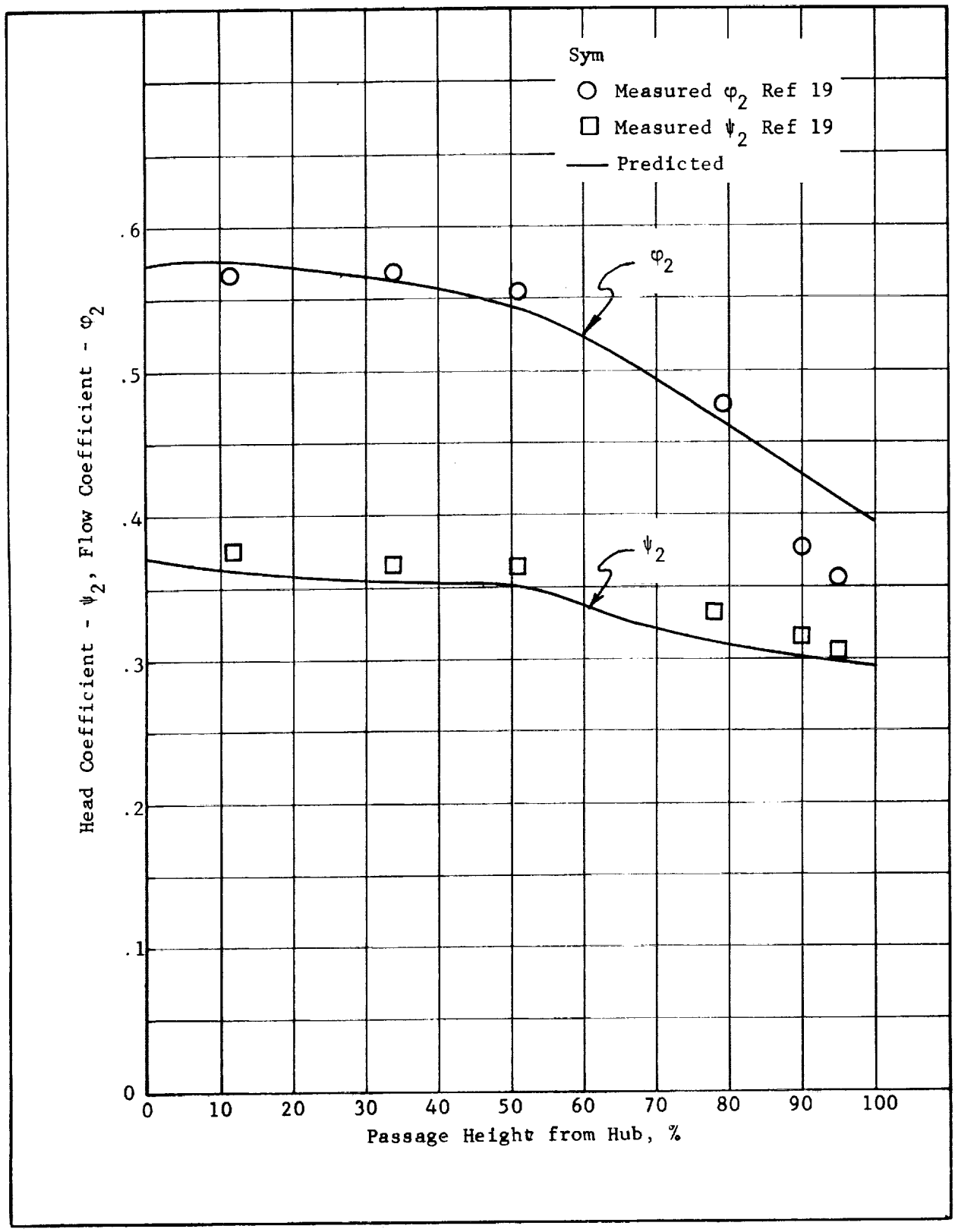

Figure 15. - Calculated and Measured Head Coefficient and Flow Coefficient vs. Passage Height

The final design was a selection of inlet geometry that could be modified between tests to observe the characteristics of various inlet angle changes. Figure 16 shows the predicted axial velocity profile at two stations for a 60° inlet angle. As the flow passes through the inducer, the axial velocity at the tip becomes more uniform. When the blade extends to the hub and the fluid is completely 'captured' between blade passages and the contour, the blade angle can be decreased more rapidly. Until this axial station is reached, the blade angle can be decreased only to the point where the inducer-free fluid pressure can support the flow field at the larger radii.

To maintain hydrodynamic similarity between the hubless inducer and the conventional inducer, the solidity at the mean radius was made identical. This resulted in higher tip and lower hub solidities when compared to the conventional inducer. The blade angles of the hubless inducer are equal to those of the conventional inducer from approximately 70% of axial length to the discharge.

The tip contour is converging from the inlet to the discharge along a conical line. The convergence ratio, discharge to inlet, is 0.946. The hub contour from the connection of the blade to the discharge is also a conical section. This conical hub contour approximates the contour of the conventional inducer over that portion of the inducer. This design concept made the discharge of the hubless inducer nearly identical to that of the conventional so that both would provide similar flow into the transition (aft) section.

2. Aft Section

The aft section is common to both inducers and is aptly called the transition section. The function of the transition section is to 'straighten' the flow coming from the front section and provide more nearly uniform axial flow and radial head to the rotor. By dividing the inducer into two sections, the blading of the rear portion could be twisted enough to accomplish these favorable conditions. An inducer with a continuous blade with comparable twist would not only be difficult to manufacture but would have higher centrifugal stresses because of its forward lean.

The selected blade form of the transition section was double circular arcs because of their characteristic sharp leading edges (which is necessary for good cavitation performance), and abundance of cascade data.

The incidence angles were set at near-zero values after accounting for the flow deviation from the forward section. This was done to account for any uncertainties in relative flow angles. The deviation angles were established from data in Ref 6 and corrected to account for rotation effects, tip leakage and radial flow shifts, based on correlations of this data and existing axial flow pump blade element performance data.

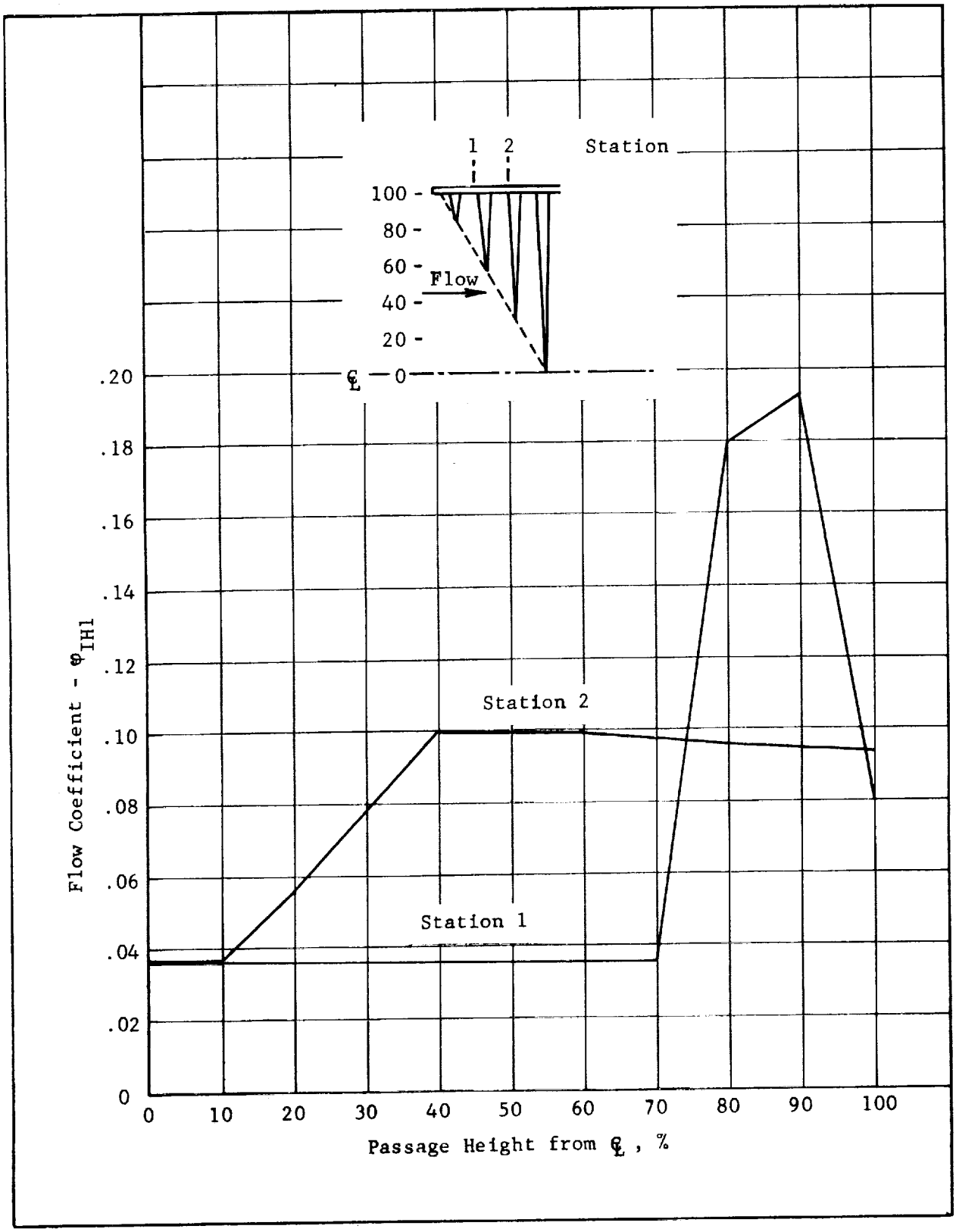

Figure 16. - Hubless Inducer Inlet Flow Coefficient vs. Passage Height

Figures 17 and 18 show the predicted performance of the transition section at the design flow. The inlet flow coefficient and mean radius was obtained by assuming constant angular momentum at each streamline discharging from the forward section. The discharge flow coefficient and mean radius had previously been selected during the one-dimensional analysis (Section III,C).

B. ROTOR

The detailed design of the rotor was initiated after the inducer testing had been completed. Therefore, some adjustments were made to the design specification of the rotor based on the test data. The only parameter in which there was a significant variation was the required torque to drive the inducer-shroud combination. Torque was measured at 30% greater than that estimated during the parametric analysis (Section III). This discrepancy will be discussed in later sections, but its only effect on the rotor was to require a higher head rise due to additional turbine head drop necessary to produce the required torque. The required head coefficient increased from 0.16 to 0.195 at the mean; this was still within the design limitations given in Ref 5.

Since the inducer average head and head distribution from test data was as predicted, the rotor inlet absolute fluid flow was assumed to be the same as the predicted inducer discharge, adjusted for the speed difference, Figure 19. The same design methods used to design the transition section of the inducer were followed for the rotor. The mass average head rise of the rotor was determined from the overall required system head rise, the inducer head rise, and the head drop through the turbine. There were several design iterations between the rotor and turbine to determine the best combined system, based on the design specification and blade geometry.

The predicted blade element performance of the rotor is shown in Figures 20 and 21. The blade inlet angles were set to give positive incidence at all radial sections for improved cavitation performance, and were greater than minimum loss incidence. The blade turning was then adjusted to obtain the required average head rise with nearly uniform discharge axial velocity. The maximum diffusion factor of 0.525 occurs at the tip stream line.

C. TURBINE

Both the turbine and rotor were designed after the inducers were tested; therefore, the power required to drive the inducer-shroud was known through direct measurement.

Two types of turbine blading were considered, constant section and twisted section. Since the relative inlet flow angle and a very wide variation hub to tip and because a wide operating range was desired, a constant section blunt leading edge blade was selected. This type blade,

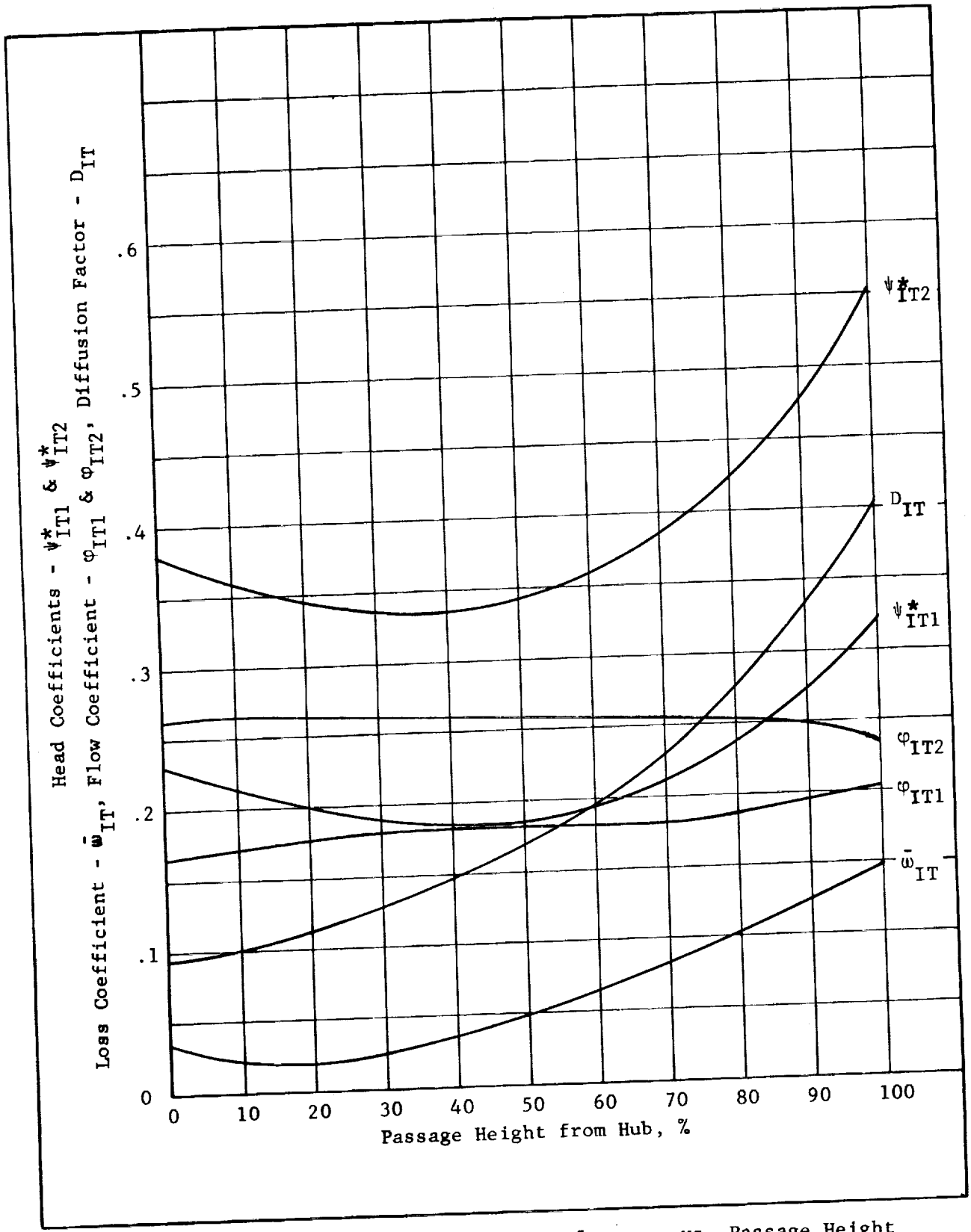

Figure 17 - Transition Blade Performance vs. Passage Height

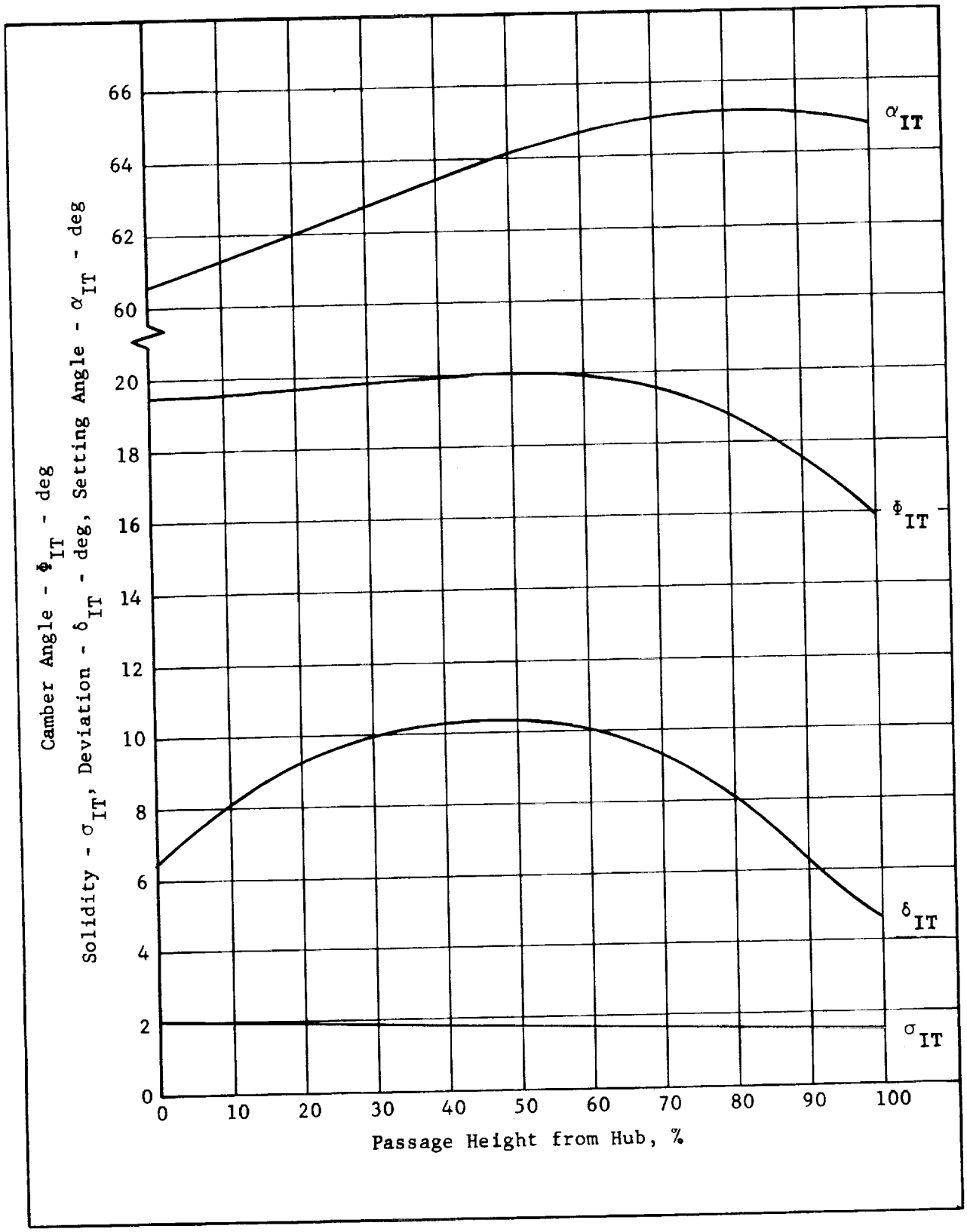

Figure 18. - Transition Blade Geometry vs. Passage Height

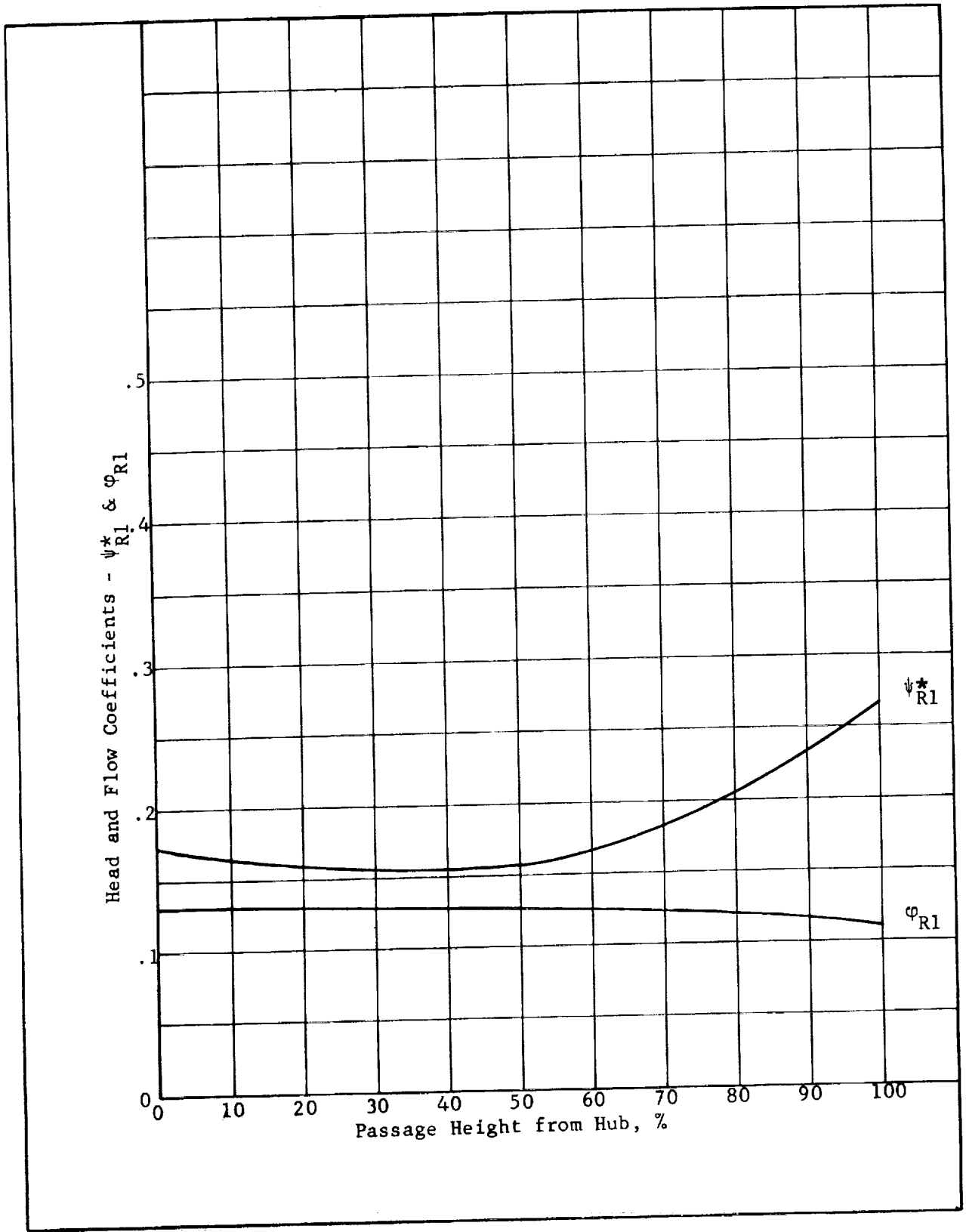

Figure 19. - Rotor Inlet Conditions vs. Passage Height

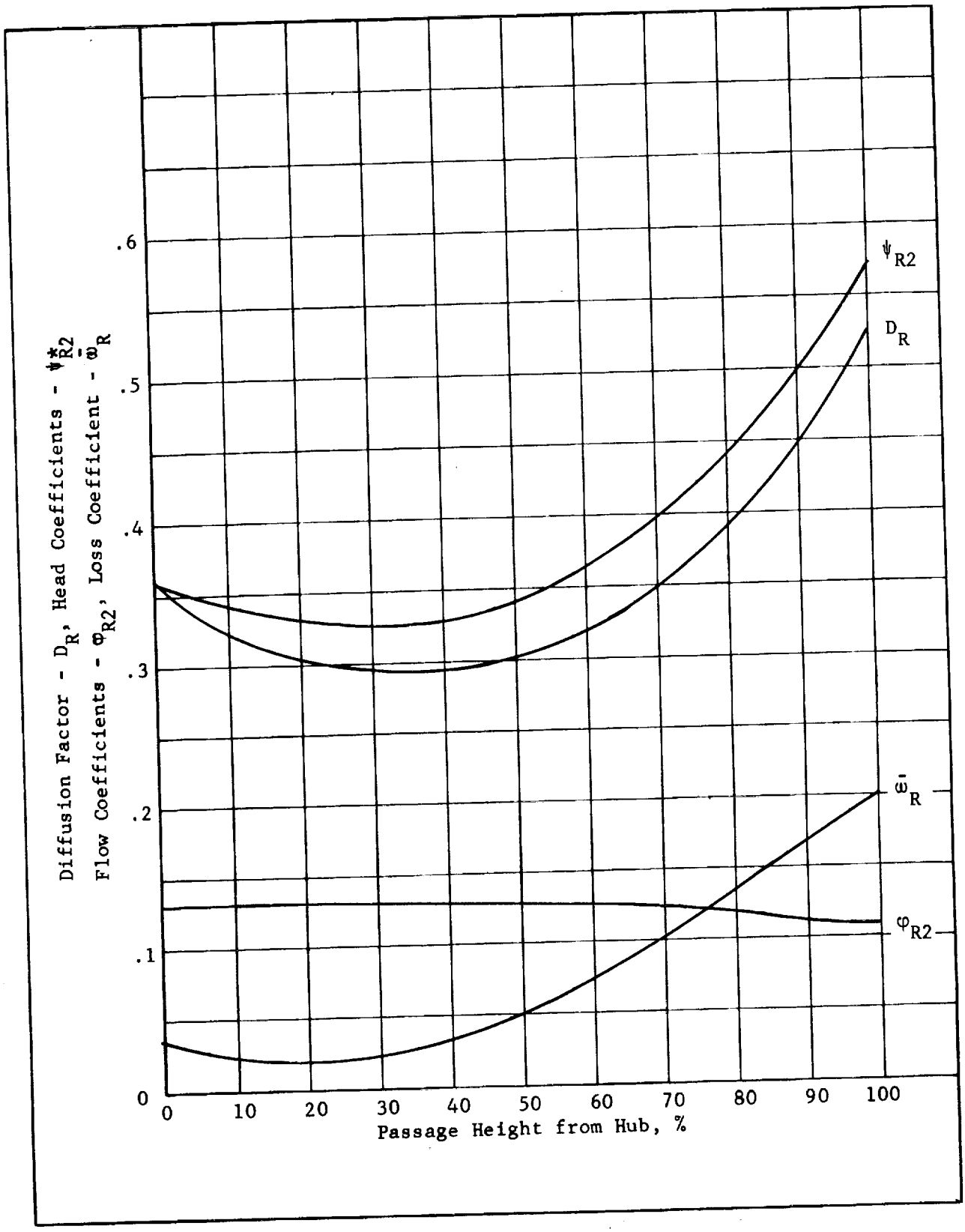

Figure 20. - Rotor Blade Performance vs. Passage Height

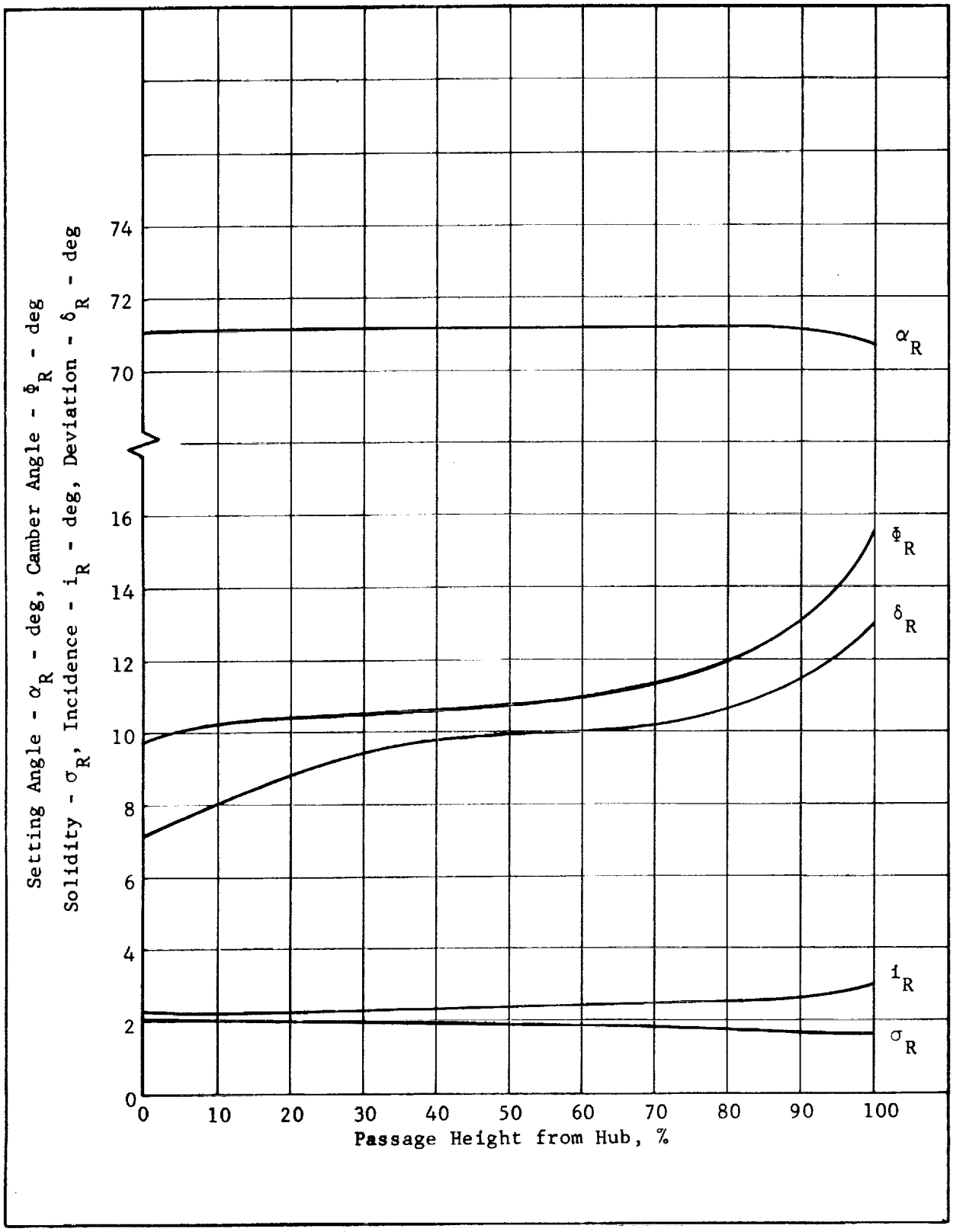

Figure 21 - Rotor Blade Geometry vs. Passage Height

although less efficient, was far more tolerant of fluid mismatch, as described in Ref 20. A constant section blade with blunt leading edge also provided a larger surface area to which the outer shroud could be attached.

Figure 22 shows the predicted blade element performance with most of the work being done at the blade tip. The discharge flow is nearly uniform, a condition most desirable for the downstream main pump. The magnitude of the discharge fluid whirl distribution is relatively small. In most design configurations, zero fluid whirl at the turbine discharge would be desirable, although the main stage blade velocity will be the speed ratio times the turbine blade velocity so that fluid whirl becomes less significant.

V. DETAILED HARDWARE AND FABRICATION

A. HARDWARE DATA

Upon completion of the hydrodynamic design, a master layout was made. This layout, Drawing No. 1158734, included all linear dimensions, blade profile dimensions, materials, specifications, tolerance stackups, concentricity and other necessary fabrication information. The drive assembly, P/N 1154352, was obtained from the program described in Ref 3. This drive unit can be either directly coupled to an electric motor through a torque meter and eddy current variable speed clutch or driven by a gas turbine. The first setup was used for steady-state cavitation and non-cavitation testing, while the latter was used for transient testing.

B. DESCRIPTION OF MAJOR HARDWARE

The hubless inducer shown in Figure 23 is in the unmodified condition which is the 60° inlet angle. The inducer was machined on a center hub, then brazed into an outer shroud, and finally machined to remove the center hub.

Figure 24 shows the front view of the conventional inducer. This inducer is contained within the shroud as shown in Figure 2. The blade contours at the discharge are identical to those of the hubless inducer.

The conventional inducer and transition (aft) section are shown in Figure 25. The transition section will mate with either the conventional or hubless inducer. This component was also made by machining the blade contour on the hub then brazing the shroud to the blade tips.

Figure 26 shows the rotor which is powered by the main shaft and is located between the inducer and hydraulic turbine. The rotor configuration is not unlike a high solidity axial flow airfoil blade. The condition shown is after the modification, during which approximately one-half the blade thickness was removed from the suction side. This modification resulted in a "flat-plate" blade with a slight amount of camber at the discharge.

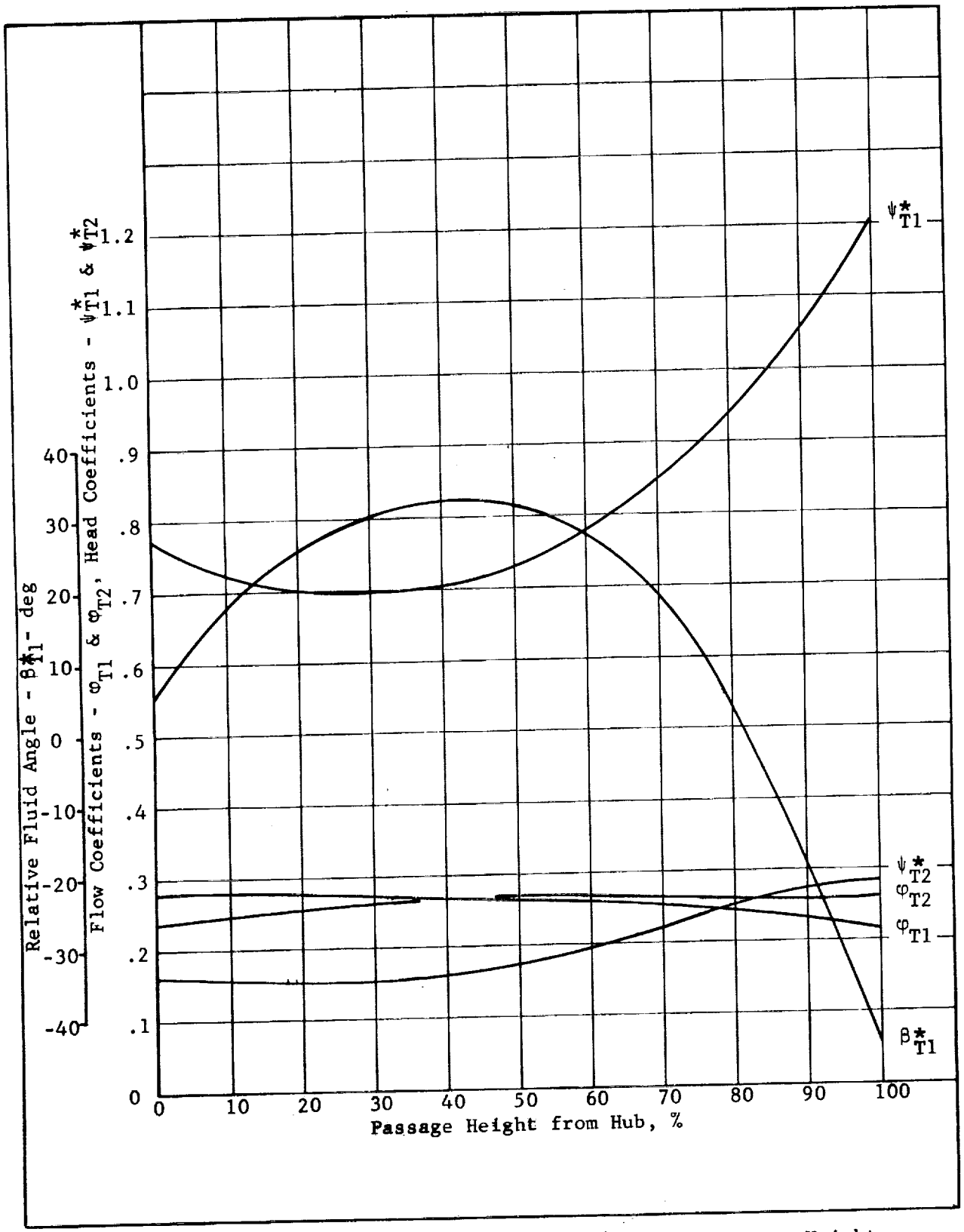

Figure 22. - Hydraulic Turbine Performance vs. Passage Height

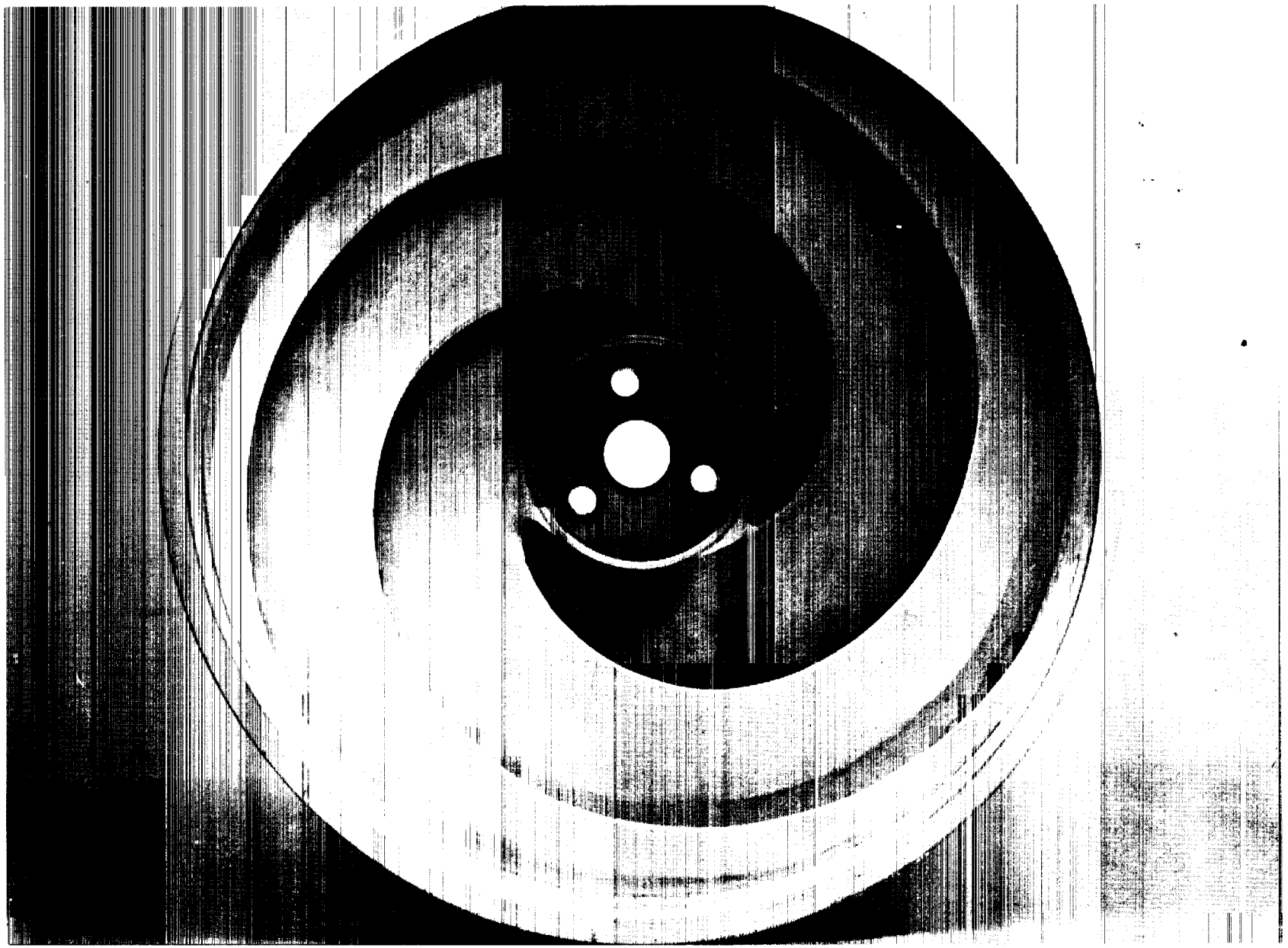

Figure 23. Hubless Inducer, P/N 1158907

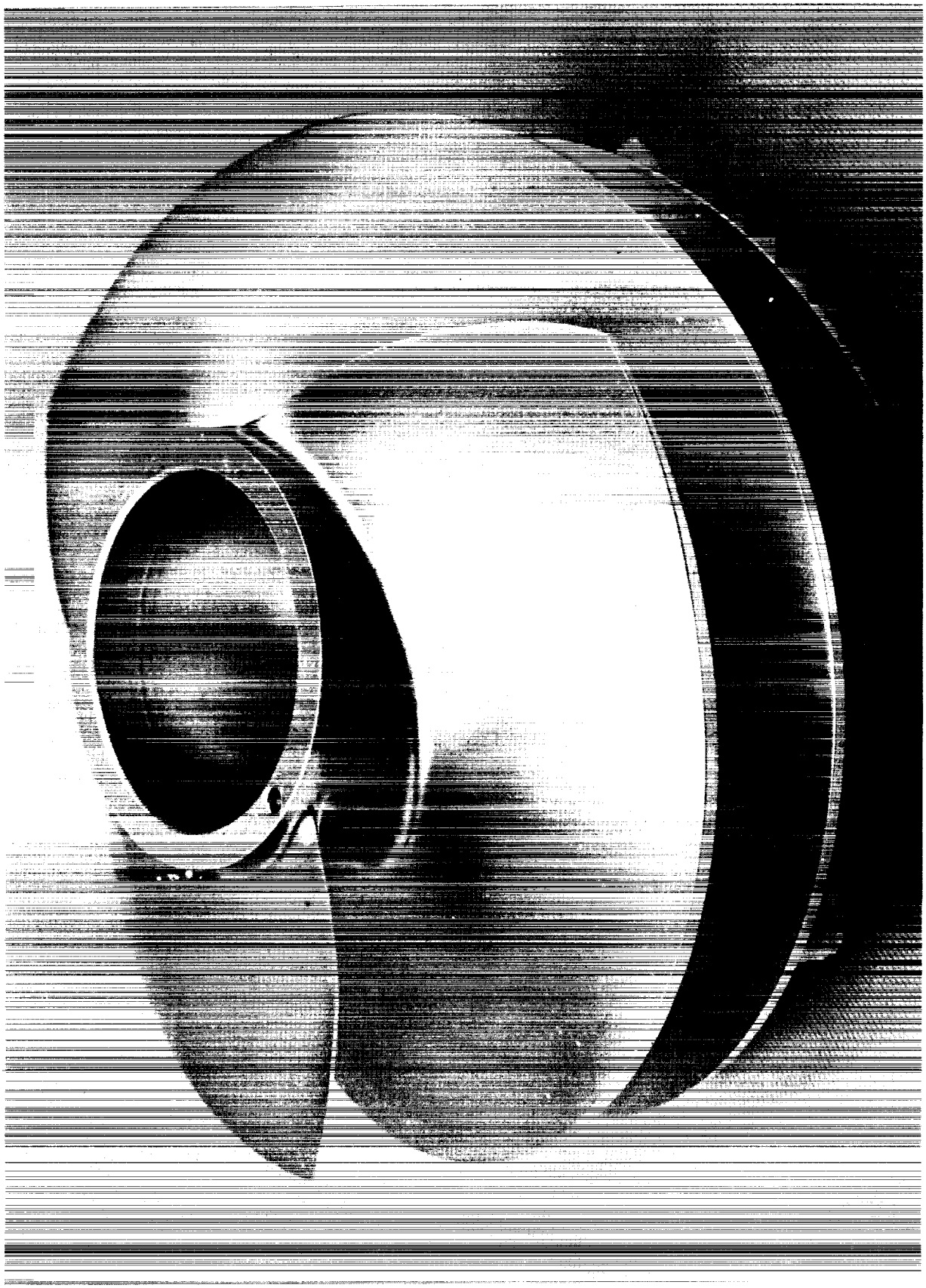

Figure 24. Conventional Inducer, P/N 1158905

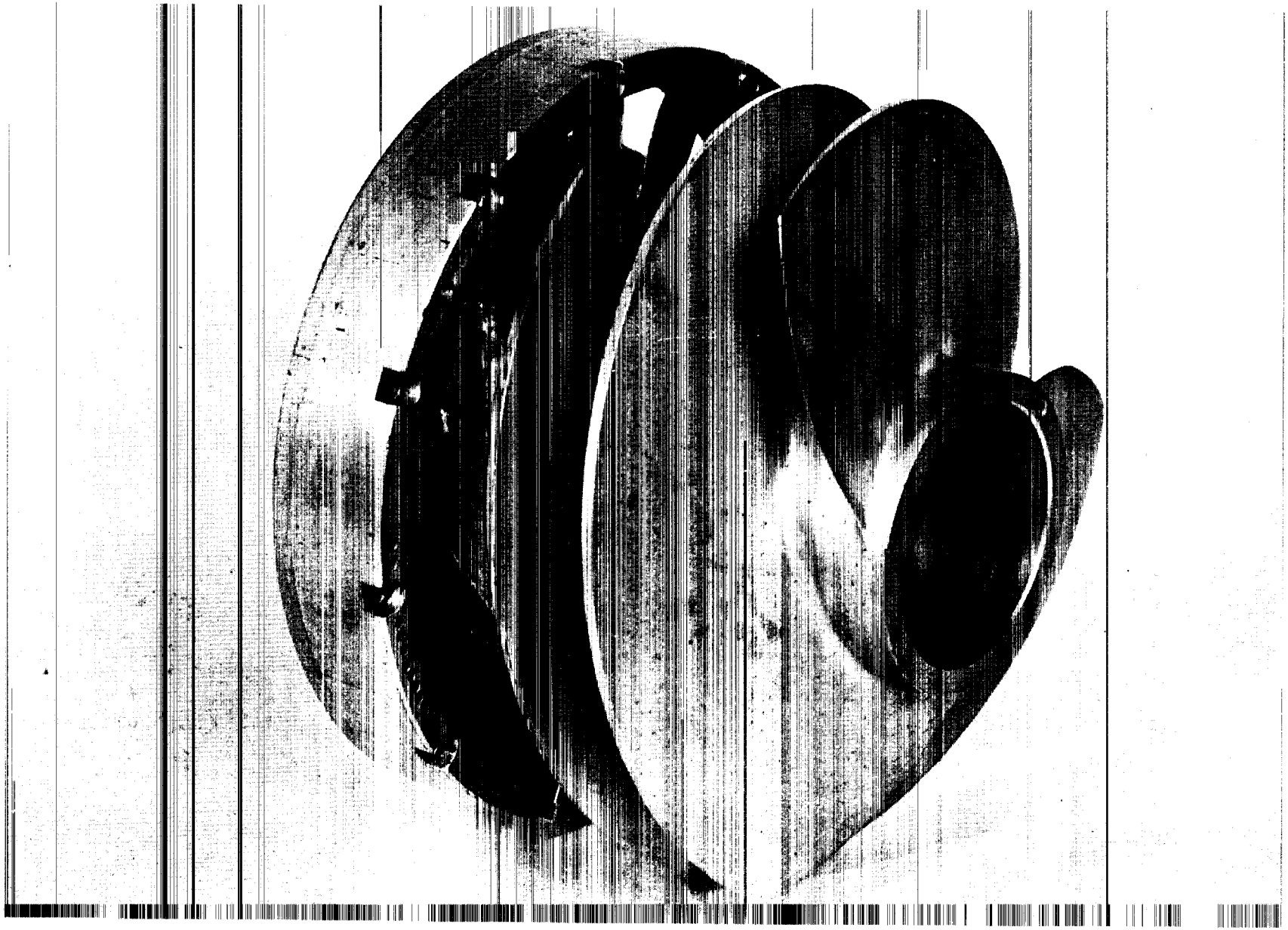

Figure 25. Transition Section, P/N 1158913

Figure 26. Rotor, P/N 1160008

The final blade row, the hydraulic turbine, is shown in Figure 27. All the flow from the rotor passes through the turbine. A labyrinth at the base of the hub shroud prevented excessive leakage around the turbine.

C. HARDWARE DIMENSIONS

A tabulation of the dimension and other pertinent design parameters for each blade row is given in Table I.

VI. TEST PROGRAM

The test program consisted of two series conducted at different time periods. During the first test series, a conventional inducer, a 60° hubless inducer with both long and short spinners, and a 45° hubless inducer with both long and short spinners were each driven directly by an electric motor. A total of 28 cavitating and noncavitating tests were made, and the performance of each inducer was obtained. The second test series was conducted using either the conventional inducer or the 45° hubless inducer with the long spinner. The inducers were powered by a full flow hydraulic turbine drive system. The rotor, which supplies power to the hydraulic turbine, was in turn driven by either the electric motor for steady-state or a GN_2 gas turbine for transient operation. A total of 23 tests was conducted; 16 at steady-state and 7 in transient.

A. TEST INSTRUMENTATION

The performance of each component (inducers, rotor, and hydraulic turbine) was obtained by using Keil probes at the discharge of each row, as shown in Figure 28. The angle at which the probes were set was determined by the performance prediction. These probes have a wide operating range so that even the off-design flow coefficient measured data are valid. The probes were placed at three radial locations (20%, 50%, 80% of hub to tip radial distance) and the pressure measured external to the pump through drilled passages which connected to the probes. When the inducers were tested separately (top of Figure 28) the probes were located directly downstream. During the later test series, these probes were removed (middle of Figure 28) and the performance of the downstream was rotor calculated by assuming that the inducer head rise was unchanged. This assumption appears valid since the measured rotor performance was unchanged with the two different performing inducers. Overall performance of all components was determined by averaging the measured pressure from the three probes.

The following types of sensors were incorporated into the measuring systems:

Flows	Turbine type flowmeter
Pressures	Strain gage pressure transducer
Temperatures	Resistance temperature transmitters
Torque	Strain gage with slip rings
Speeds	Magnetic coil type

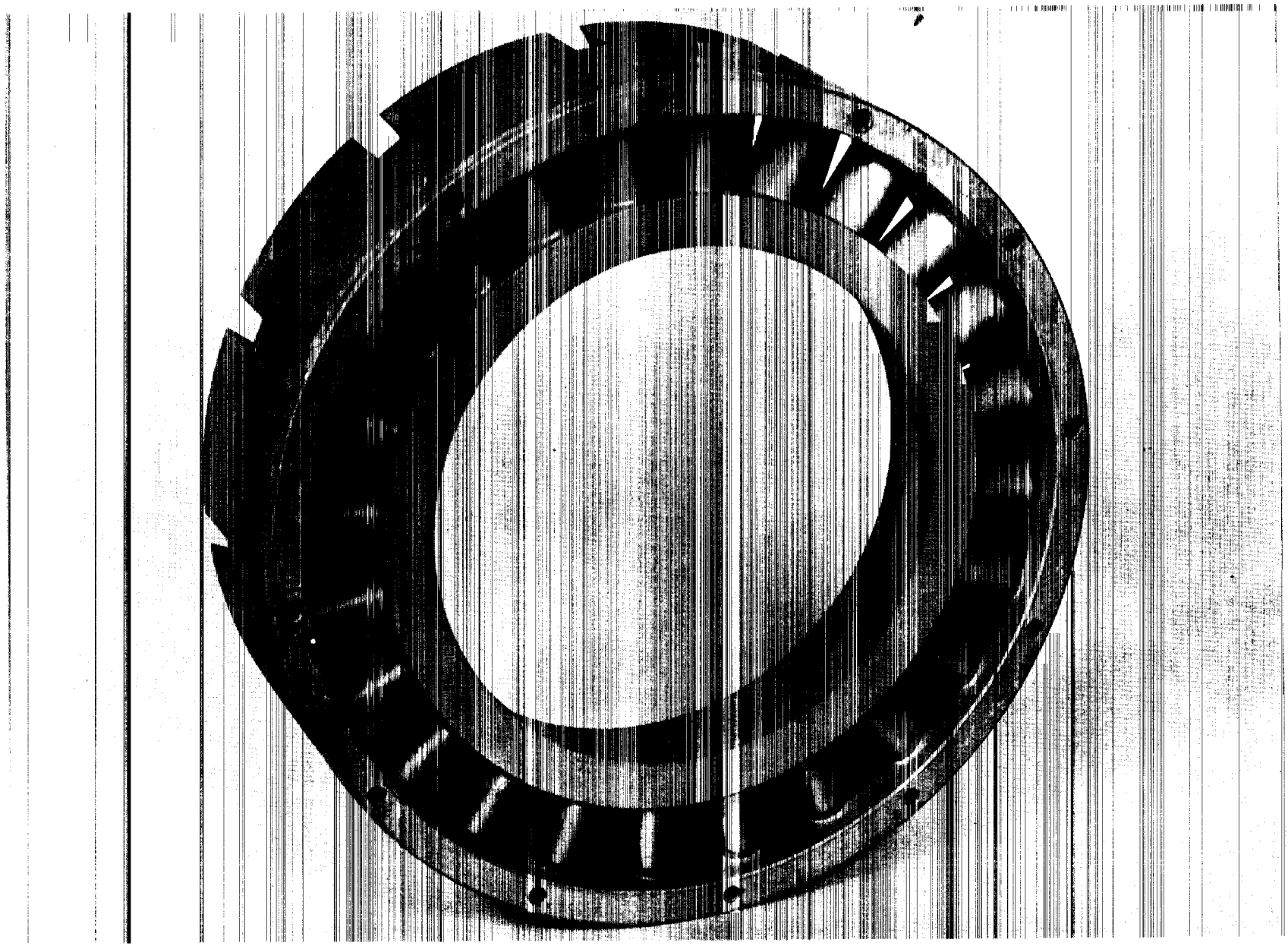

Figure 27. Hydraulic Turbine, P/N 1160032

TABLE I. - BLADE DIMENSIONS AND DESIGN PARAMETERS

	Inducer				
	Hubless	Conventional	Transition	Rotor	Hydraulic Turbine
Inlet Flow Coefficient	.071	.085	.179	.119	.250
Exit Flow Coefficient	.146	.146	.250	.119	.250
Head Coefficient[1]	.146	.146	.146	.162	.674
Tip Diameter Inlet	7.720 in (.196m)	7.720 in (.196m)	7.142 in (.181m)	7.116 in (.180m)	7.144 in (.181m)
Tip Diameter, Exit	7.314 in (.186m)	7.314 in (.186m)	7.142 in (.181m)	7.116 in (.180m)	7.144 in (.181m)
Hub/Tip Ratio, Inlet	0	.4	.705	.8	.8
Hub/Tip Ratio Exit	.65	.65	.8	.8	.8
Number of Blades	3	3	15	11	24
Blade Tip Clearance	-	.035 in (.00089m)	-	.012 in (.00030m)	-
Leading Edge Thickness	.020 in (.00051m)	.020 in (.00051m)	.020 in (.00051m)	.030 in (.00076m)	-
TIP					
Solidity	4.06	2.05	1.54	1.57	1.4
Cord Length	30.87 in (.835m)	16.6 in (.422m)	2.300 in (.00585m)	3.184 in (.0810m)	1.3 in (.0330m)
Maximum Thickness/Cord	-	-	.06	.06	.33
Inlet Blade Angle	85.0°	81.57°	73.0°	78.5°	-
Exit Blade Angle	80.5°	80.5°	51.2°	63.0°	69.7°
HUB					
Solidity[2]	2.2/1.6	3.03	2.04	1.99	1.4
Cord Length	5.0/4.5 in (.127/.114m)	9.80 in (.249m)	2.300 in (.0585m)	3.250 in (.0825m)	1.3 in (.0330m)
Maximum Thickness/Cord	-	-	.06	.10	.33
Inlet Blade Angle	-	69.7°	70.5°	76.0°	-
Exit Blade Angle	60.0°	60.0°	50.5°	66.3°	69.7°

(1) Based on tip discharge diameter of indicated component

(2) 60° hubless/45° hubless

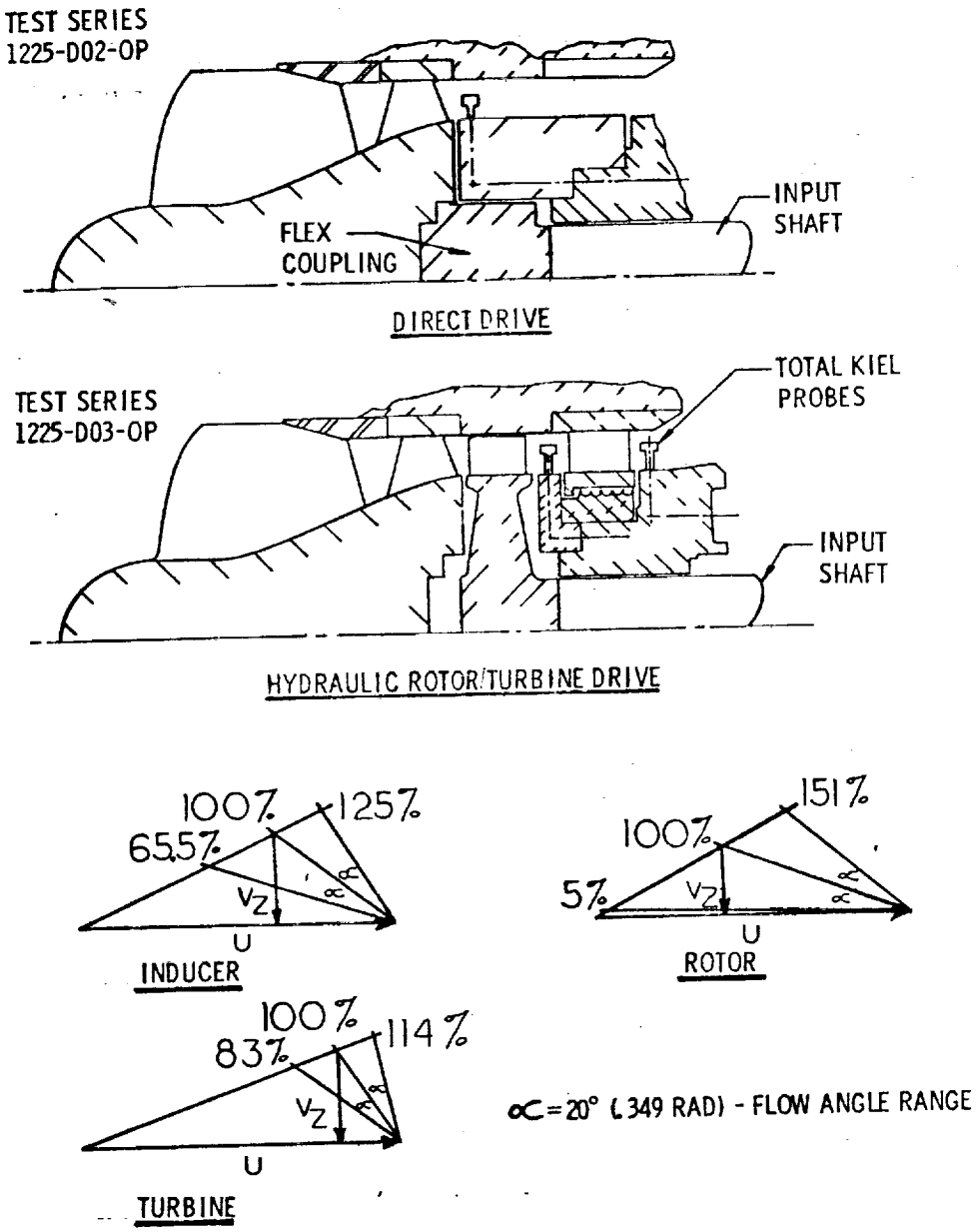

Figure 28. - Kiel Probe Location and Pressure Measuring Capability

The output from these sensors was fed through an analog-to-digital system, Aerojet's Automatic Data Control System. Each parameter or channel is "swept" 30 times per second and the data is recorded on magnetic tapes. Three-second time sweeps were used during steady-state testing, while continuous sweeps were utilized during transient operation. The steady-state data for each function were averaged and statistically analyzed over the 3-second time interval. This statistical analysis of each function included the standard deviation and the maximum difference from the mean. Then the data were examined and considered to be acceptable if the two-sigma deviation was less than 1% of the mean.

The above described average values were computed using Job No. 3001. The output from this computer program, which has identical printed and punch card output, was then used as input to a data reduction program. The test data were utilized in this data reduction program to produce normalized pump performance.

Visual gage and strip charts were used to record critical or "redline" parameters, as well as aids in the setup of a test. The strip charts also provided "quick-look" information and served as backup for the digital recordings.

High frequency data was recorded for the purpose of determining pressure oscillation during cavitation and transient conditions. These sensors were flush mounted at the pump suction and discharge. The output was recorded on magnetic tape which served as input to a spectral density computer program (Job No. 2901).

B. TEST FLOW FACILITY

Figure 29 shows a flow schematic of the test loop and the relative position of the necessary components. The hydrostatic bearing flow was supplied by a facility pump and was directly coupled to the loop so that there was no net gain or loss in fluid. Figure 30 is a photo of the test bay showing the associated valves and piping.

C. TEST NUMBER AND TEST TYPE

Table II shows the test number and type of test for the two test series. Also shown are the speed and flow range for each test as well as the type of components tested.

VII. TEST RESULTS AND PERFORMANCE EVALUATION

All the test results discussed in this section were obtained from water-loop testing, which was completed in two test series. The three basic type of tests conducted were non-cavitating steady-state, cavitating steady-state, and cavitating transient.

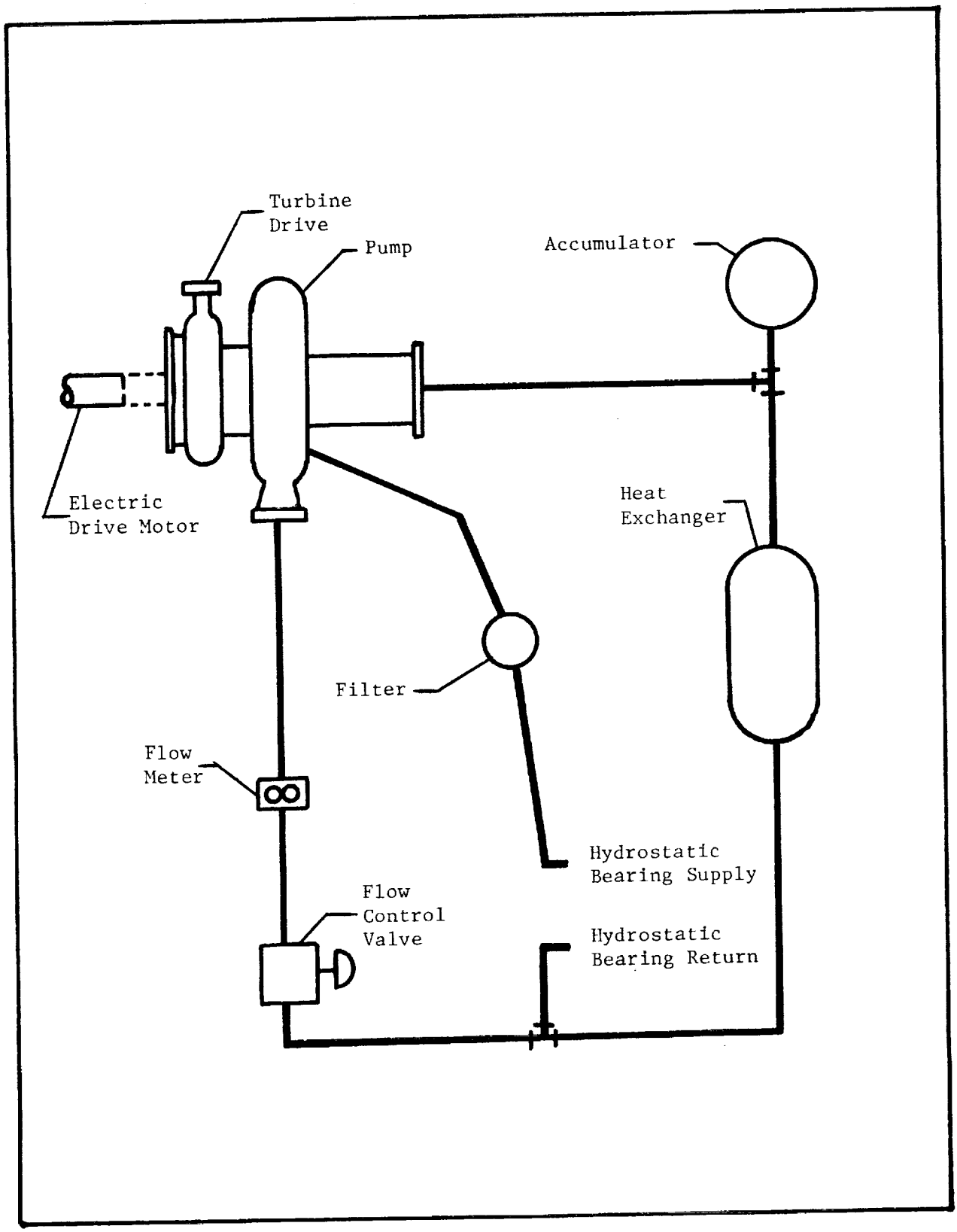

Figure 29. - Test Facility Flow Schematic

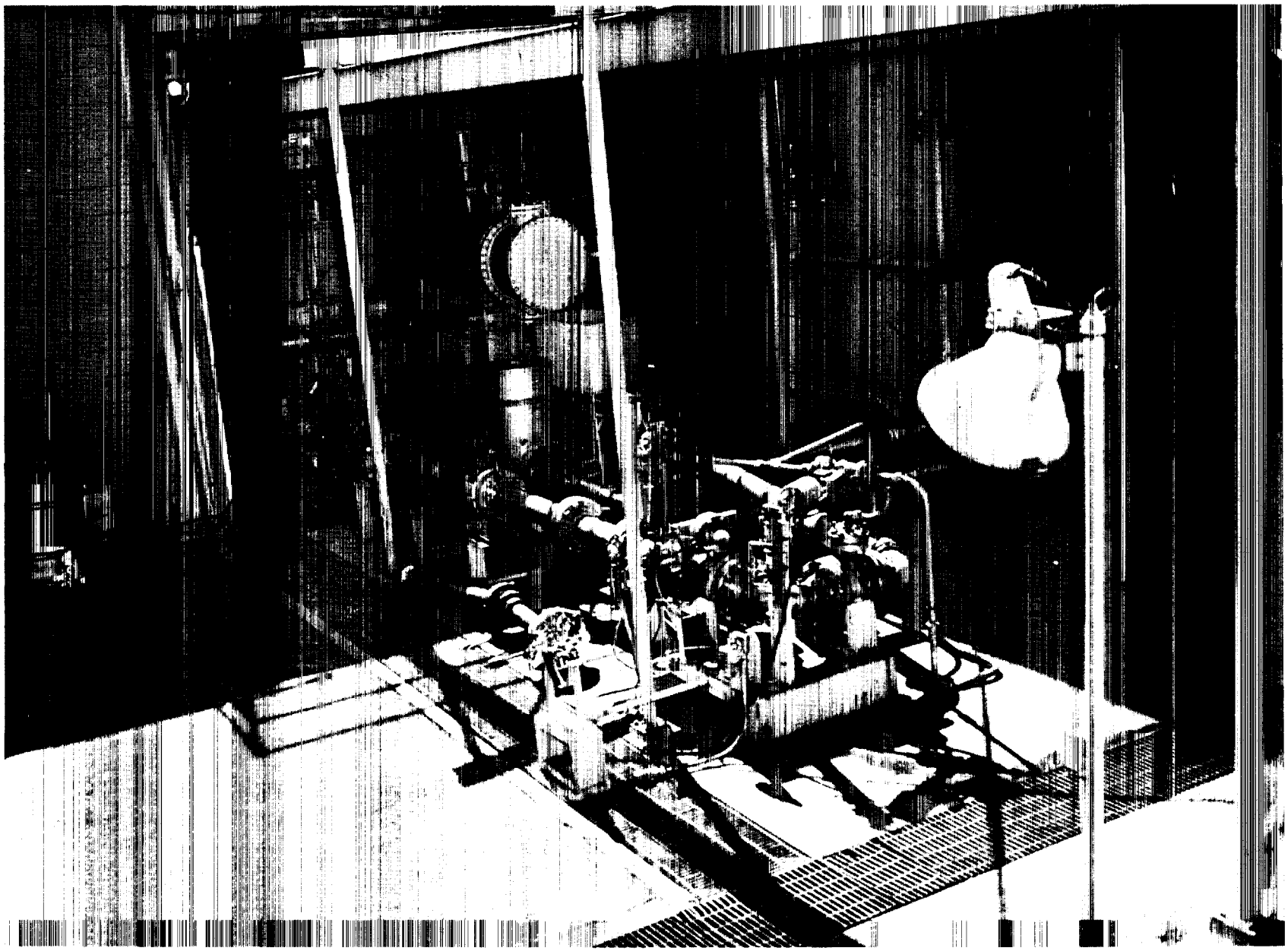

Figure 30. Test Facility Zone D-3A

TABLE II. - TEST NUMBER AND TEST TYPE

Test Number	Test Type	Speed, % Design	Flow/Speed, % Design	Components			
				Hubless	Conventional	Rotor	Turbine
1225-D02-OP-001	Head Flow	40	18-130		X		
-002	Head Flow	60	24-130		X		
-003	Head Flow	80	60-130		X		
-004	Head Flow	40	18-120	60° Long Spinner			
-005	Head Flow	60	25-122	60° Long Spinner			
-006	Head Flow	80	63-123	60° Long Spinner			
-007	Head Flow	100	65-140	60° Long Spinner			
-008	Cavitation	100	100	60° Long Spinner			
-009	Cavitation	100	100	60° Long Spinner			
-010	Cavitation	100	100	60° Long Spinner			
-011	Cavitation	100	80	60° Long Spinner			
-012	Cavitation	100	100	60° Short Spinner			
-013	Cavitation	100	110	60° Short Spinner			
-014	Cavitation	100	80	60° Short Spinner			
-015	Head Flow	100	65-132		X		
-016	Cavitation	100	100		X		
-017	Cavitation	100	80		X		
-018	Cavitation	100	110		X		
-019	Cavitation	100	100		X		
-020	Cavitation	100	100		X		
-021	Head Flow	100	65-123	45° Long Spinner			
-022	Head Flow	60	12-123	45° Long Spinner			
-023	Cavitation	100	104	45° Long Spinner			
-024	Cavitation	100	82	45° Long Spinner			
-025	Cavitation	100	115	45° Long Spinner			
-026	Cavitation	100	104	45° Short Spinner			
-027	Cavitation	100	82	45° Short Spinner			
-028	Cavitation	100	115	45° Short Spinner			
1225-D03-OP-001	Head Flow	40	17-116	45° Long Spinner		X	X
-002	Head Flow	60	11-118	45° Long Spinner		X	X
-003	Head Flow	80	65-117	45° Long Spinner		X	X
-004	Head Flow	100	70-118	45° Long Spinner		X	X
-005	Cavitation	100	100	45° Long Spinner		X	X
-006	Head Flow	100	72-118	45° Long Spinner		X	X
-007	Cavitation	100	100	45° Long Spinner		X	X
-008	Cavitation	100	110	45° Long Spinner		X	X
-009	Cavitation	100	80	45° Long Spinner		X	X
-010	Head Flow	40	0-118		X	X	X
-011	Head Flow	60	0-120		X	X	X
-012	Head Flow	80	63-123		X	X	X
-013	Head Flow	100	65-120		X	X	X
-014	Cavitation	100	100		X	X	X
-015	Cavitation	100	110		X	X	X
-016	Cavitation	100	80		X	X	X
-017	Transient	0-100	--		X	X	X
-018	Transient	0-100	--		X	X	X
-019	Transient	0-100	--	45° Long Spinner		X	X
-020	Transient	0-100	--	45° Long Spinner		X	X
-021	Head Flow & Cavitation	100	69-127 & 100		X	X	X
-022	Cavitation	100	80		X	X	X
-023	Cavitation	100	110		X	X	X

The test results presented for each blade row are based upon the average of the three Kiel probe readings, unless otherwise noted.

A. STEADY STATE NON-CAVITATING

The steady state non-cavitating tests were conducted with suction pressure sufficiently high to preclude any cavitation. The drive mode was an electric motor capable of maintaining constant speed to within $\pm$ 0.1%.

1. Conventional Inducer

Figure 31 shows the inducer efficiency and normalized input torque for several speeds over a flow range of 15 to 130% of the discharge flow coefficient. The measured input torque (and, consequently, the efficiency) includes the inducer torque plus the shroud torque. The shroud torque was calculated to be 38.8 lb-ft (52.6N-m) at the design speed. Since there was no direct measurement to verify the calculated shroud drag torque, a value was obtained by subtracting the inducer torque at design flow from the measured input torque; this resulted in a shroud torque value 30% higher than calculated. This value was then normalized with speed and was used at all other speeds and flow coefficients.

The inducer head coefficient and efficiency as a function of flow coefficient are shown in Figure 32. Again, it is noted that the inducer efficiency at the design flow was set to the design value. This is justified by the fact that the measured head coefficient has the same value as the design predicted value, therefore, the efficiency at the design point should be near the predicted value. Since the shroud drag at off-design flow coefficient was constant (at constant speed), the off-design efficiency will be true relative to the design point. There appears to be little or no speed effect imposed on the normal data scatter. The inducer shows some stall at approximately 45% of the design flow coefficient. The maximum flow coefficient was determined by the facility flow loop resistance with a fully open valve.

The head rise coefficients at four radial stations are shown as a function of discharge flow coefficient in Figure 33. The upper three are total head coefficients measured with total Kiel probes, while the lower one is a static head coefficient measured with a wall tap. Over the flow range shown there is no evidence of inducer stall at the low flow, or inducer choking at the high flow. It appears that zero slope or stall will occur first at the 80% streamline; some stall did occur at slightly lower flow coefficient, as indicated by Figure 32. Figure 34 shows the measured head coefficient at the various radial stations; also shown is the design prediction. The mass-averaged design-predicted head coefficient and the head coefficient determined by average of the three probes agreed within 1%. At the 80% radial station, the measured head coefficient was 13% higher than the predicted value. An average was used to determine blade row performance since the velocity and mass flow distribution can not be obtained from Kiel probe readings.

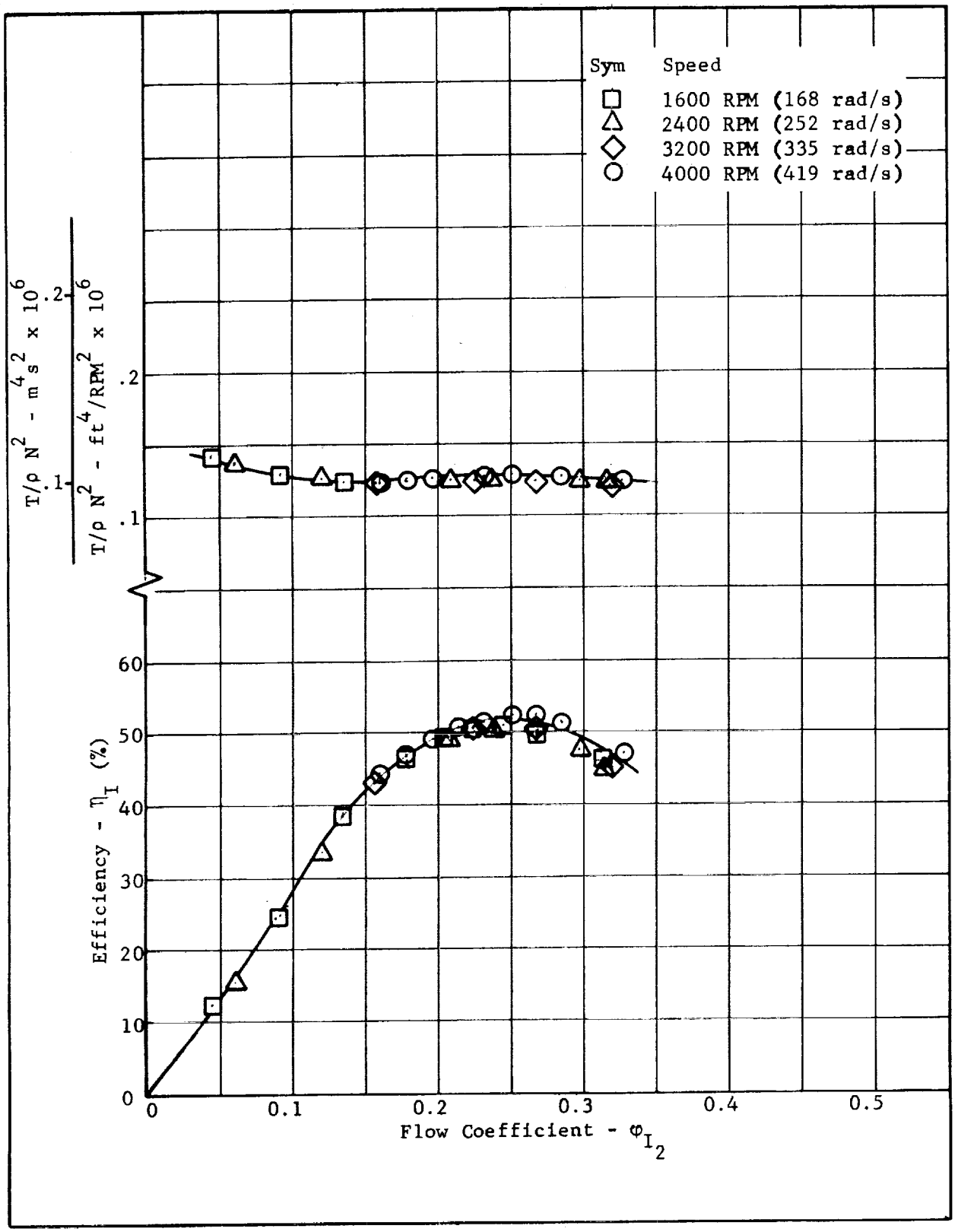

Figure 31. - Conventional Inducer, Combined Inducer and Shroud Normalized Torque and Efficiency vs. Flow Coefficient (Non-Cavitating)

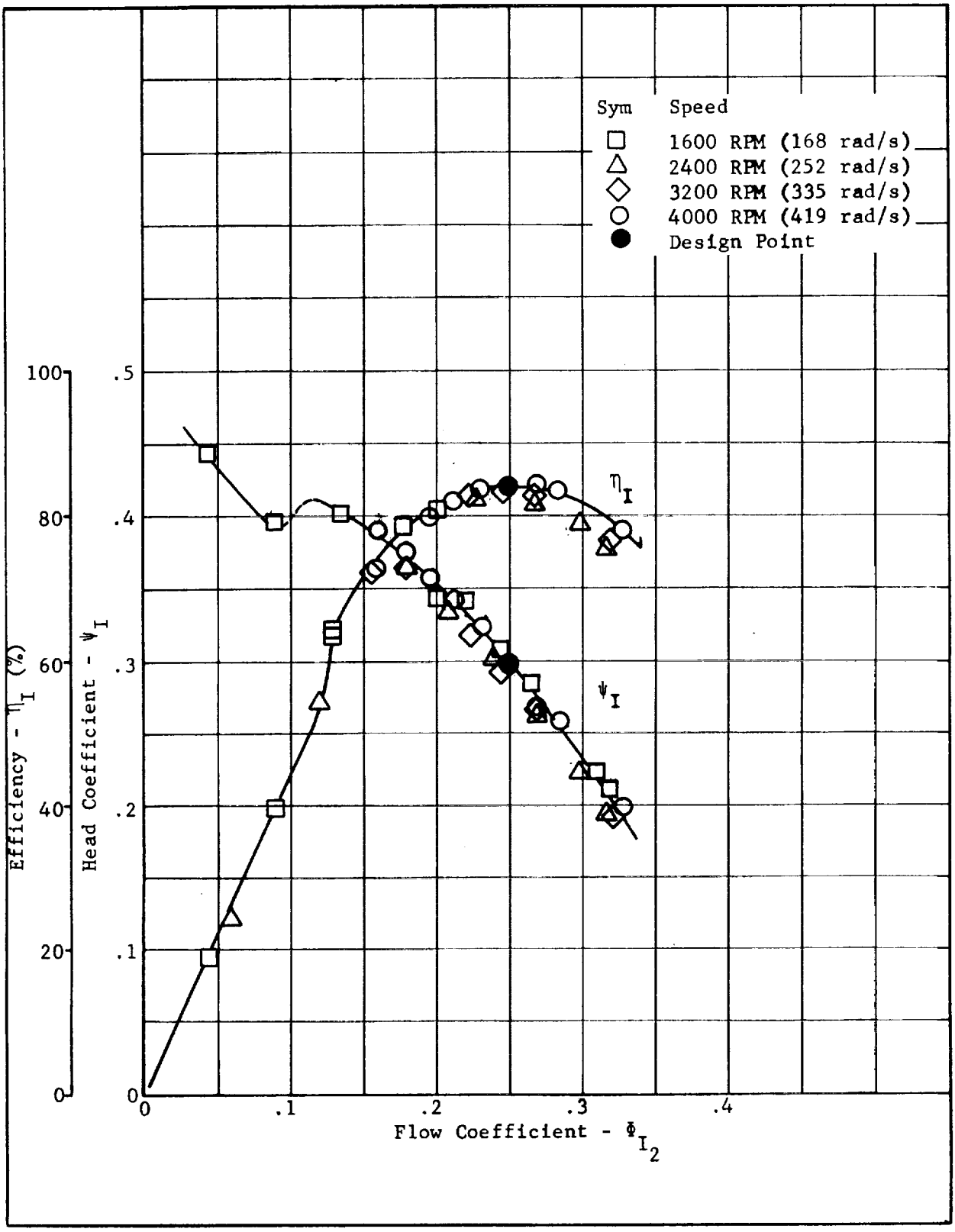

Figure 32. - Conventional Inducer, Head Coefficient and Efficiency vs. Flow Coefficient (Non-Cavitating)

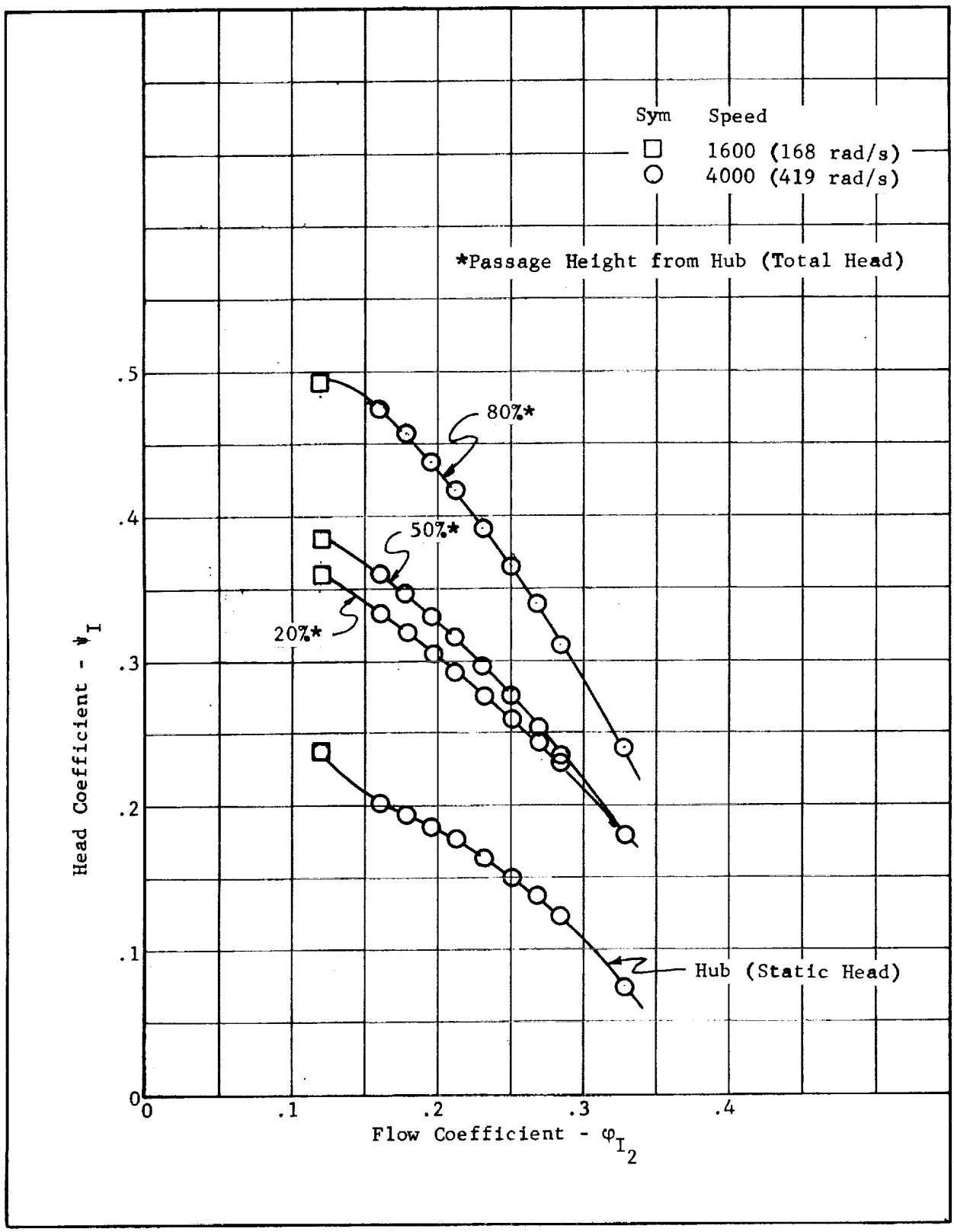

Figure 33. - Conventional Inducer, Head Coefficients vs. Flow Coefficient at Four Radial Measuring Stations (Non-Cavitating)

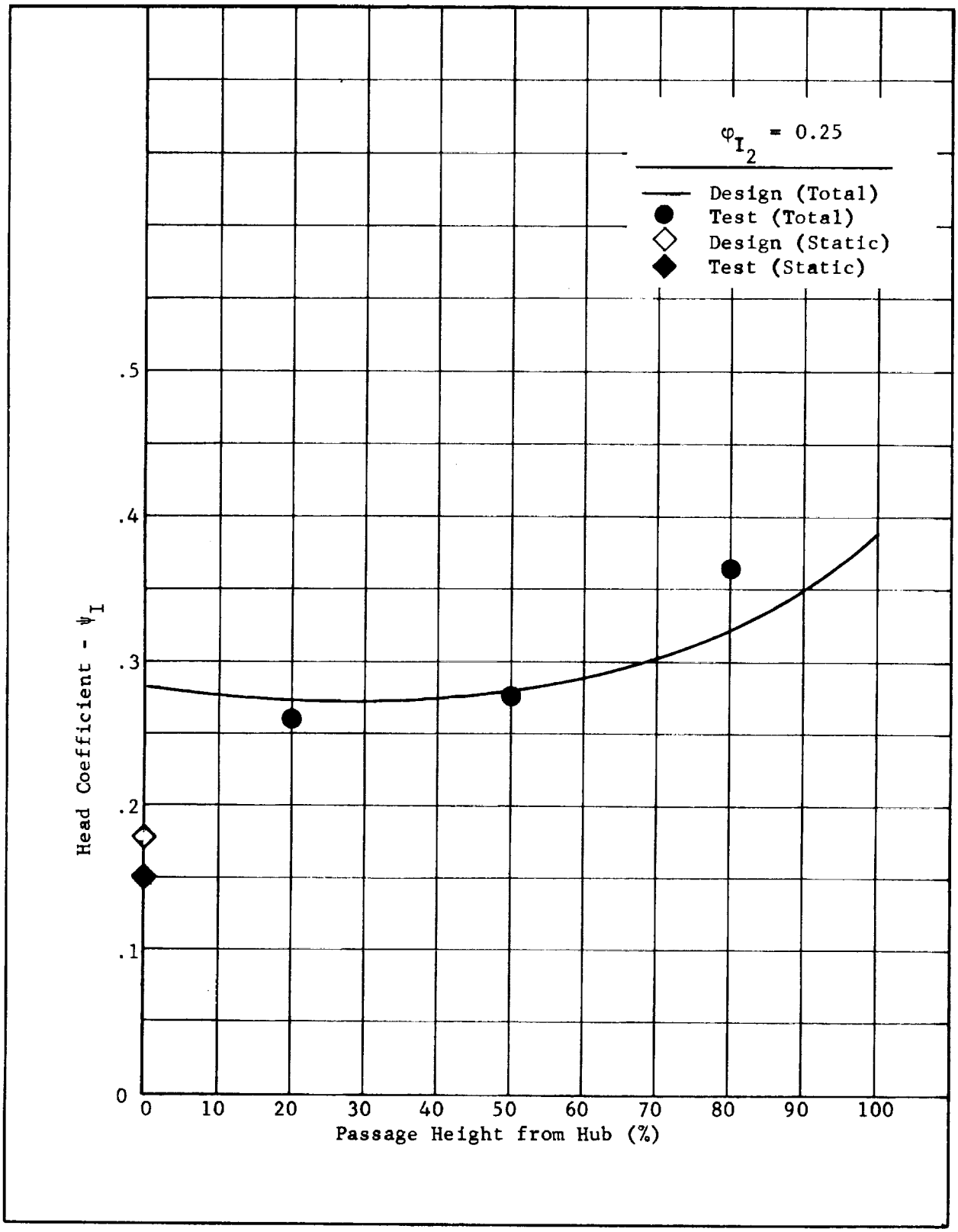

Figure 34. - Conventional Inducer, Radial Head Coefficient Distribution at Design Flow Coefficient (Non-Cavitating)

2. Hubless Inducer with 60° Inlet

Figure 35 shows the normalized input torque and efficiency for several speeds over a flow coefficient range of 25% to 125% of the design flow coefficient. The input torque appears flat and continuous while the efficiency has a double peak. The head coefficient shown on Figure 36 has an inflection at the same flow coefficients. Also shown is the inducer efficiency without the shroud drag torque. The shroud drag torque used to calculated efficiency was exactly the same as that determined from the conventional inducer testing. The inflection in the head flow and efficiency flow curves can most likely be attributed to flow shifts within the inducer. Most of the head is generated near the tip of the inducer as shown in Figure 37. The head values at radial stations 20% and 50% are almost the same and are approximately 60% of the head at the 80% radial station.

3. Hubless Inducer with 45° Inlet

Figure 38 shows the normalized torque and efficiency vs. flow coefficient for two different speeds over a flow coefficient range of 12 to 125% of the design. Again the efficiency shown is based on input torque, which includes both inducer torque and shroud drag torque. The head coefficient and efficiency vs. flow coefficient curves shown on Figure 39 have inflections which are most likely caused by the radial flow shifts within the inducer. Figure 40 shows the head coefficient at four radial stations. This curve also shows that flow shifts are occuring at two flow coefficients: 0.16 and 0.25.

4. Inducer Comparison

By juxtapositioning Figures 31, 35 and 38, Figures 32, 36 and 39, and Figures 33, 37 and 40, the non-cavitating performance comparison of the conventional, 60° hubless, and 45° hubless inducers can be made. For the first set of figures it can be seen that the normalized input torque is the same for all inducers above a 80% design flow (0.2 flow coefficient). The efficiencies at the design flow are 52%, 42% and 41%, respectively. The second set of figures shows that the inducer efficiency excluding shroud drag is 85% (design value), 69% and 68%, respectively. The head rise coefficients are displaced by the same relative amount as the efficiencies. The final set of figures shows that head coefficients at each radial station for both hubless inducers is considerably less than that of the conventional inducer; this implies that the losses through hubless inducers are greater than those for the conventional inducer, since the discharge blade angles are the same for all three inducers. The tip head coefficient for both hubless inducers should be the same since no modification to the inducer was made at the tip. The solidity at the tip is much greater for the hubless inducers, which could account for the higher losses due to form drag. It appears that the head - flow relationship of a hubless inducer could be 'tailored' by modification of the inlet angle, although the performance would most likely not exceed that of a conventional inducer.

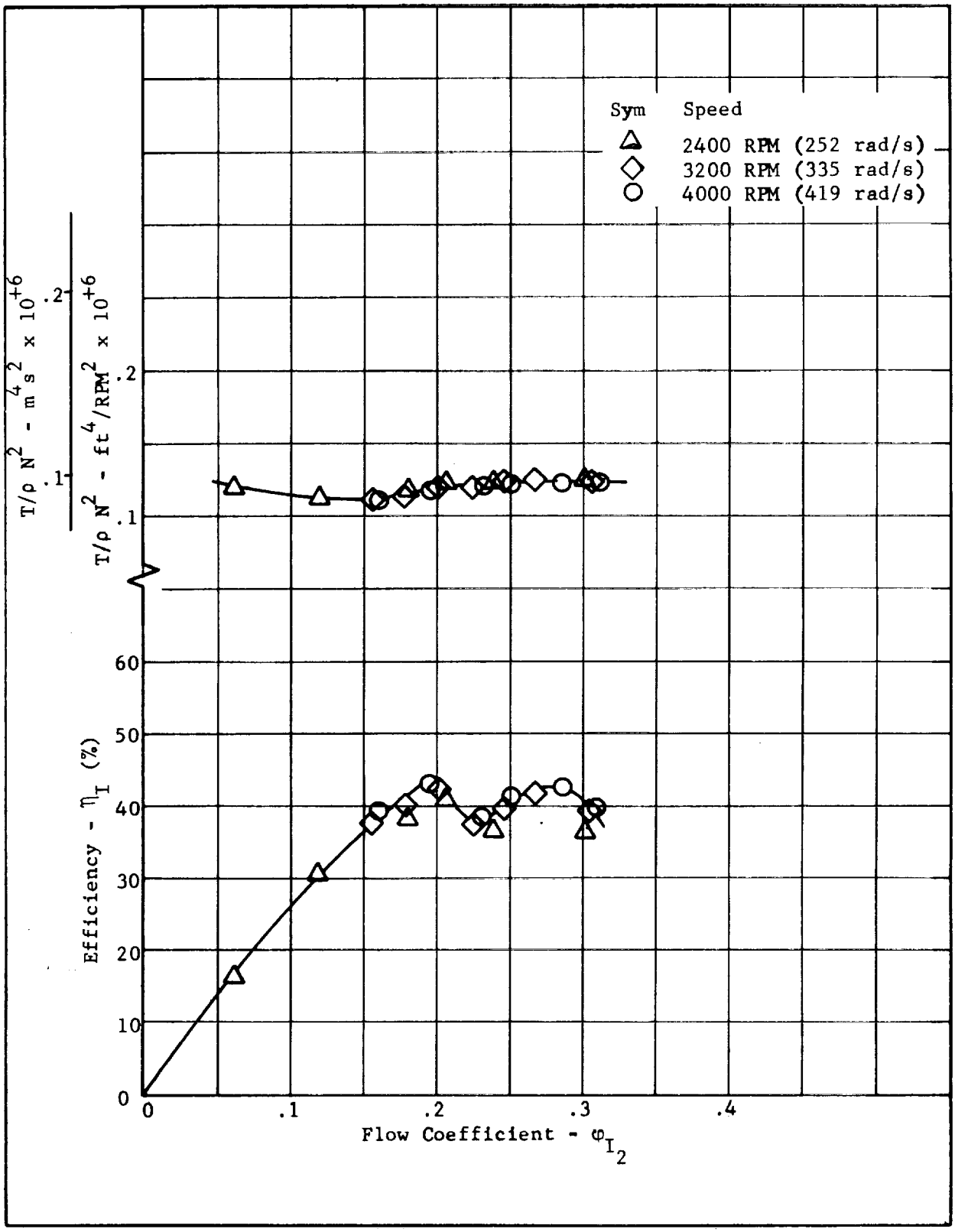

Figure 35. - Hubless Inducer (60°), Combined Inducer and Shroud Normalized Torque and Efficiency vs. Flow Coefficient (Non-Cavitating)

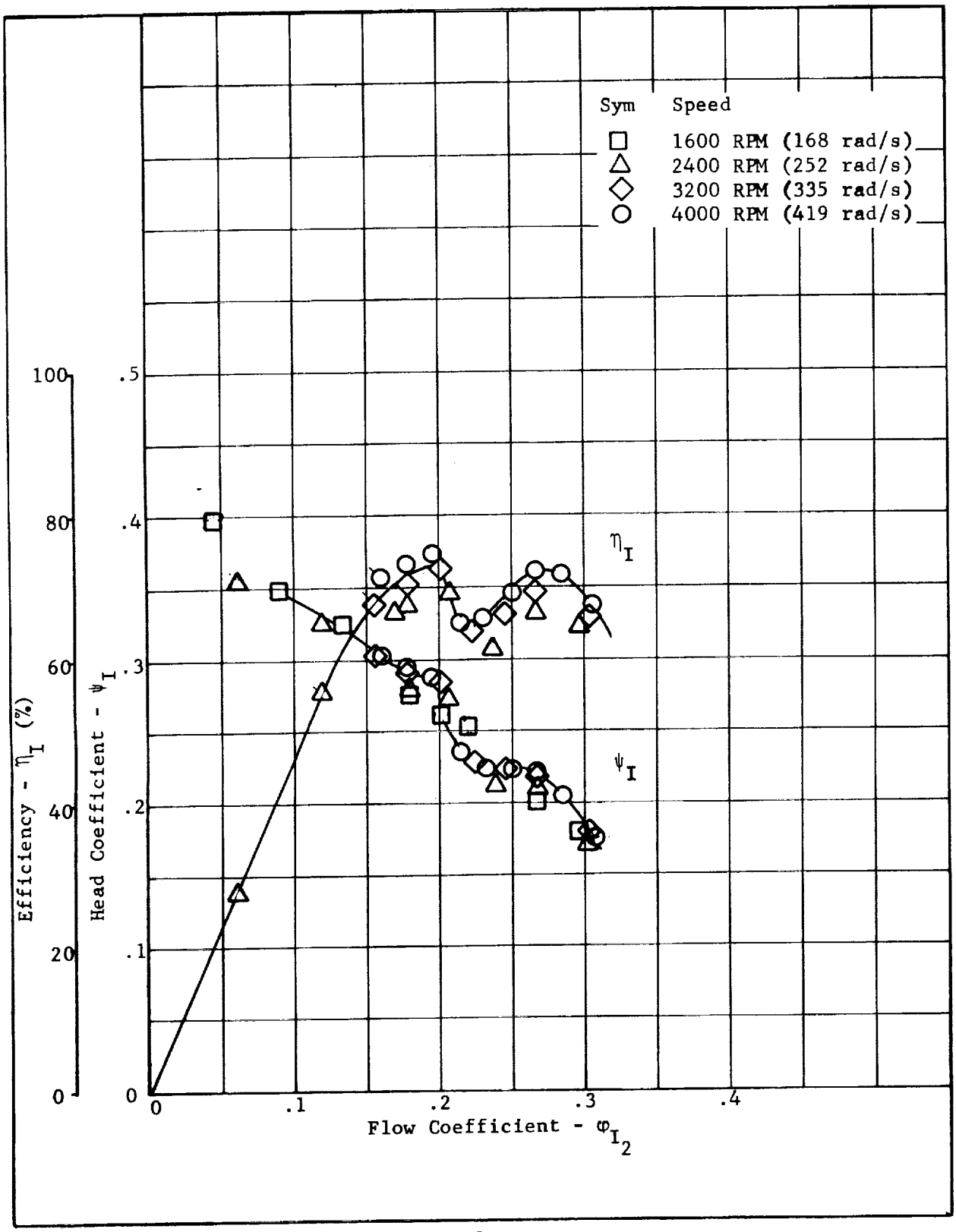

Figure 36. - Hubless Inducer (60°), Head Coefficient and Efficiency vs. Flow Coefficient (Non-Cavitating)

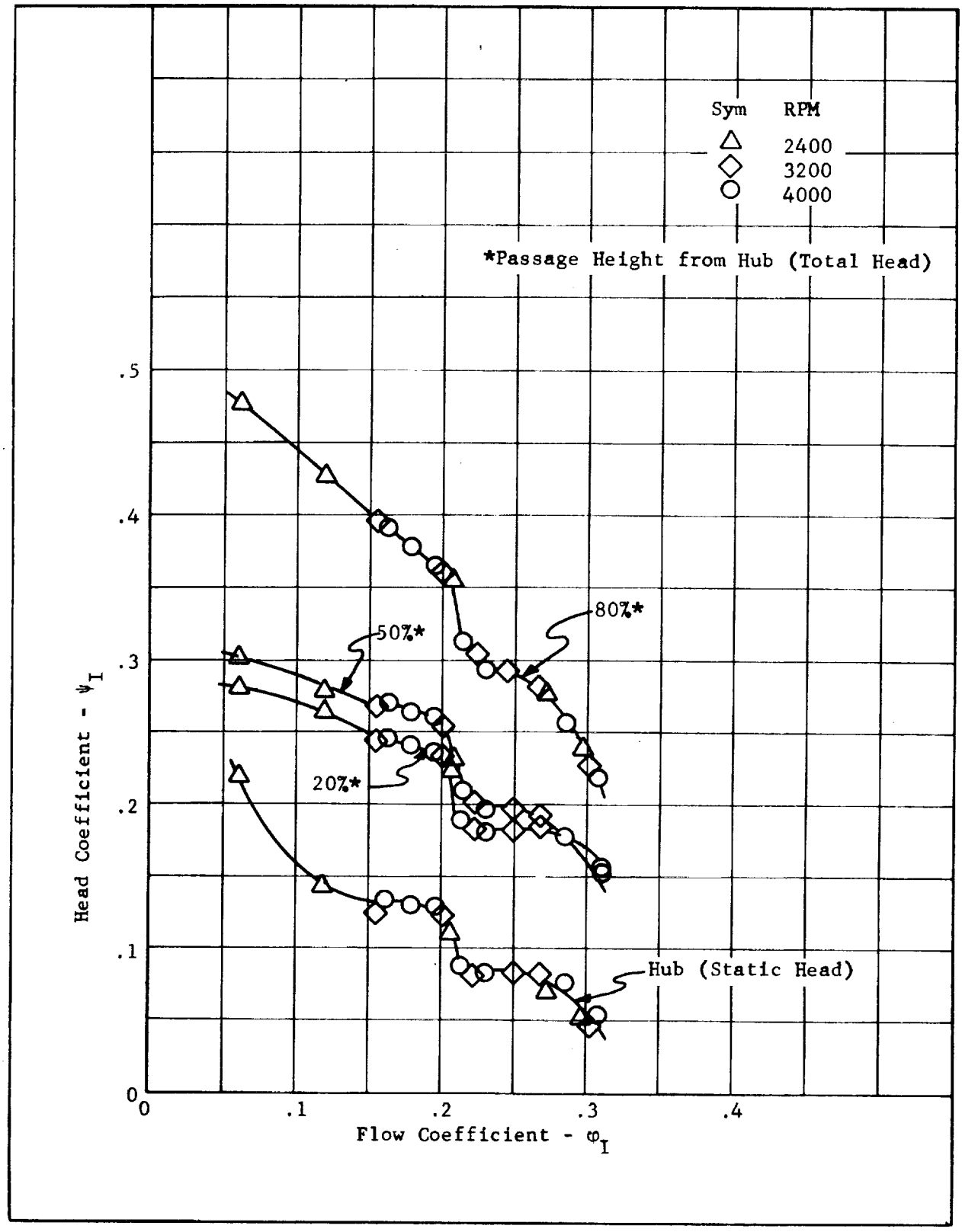

Figure 37. - Hubless Inducer (60°), Head Coefficients vs. Flow Coefficient at Four Radial Measuring Stations (Non-Cavitating)

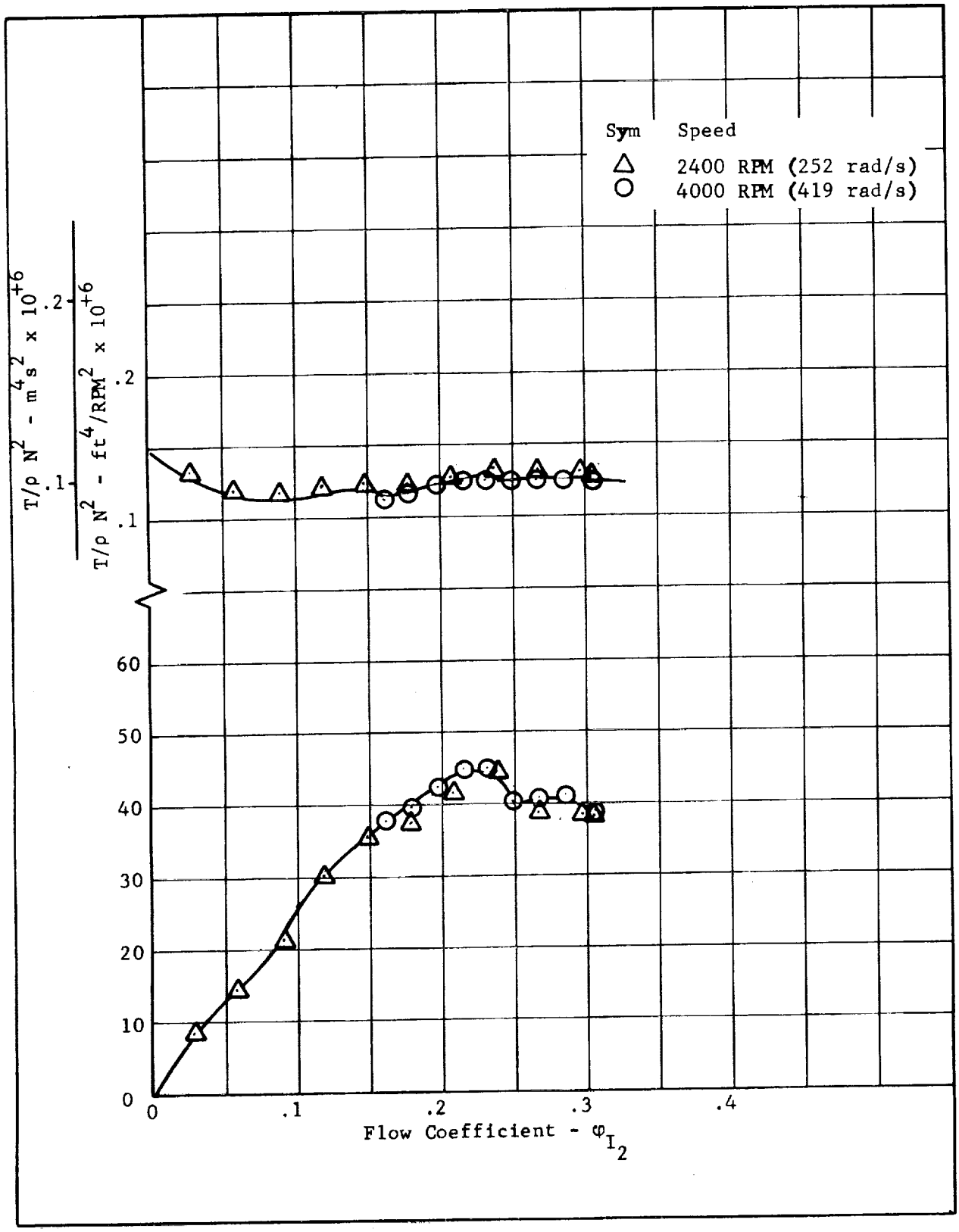

Figure 38. - Hubless Inducer (45°), Combined Inducer and Shroud Normalized Torque and Efficiency vs. Flow Coefficient (Non-Cavitating)

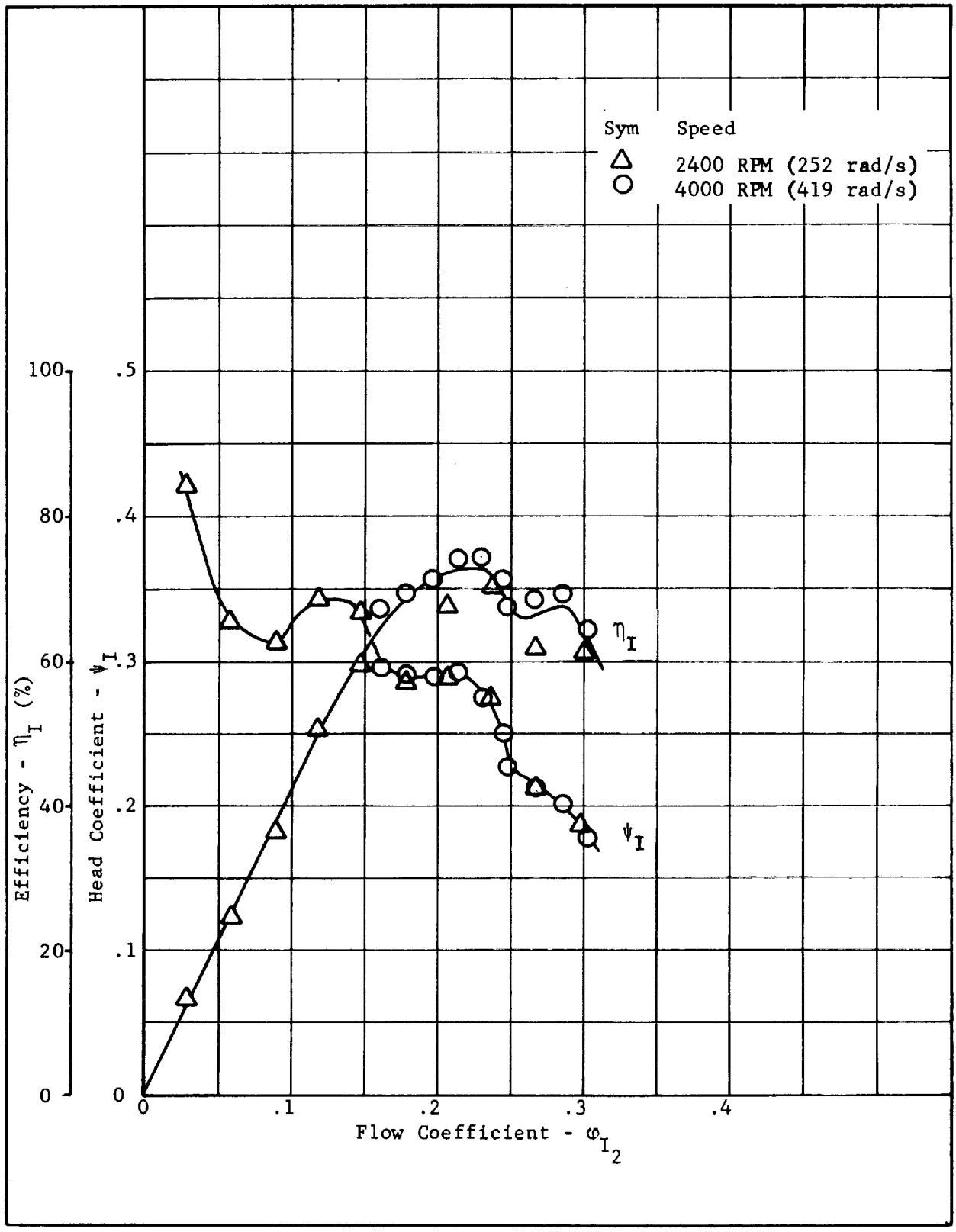

Figure 39. - Hubless Inducer (45°), Head Coefficient and Efficiency vs. Flow Coefficient (Non-Cavitating)

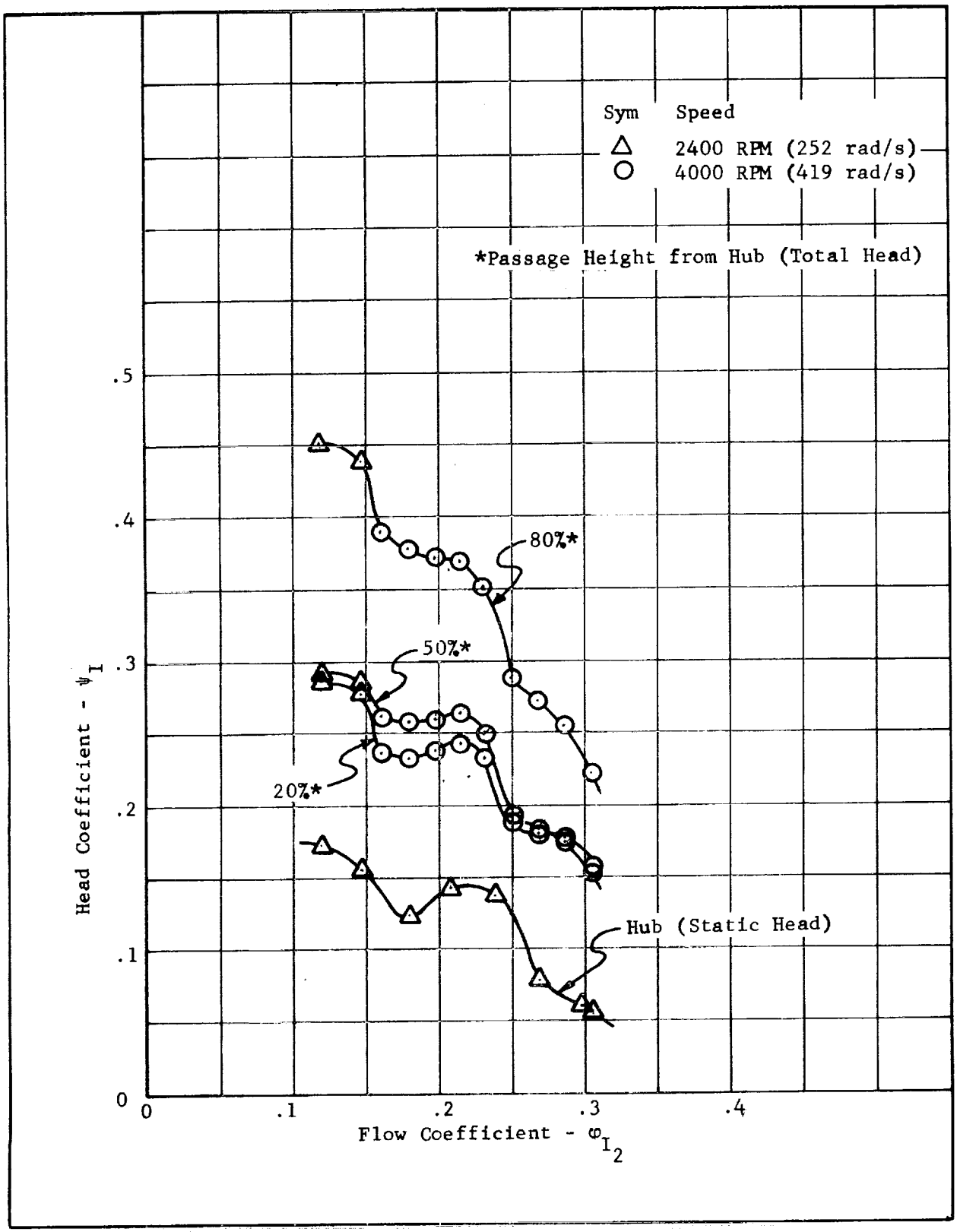

Figure 40. - Hubless Inducer (45°), Head Coefficients vs. Flow Coefficient at Four Radial Measuring Stations (Non-Cavitating)

5. Rotor

The rotor efficiency and head coefficient vs. flow coefficient for several speeds over a flow range of 0 to 120% of design is shown in Figure 41. There does not appear to be a speed effect, although the data scatter is greater than normal. Part of the data scatter could be attributed to the calculated rotor inlet pressure, which was obtained from curve fits of the data taken from Figures 33, 37, and 40. The rotor efficiency was approximately four points lower than design, although the maximum did occur near the design flow coefficient. The input torque used in the efficiency calculation includes the torque from bearing and seal, which are located between rotor and torque meter; this could account for the four percentage points in efficiency.

The head coefficient at design flow agrees with the design prediction within 1%. It appears that the rotor has two inflections, one at 0.104 and the other at 0.055. The first is rotor stall, which occurs at 85% design flow. The second, at flow coefficient 0.055, is most likely caused by inducer stall. From this point to zero flow coefficient, the peak-to-peak discharge pressure oscillations increased slightly (zero flow testing was conducted only at reduced speed, 60% of design).

The head coefficient at each of the four radial measuring stations is shown in Figure 42. It appears that the station nearest the hub stalls first and that the stall progresses toward the tip as the flow is decreased. The data shown is over a flow range of 65 to 120% of design and was taken when the conventional inducer was in the buildup.

Figure 43 again shows the rotor head coefficient, with the solid line representing the results from Figure 42 and the symbol data taken from tests with the hubless inducer in the buildup. Since each of these inducers had significantly different head - flow coefficient relationships, the agreement indicated by this plot verifies the validity of the method of determining rotor performance.

The actual measured radial head coefficients at the design flow are shown in Figure 44, where the line represents the predicted method and, again, shows reasonable agreement.

6. Hydraulic Turbine

Turbine parameters are normally shown vs. blade velocity/gas velocity, but, for this report, the independent abscissa is flow coefficient: fluid axial velocity/blade velocity. The method was used so that the reader may relate from a pump figure to a turbine figure without changing the flow reference.

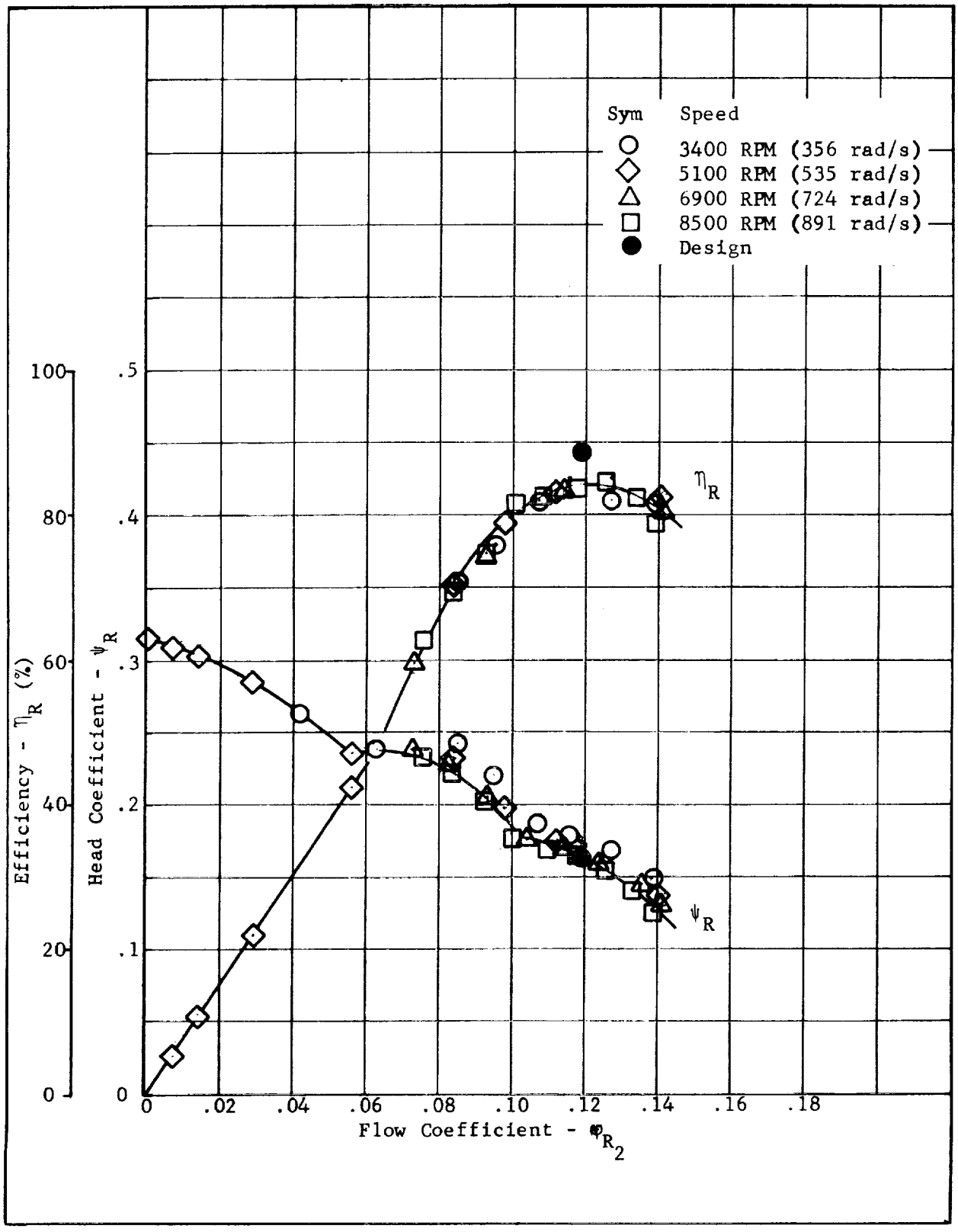

Figure 41. - Rotor, Head Coefficient and Efficiency vs. Flow Coefficient (Non-Cavitating)

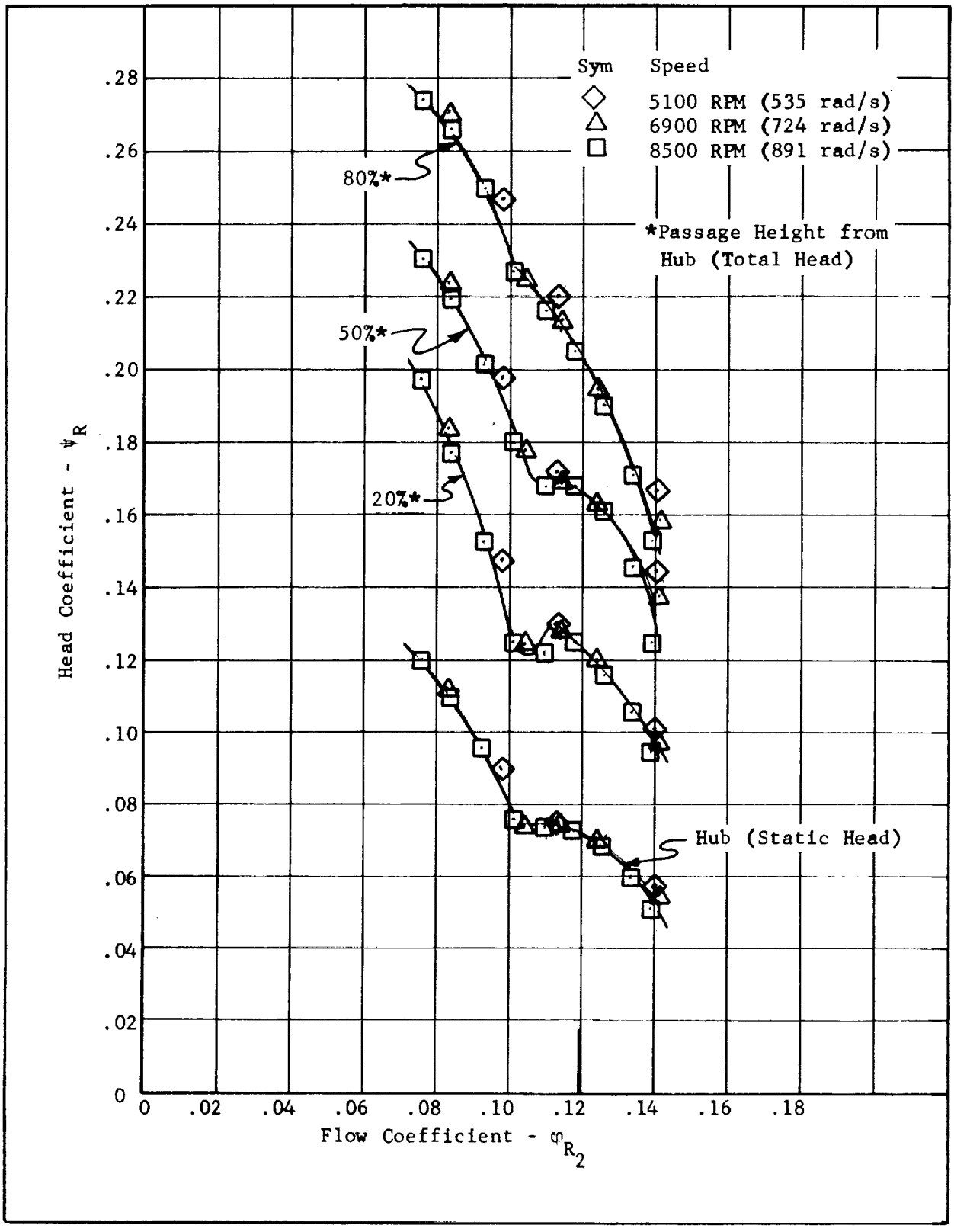

Figure 42.- Rotor, Head Coefficients vs. Flow Coefficient at Four Radial Measuring Stations (Non-Cavitating)

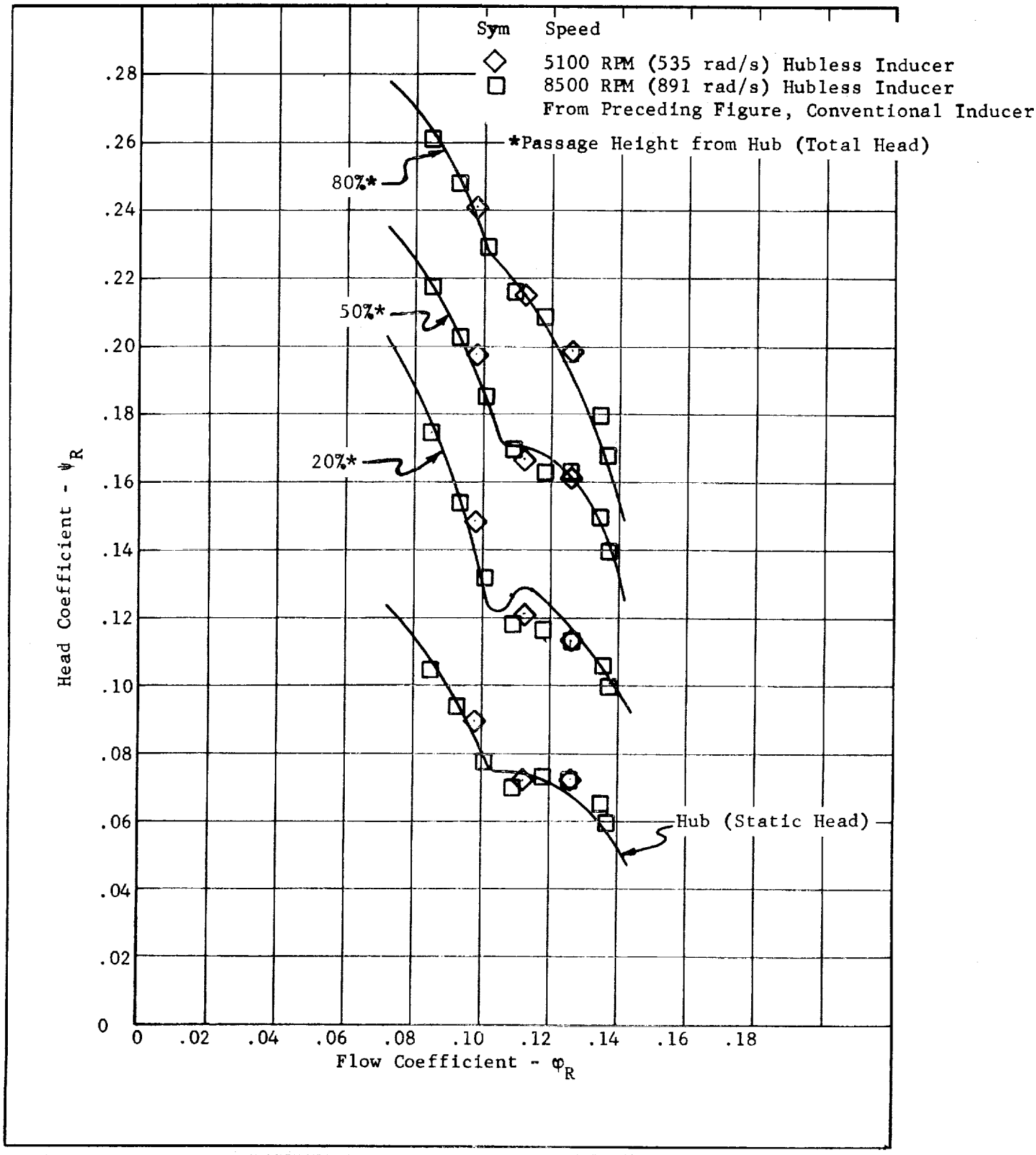

Figure 43.- Rotor, Radial Head Distribution Comparison with Hubless and Conventional Inducers (Non-Cavitating)

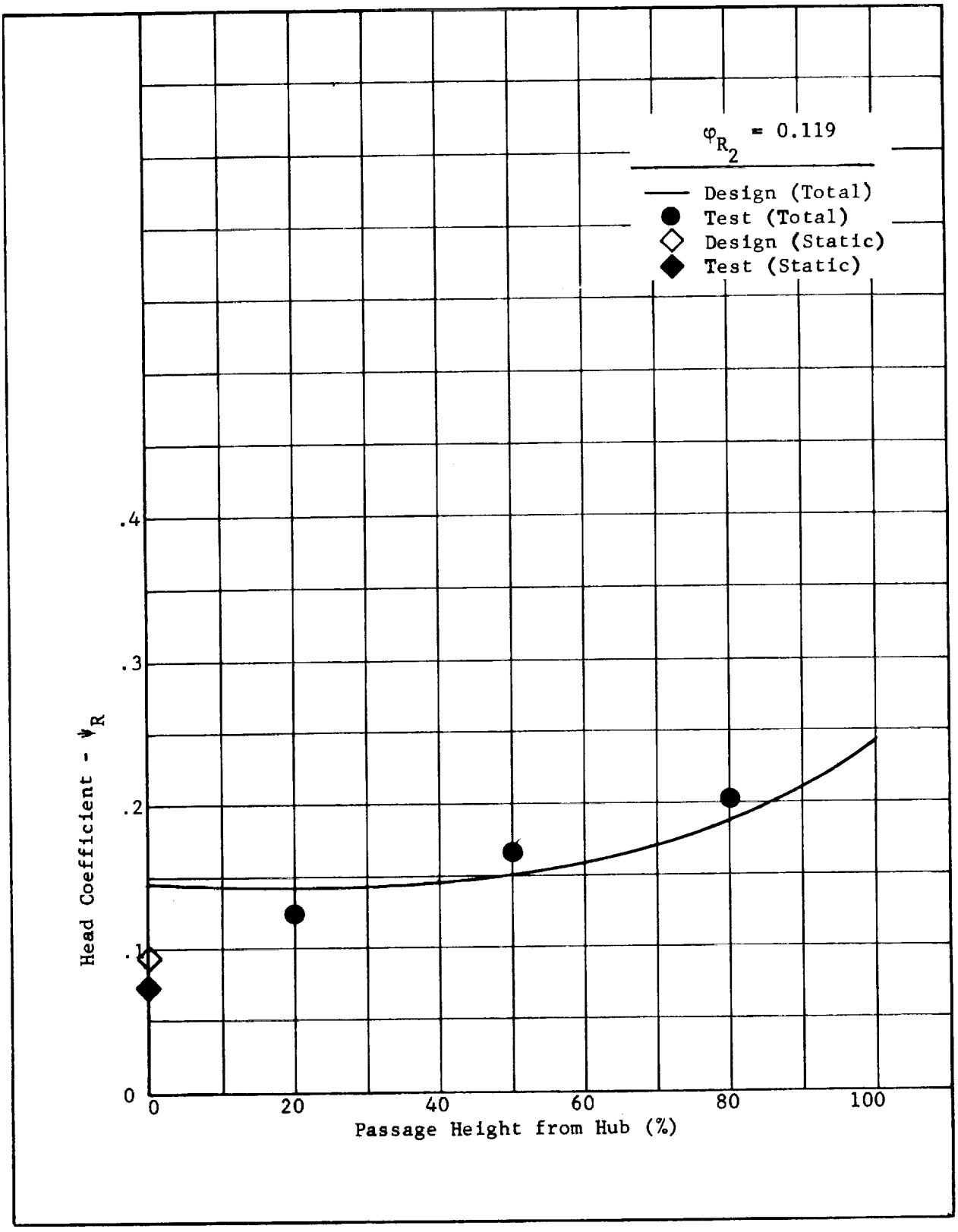

Figure 44. - Rotor, Radial Head Coefficient Distribution at Design Flow Coefficient (Non-Cavitating)

The performance of the hydraulic turbine is shown in Figures 45 and 46. The first figure shows the overall head drop coefficient and efficiency vs. flow coefficient. The torque was calculated from the inducer and shroud torque shown on Figures 31, 35, and 38. The head drop coefficients on Figure 46 show large variations between hub and tip. Almost all of this variation is caused by the turbine inlet head distribution since the turbine head distribution was nearly constant from hub to tip. The design head drop was less than that actually measured by 14%, most likely due to the non-uniform inlet condition, which caused higher turbine inlet losses. The efficiency shown appears to be invalid below a flow coefficient of 0.25. This is most likely caused by the Keil probe measurements at off-design flow, as discussed previously.

7. Overall Performance

The overall performance is defined as the head rise from inducer suction to hydraulic turbine discharge, since this represents the available head to the doenstream main stage (see Figure 2 for component location). Figure 47 shows the speed ratio and discharge head coefficients (from suction) for each blade row, inducer, rotor, and hydraulic turbine, based on the rotor tip velocity. The design values are also shown for comparison with the test data. The speed ratio is constant within 6% of the design value over the entire flow range tested. The efficiency and normalized input torque for the overall machine is shown in Figure 48. The overall efficiency of 40% at the design compares to 30% predicted overall efficiency of a part flow hydraulic turbine driven inducer which was designed for nearly the same operating conditions. The input torque represents the torque necessary to drive the boost pump, and would be added to the main pump torque in determining the total pump drive requirements.

B. STEADY-STATE CAVITATING

The steady-state cavitating tests were conducted at constant flow coefficient, with the suction pressure decreased from the non-cavitating condition, until at least 10% head loss was measured. The drive mode was an electric motor capable of maintaining constant speed to within $\pm$ 0.1%.

All cavitation testing was conducted with water temperature at 160°F (345°K) except for one test on the hubless inducer. The difference in available thermodynamic head between ambient temperature water and water at 160°F (345°K) is insignificant, per Ref 21; therefore, no attempt was made to normalize the data to standard water temperature.

The head coefficient for the inducer cavitation performance was obtained from the Kiel probes rather than from static taps in the discharge line. During cavitation the Kiel probes gave erratic readings and were therefore not used. Consequently, the head coefficients obtained from the cavitation curves will not agree with the head coefficients previously shown. The relative head coefficient value, however, is adequate to determine the percentage head loss.

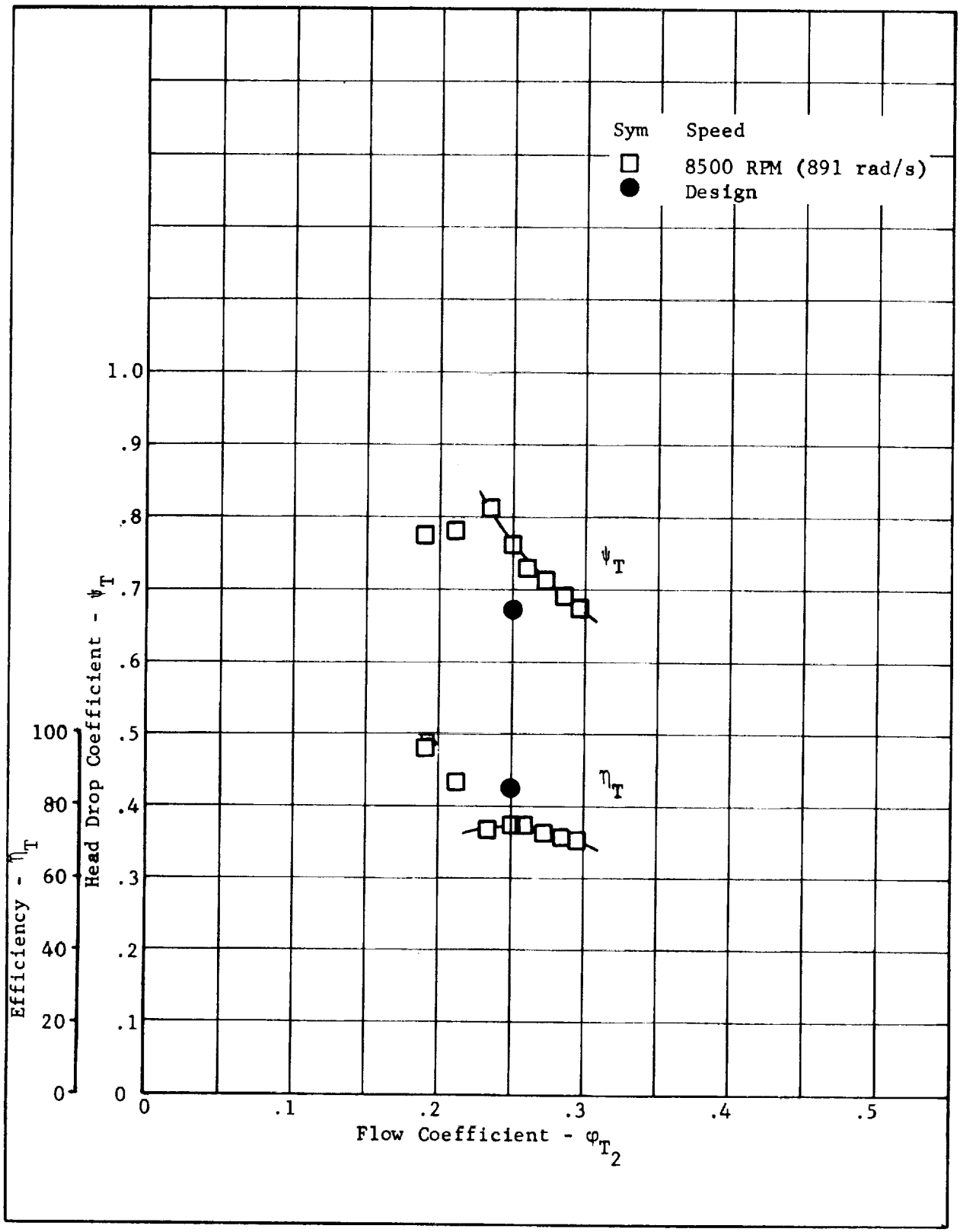

Figure 45. - Turbine, Head Coefficient and Efficiency vs. Flow Coefficient (Non-Cavitating)

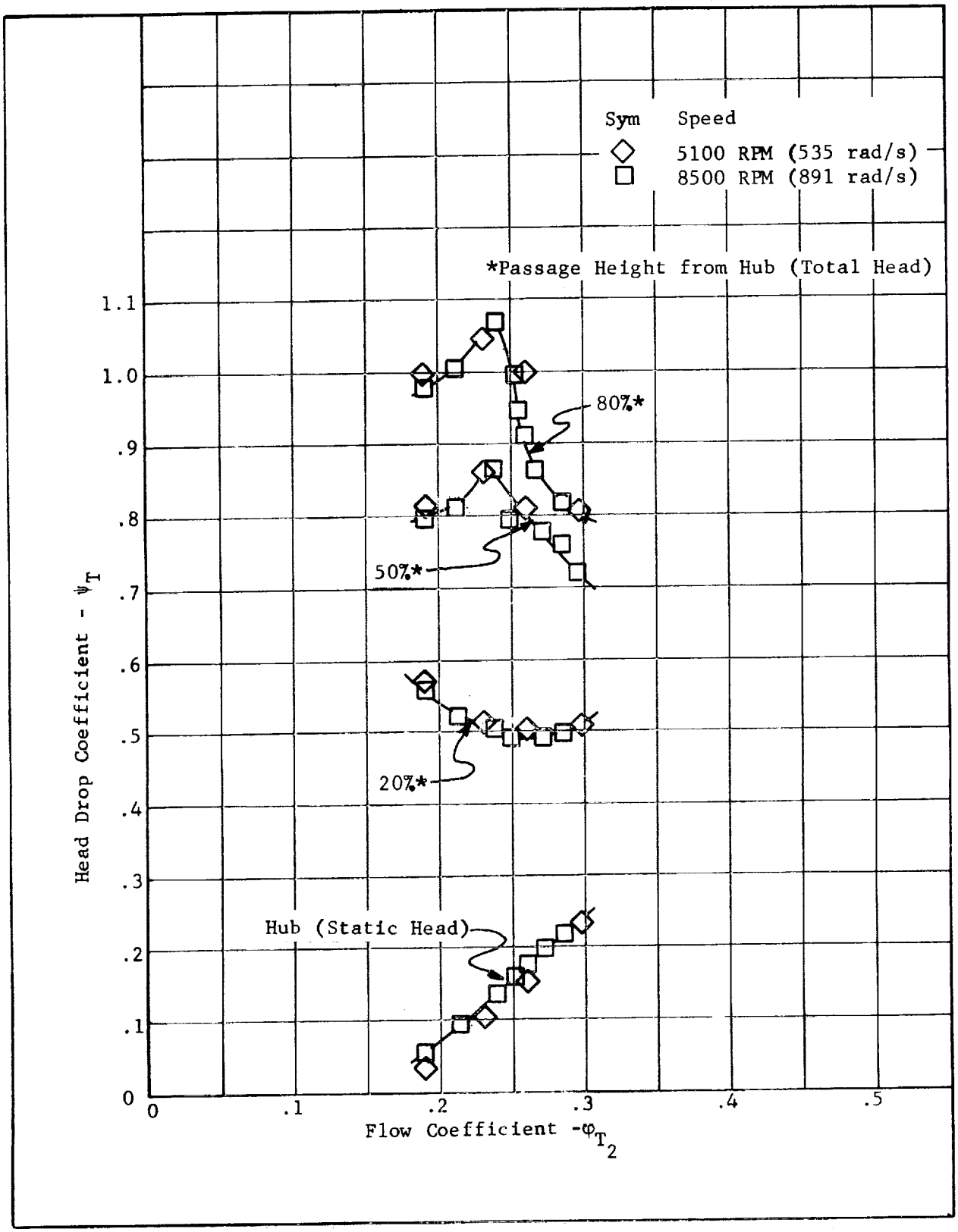

Figure 46. - Turbine, Head Coefficients vs. Flow Coefficient at Four Radial Measuring Stations (Non-Cavitating)

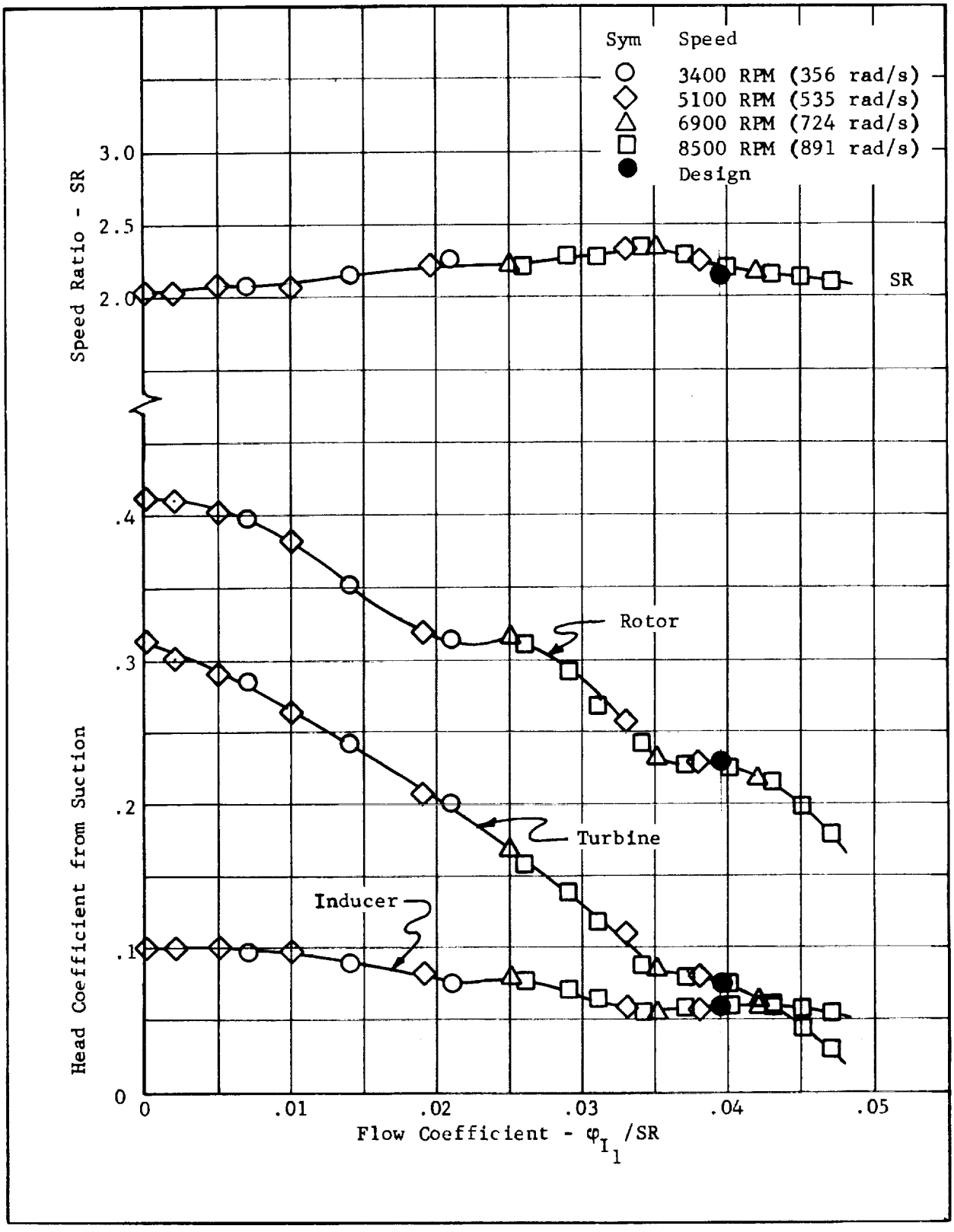

Figure 47. - Boost Pump (with Conventional Inducer), Head Coefficients and Speed Ratio vs. Flow Coefficient (Non-Cavitating)

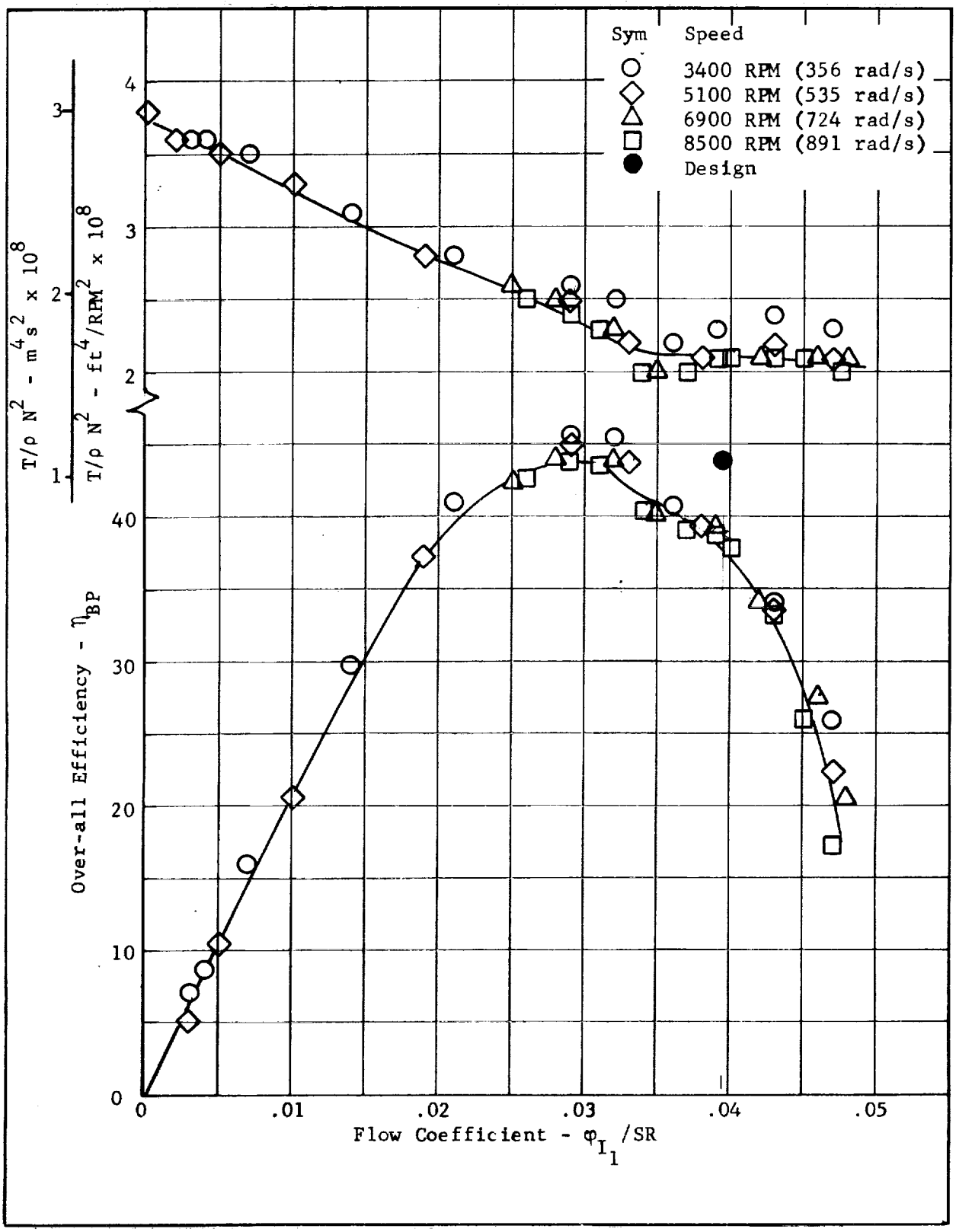

Figure 48. - Boost Pump (with Conventional Inducer), Normalized Torque and Efficiency vs. Flow Coefficient (Non-Cavitating)

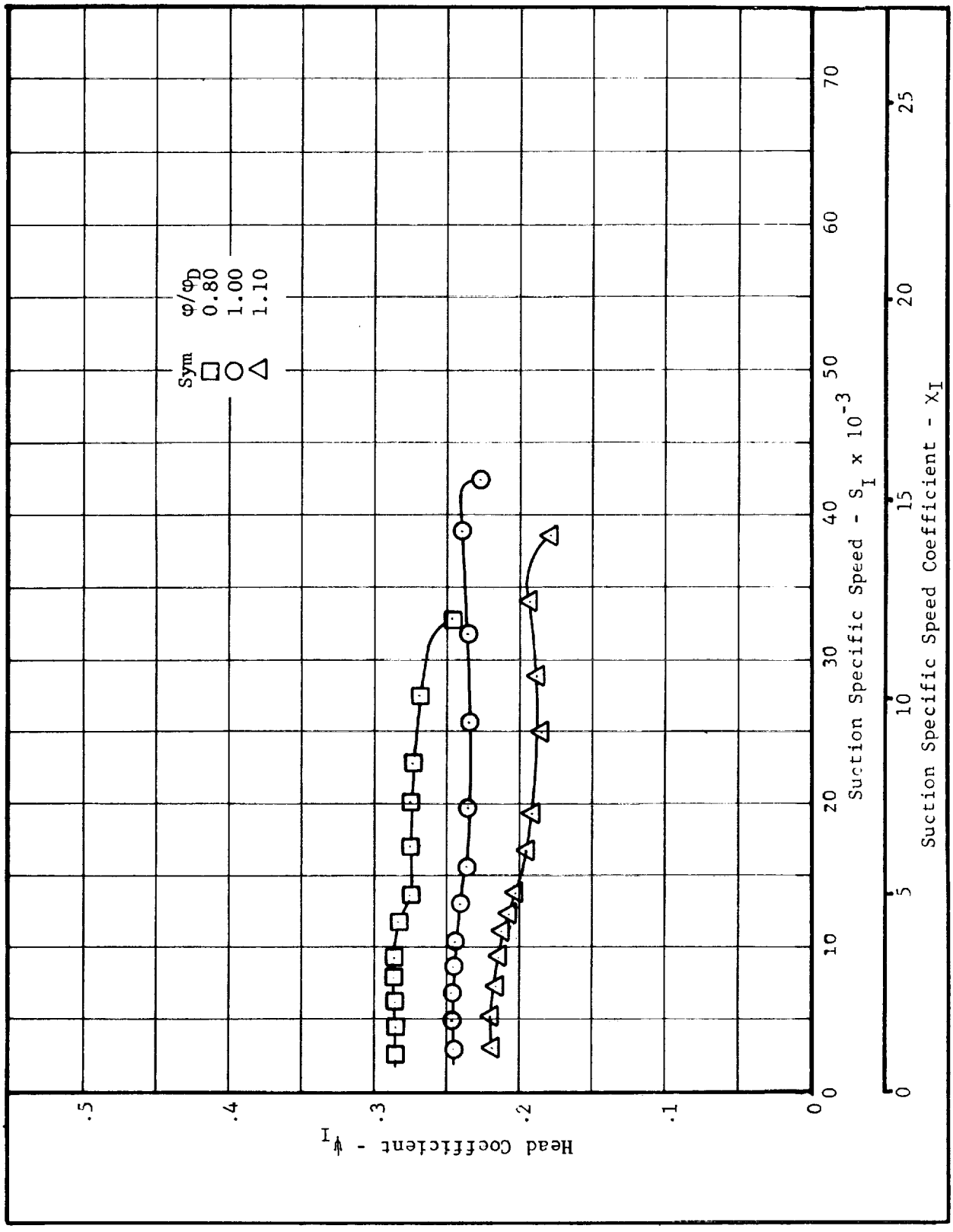

Conventional Inducer, Head Coefficients vs. Suction Specific Speed (Cavitating)

Figure 49

1. Conventional Inducer

Figure 49 shows the cavitation performance of the conventional inducer at three different flow coefficients. The highest suction specific speed values shown are very near complete breakdown since further decreases in suction head were not possible at constant flow coefficient. At the design flow coefficient, head breakdown occurs at 43,000 (15.7) which is equivalent to $\tau/\phi^2 = 2.67$, the minimum value per Ref 12. Both the 80% and 110% flow show less margin than the design.

2. Hubless Inducer (60°)

Figure 50 shows the 60° long spinner hubless inducer cavitation performance at two flow coefficients. At the 80% flow coefficient, the water temperature exceeded 190°F. At this flow, 10% head loss could not be obtained because of the facility flow limit. It appears, however, that the value would exceed 50,000 (18.2).

The data for the 60° short spinner hubless inducer is shown on Figure 51 at three flow coefficients. At 80% flow the inducer pumped without excessive loss up to a suction specific speed of 59,000 (21.5). This is reasonably close to the predicted value (by Ref 12) for an inducer with this inlet blade tip angle. The incidence to blade angle ratio for optimum performance is near the 80% flow since the hubless inducer does not have hub blockage (16%).

3. Hubless Inducer (45°)

Figure 52 and 53 show the 45° hubless inducers, with the long spinner and short spinner, respectively, at three different flow coefficients. These flow coefficients were chosen (see Figure 39), so as to not fall on a discontinuing portion of the head flow curve. The maximum suction specific speed was approximately the same for both spinners. Again the maximum suction specific speed value shown represents the near breakdown point since any decrease in suction pressure caused the head to drop below that required to pump the test flow loop.

4. Inducer Comparison

a. Comparison of Previous Data

Figure 54 shows the cavitation performance of all the inducers at the design flow coefficient. The difference in head coefficient at low suction specific speed (non-cavitating) is indicative of the head - flow relationship discussed in previous sections. The conventional inducer shows the typical drop in head, usually less than 5%, at about 15,000 (5.5) suction specific speed and then a slight increase until breakdown. The 60° hubless, however, showed an almost continuous increase in head until breakdown occurred. The 45° hubless had a continual decrease in head as the suction specific speed was increased. Both the conventional inducer and the 60° short spinner hubless inducer obtained approximately the maximum suction specific speed possible for

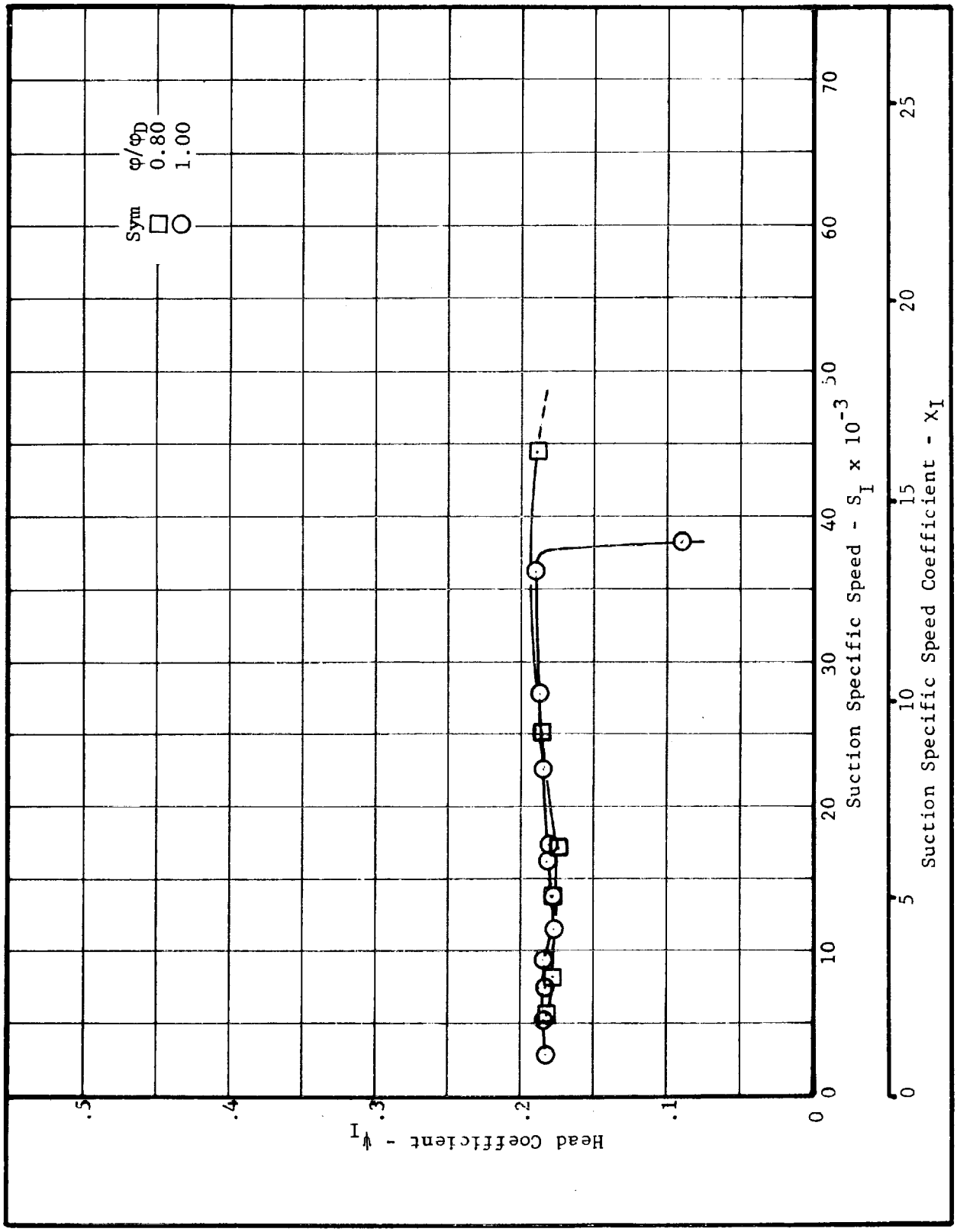

Hubless Inducer (60°) with Long Spinner, Head Coefficients vs. Suction Specific Speed (Cavitating)

Figure 50

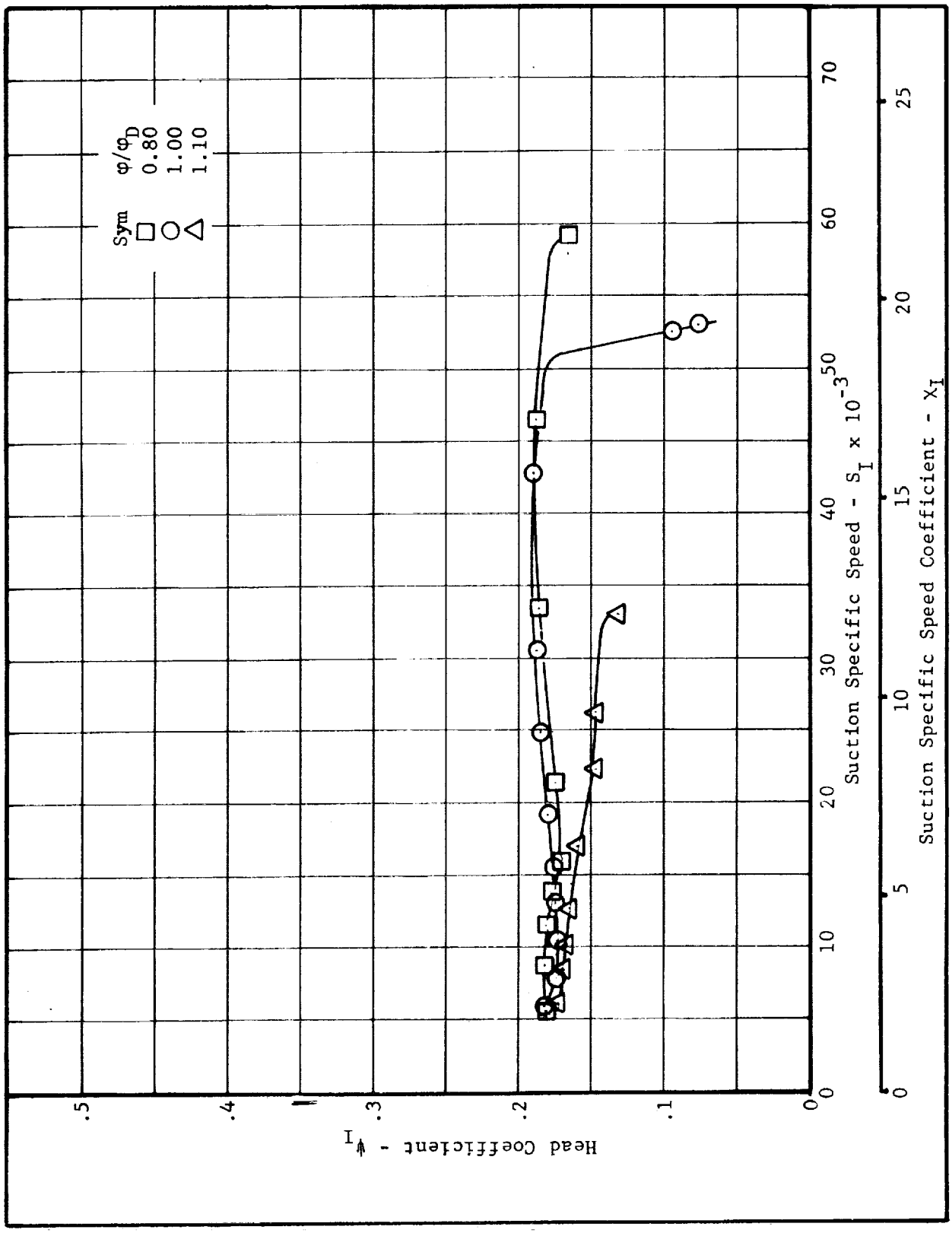

Hubless Inducer (60°) with Short Spinner, Head Coefficients vs. Suction Specific Speed (Cavitating)

Figure 51

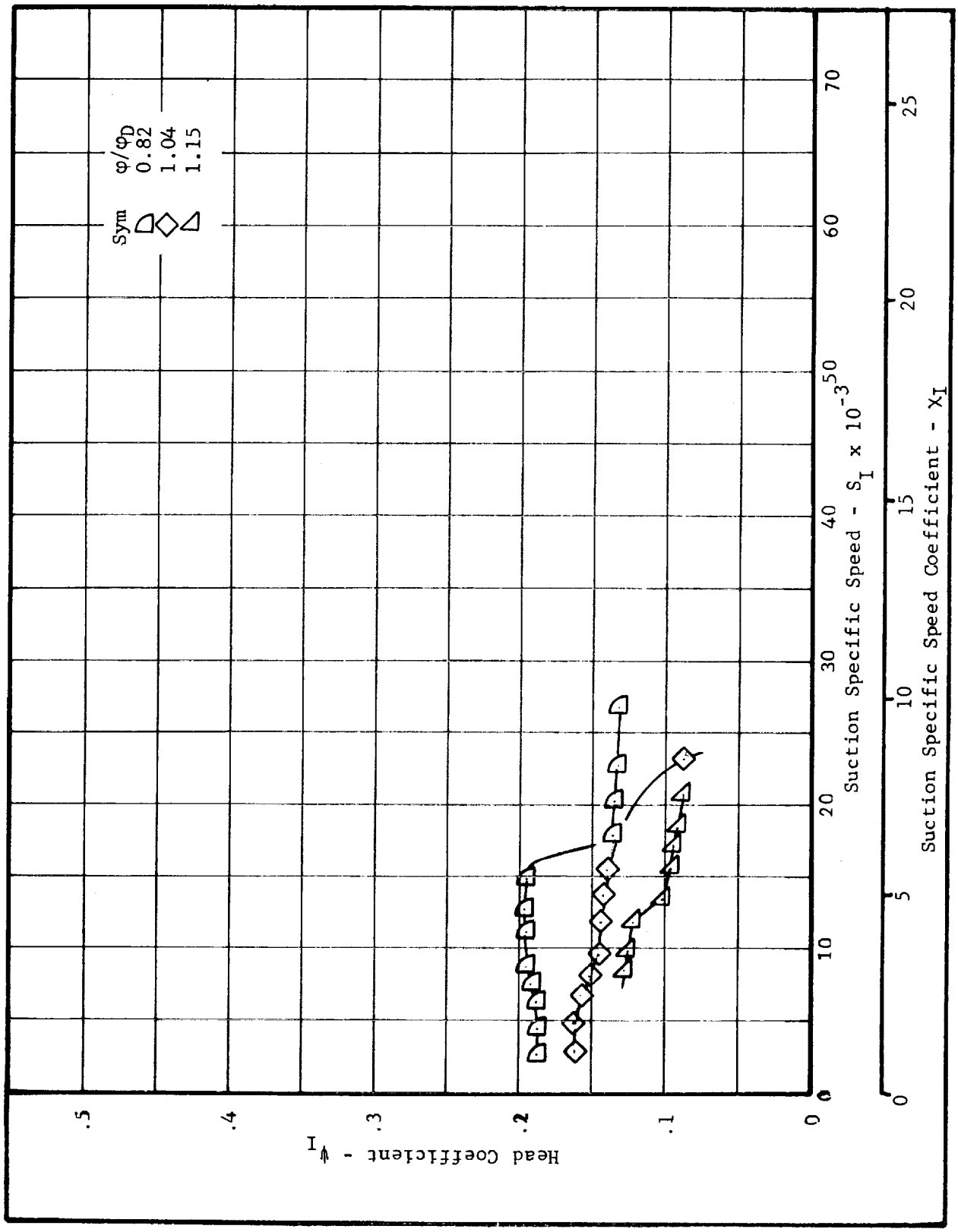

Hubless Inducer (45°) with Long Spinner, Head Coefficients vs. Suction Specific Speed (Cavitating)

Figure 52

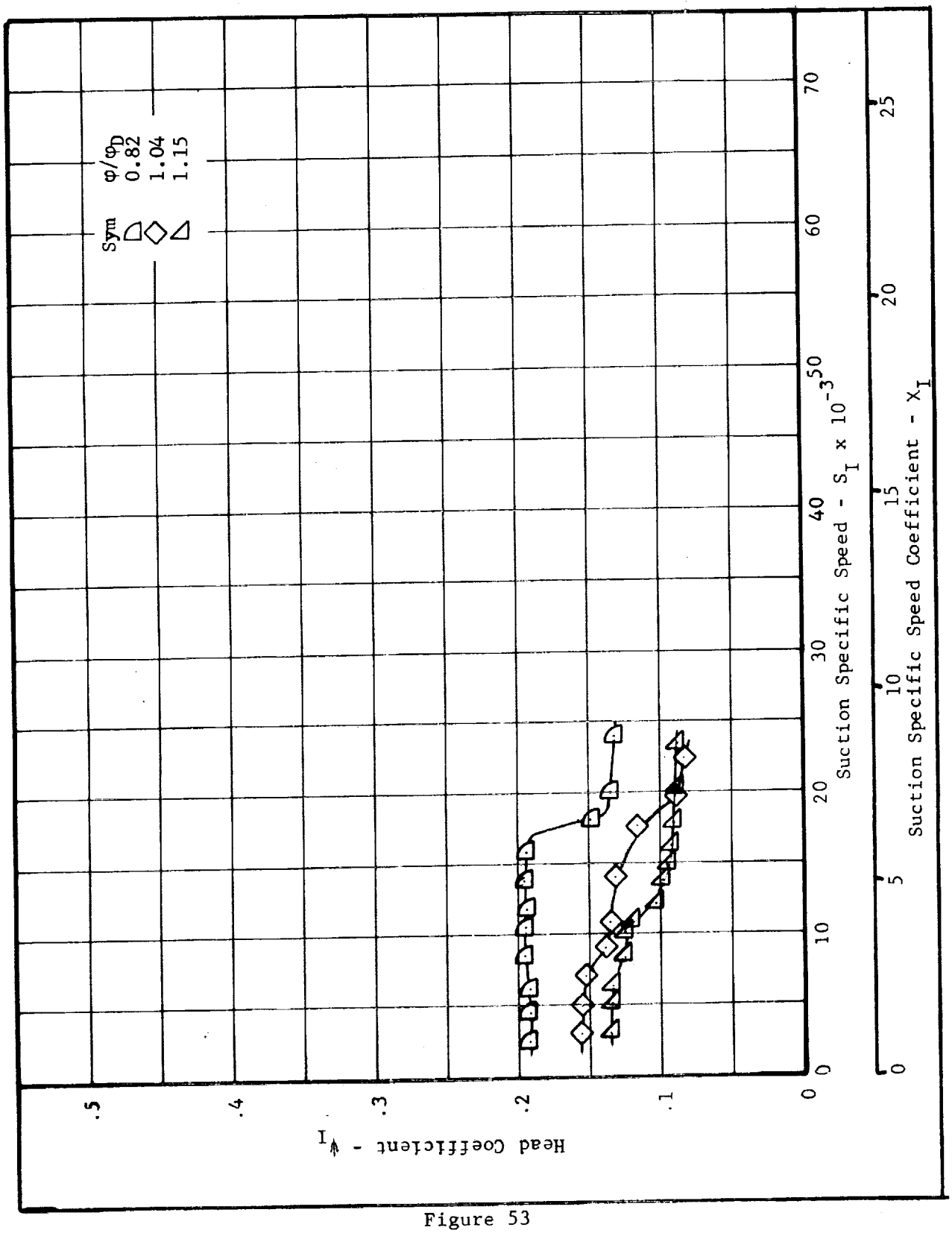

Hubless Inducer (45°) with Short Spinner, Head Coefficients vs. Suction Specific Speed (Cavitating)

Figure 53

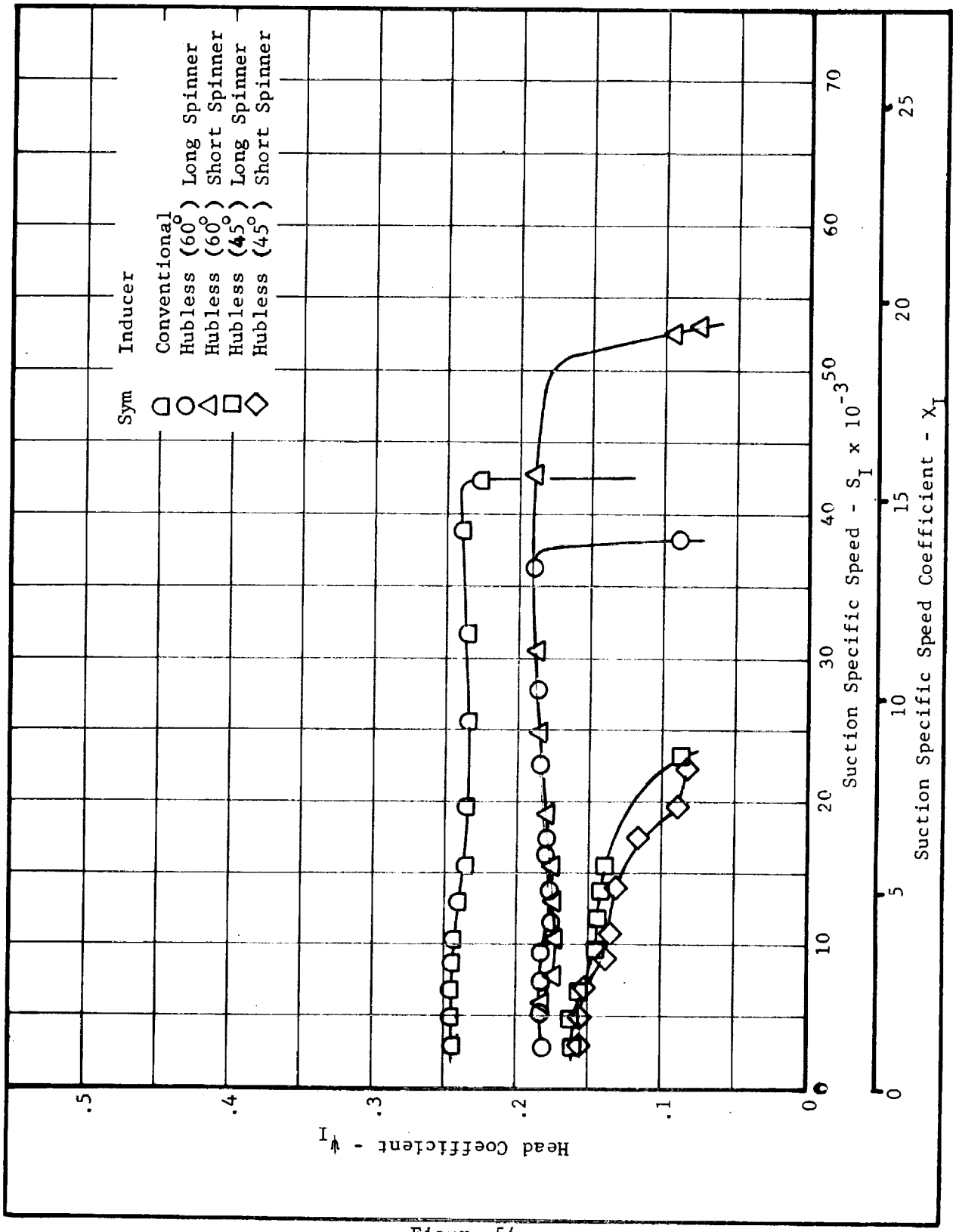

Figure 54

Inducer Comparison, Head Coefficients vs. Suction Specific Speed (Cavitating)

their respective inlet blade tip angles (per Ref 12). It appears that decreasing the inlet angle from 60° to 45°, which makes the inducer more 'hubless', has adverse effect on the cavitation performance. This is most likely caused by absence of head which can be generated at the inducer inlet eye.

The large variation in breakdown suction specific speed between the long and short spinner for the 60° hubless inducer is not apparent but could possibly be the result of providing a cavity where vapor can collapse before passing into the inducer.

b. Comparison of High Frequency Data

Figures 55 and 56 show a comparison of the high frequency pressure oscillations at the suction and discharge, respectively. All the data shown was in a frequency range of between 5 and 30 Hertz, with the predominent frequency being 20 Hertz. Any data recorded outside this range was either exactly 60 Hertz, which was undoubtedly electrical noise, or had an insignificant peak-to-peak pressure magnitude. The ordinate value on Figure 55 represents the peak-to-peak normalized head coefficient; a value of 0.03 would be approximately 10% of the discharge head coefficient. The ordinate value on Figure 56 is a ratio of the peak-to-peak pressure to the discharge pressure. The abscissa value for both figures is the normalized suction pressure parameter. The conventional inducer shows smooth suction operation at the design flow over the total suction pressure range. At the 80% flow the ψ_{pp} has increased, but returns to approximately the same value as the design when complete cavitation is approached. The 110% flow pressure oscillations, in general, fall between the design and 80% flow but has a resonance at $\tau = 0.1$.

The 60° hubless inducer has suction pressure oscillations slightly higher than the conventional with little difference between the long and short spinner. Peak-to-peak pressure oscillations were largest for the 45° hubless inducer, occurring over the entire suction pressure range. There was no difference in pressure magnitude between short and long spinner. In almost every case the design flow pressure oscillations were less than the 80% and 110% flow conditions.

The discharge peak-to-peak pressure oscillations (Figure 56) were less than 10% of the discharge pressure for all inducers down to a τ value of 0.2. From $\tau = 0.2$ to $\tau = 0.075$, the conventional inducer and both the short and long spinner versions of the 60° hubless decreased in pressure oscillation to approximately 2%. The 45° hubless inducer, short and long spinner, increase in pressure oscillation over the same range. From $\tau = 0.075$ to minimum, all inducers show an increase in discharge pressure oscillation, with the 45° hubless having the highest value of 25%.

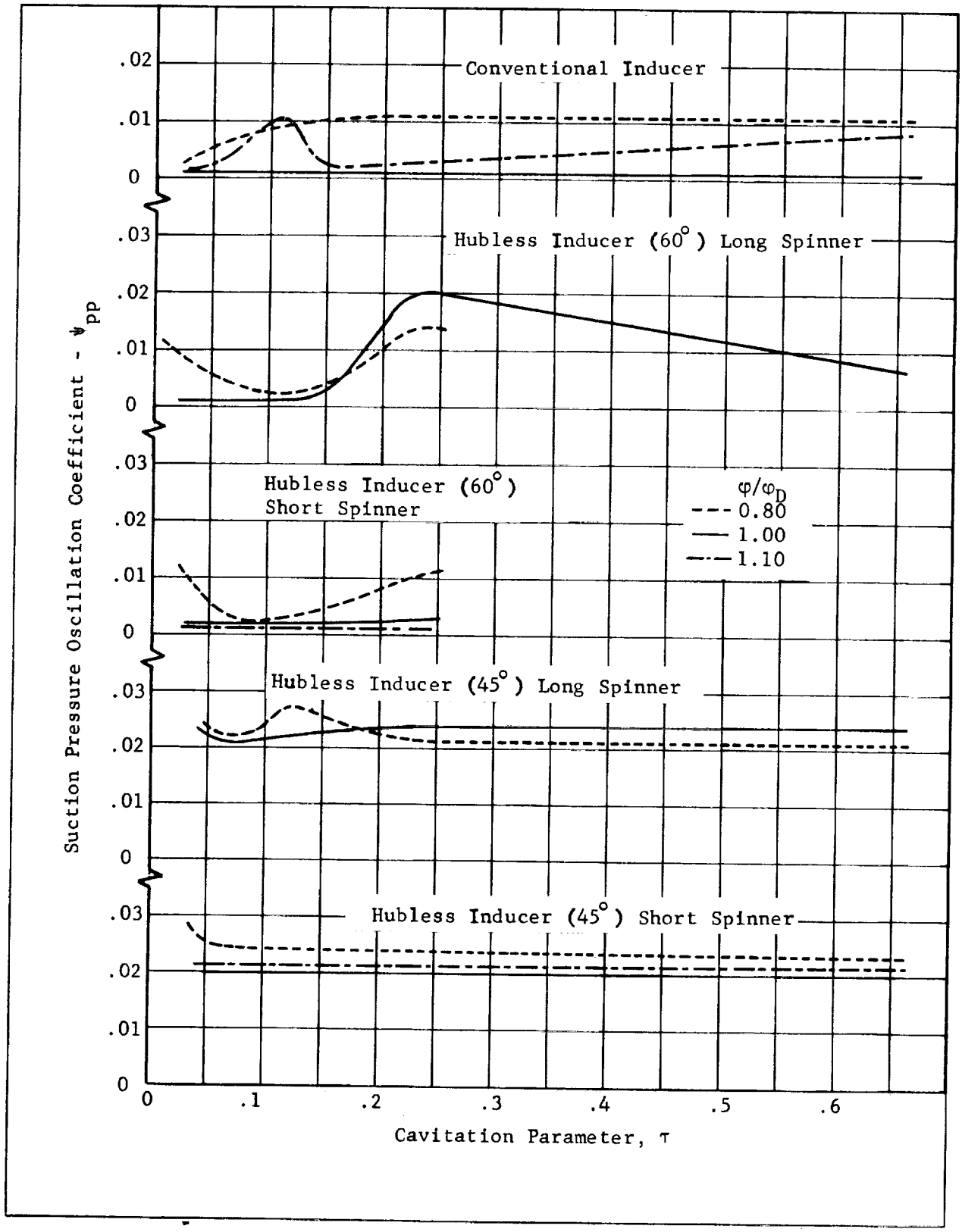

Figure 55. - Inducer Comparison, Suction Pressure Oscillation Coefficient vs. Cavitation Parameter (Cavitating)

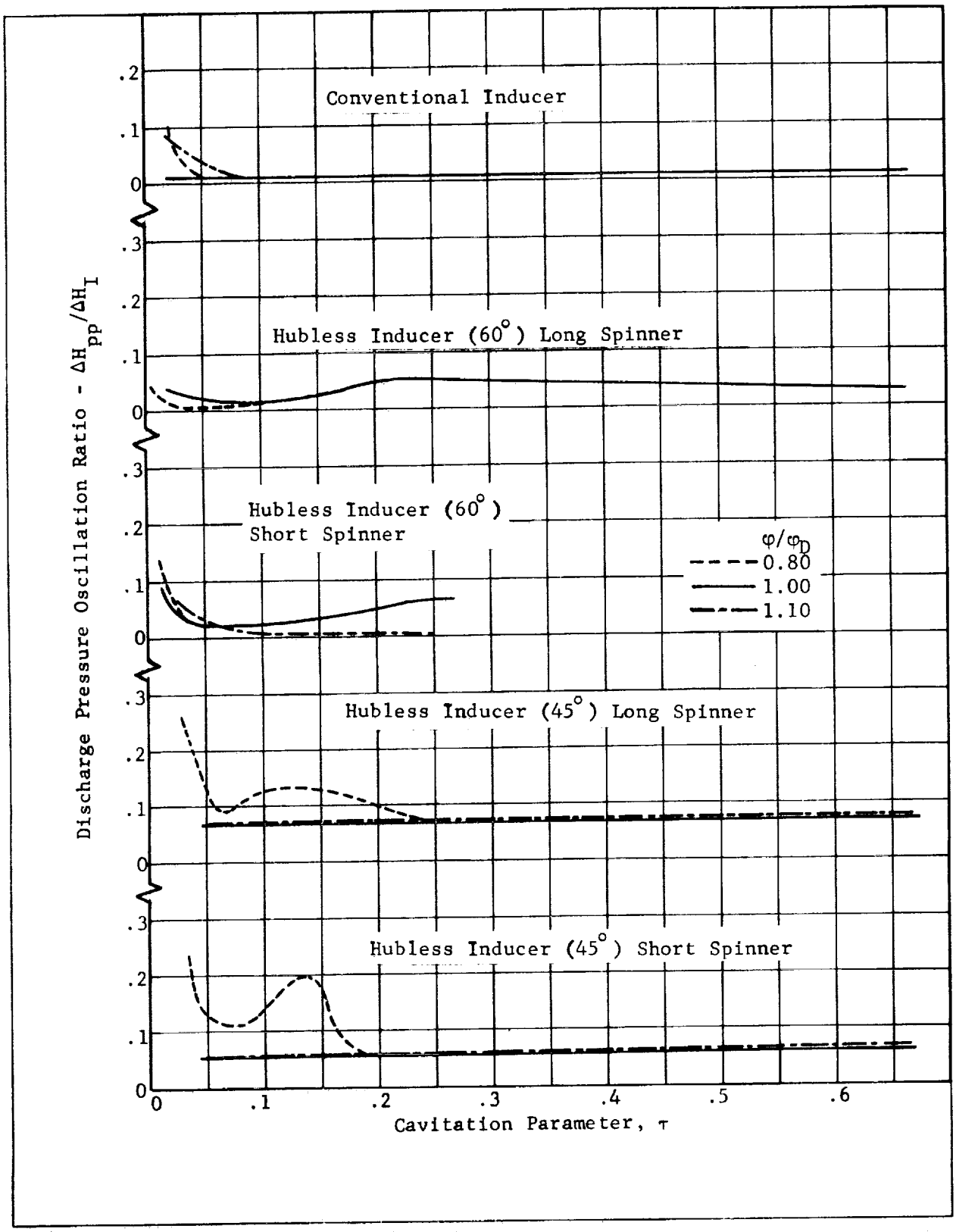

Figure 56.- Inducer Comparison, Discharge Pressure Oscillation Ratio vs. Cavitation Parameter (Cavitating)

5. Rotor

The rotor cavitation performance at three flow coefficients is shown in Figure 57. The NPSH at the rotor was computed by adding the NPSH of the inducer to the total head rise of the inducer and does not account for fluid temperature increase in the inducer or fluid prewhirl at the rotor inlet. The maximum suction specific speed at 2% head loss was 6600 (2.4) at the design flow coefficient. This compares with the design point value of 7420 (2.7) at 2% head loss. The off-design cavitation performance was 6000 (2.2) for the 78% flow and 5200 (1.9) for the 108% flow at 2% head loss. In all cases the head loss increased uniformly as the suction specific speed was increased over the test range. Data was taken until approximately 10% head loss occurred, which was equivalent to 30% loss in the overall boost pump head rise.

6. Overall Performance

The overall boost pump cavitation performance is shown in Figure 58 at three different flows. Essentially all the head loss shown is due to the rotor cavitation. The inducer is operating at a maximum of 20,000 (7.3) which, as can be seen on Figure 49, represents negligible head loss. If the rotor would have had less than 2% head loss at 7420 (2.7) suction specific speed then the boost pump would have operated with negligible loss to 92,000 (33.6). This represents a 12% increase in the suction specific speed performance of the rotor. The value of the 92,000 (33.6) is equal to 43,000 (15.7) inducer suction specific speed times the shaft speed ratio and is the maximum obtainable boost pump suction performance.

C. TRANSIENT PERFORMANCE

The transient tests were conducted in both cavitating and non-cavitating conditions, using a GN_2 powered turbine to drive the boost pump. The flow loop flow control valve was preset to the desired steady-state flow coefficient and the manually operated GN_2 power valve was opened to the desired rate. This method produced start transients with a minimum of 1.5 sec elapsed time from zero to design speed; there was no limit to the maximum start time. The shutdowns were not controlled and were accomplished simply by closing the GN_2 power valve through the emergency override system.

1. Conventional Inducer

Figure 59 shows the start transient of the boost pump with the conventional inducer at the design steady-state flow and non-cavitation conditions. This transient acceleration represents the 'fastest' start possible within drive limitations. The suction pressure was set to a level which precluded cavitation within the boost pump. As indicated by Curve 7, the inducer - turbine are essentially locked to the rotor after 1.5 sec of elapsed time. The boost pump does not operate along a specific speed line as it would if the start was infinitely long. This can be seen by Curves 8 and 9, which are directly proportional to their respective flow coefficients. Curve 8 shows that the

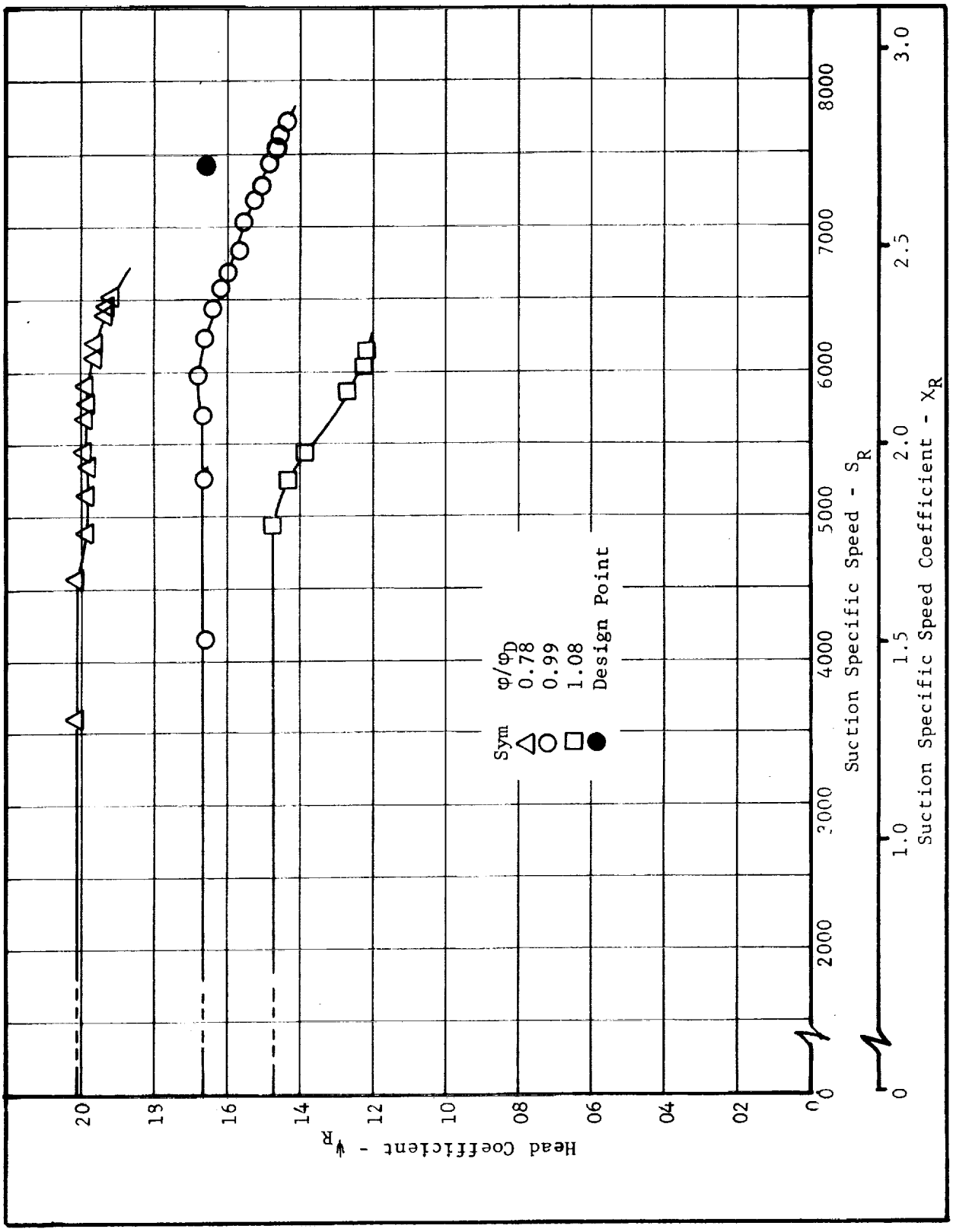

Rotor, Head Coefficients vs. Suction Specific Speed (Cavitating)

Figure 57

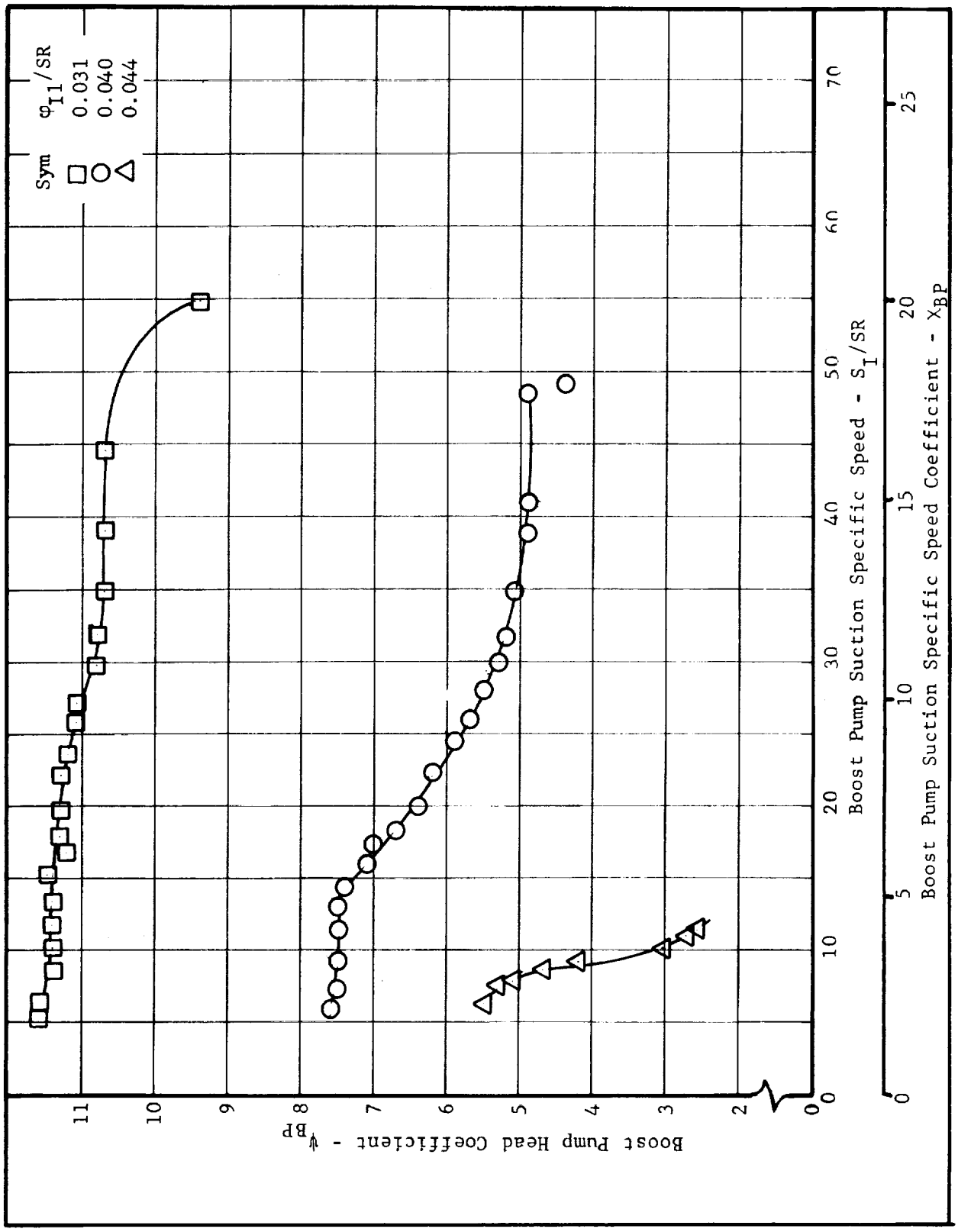

Boost Pump (with Conventional Inducer), Head Coefficients vs. Suction Specific Speed (Cavitating)

Figure 58

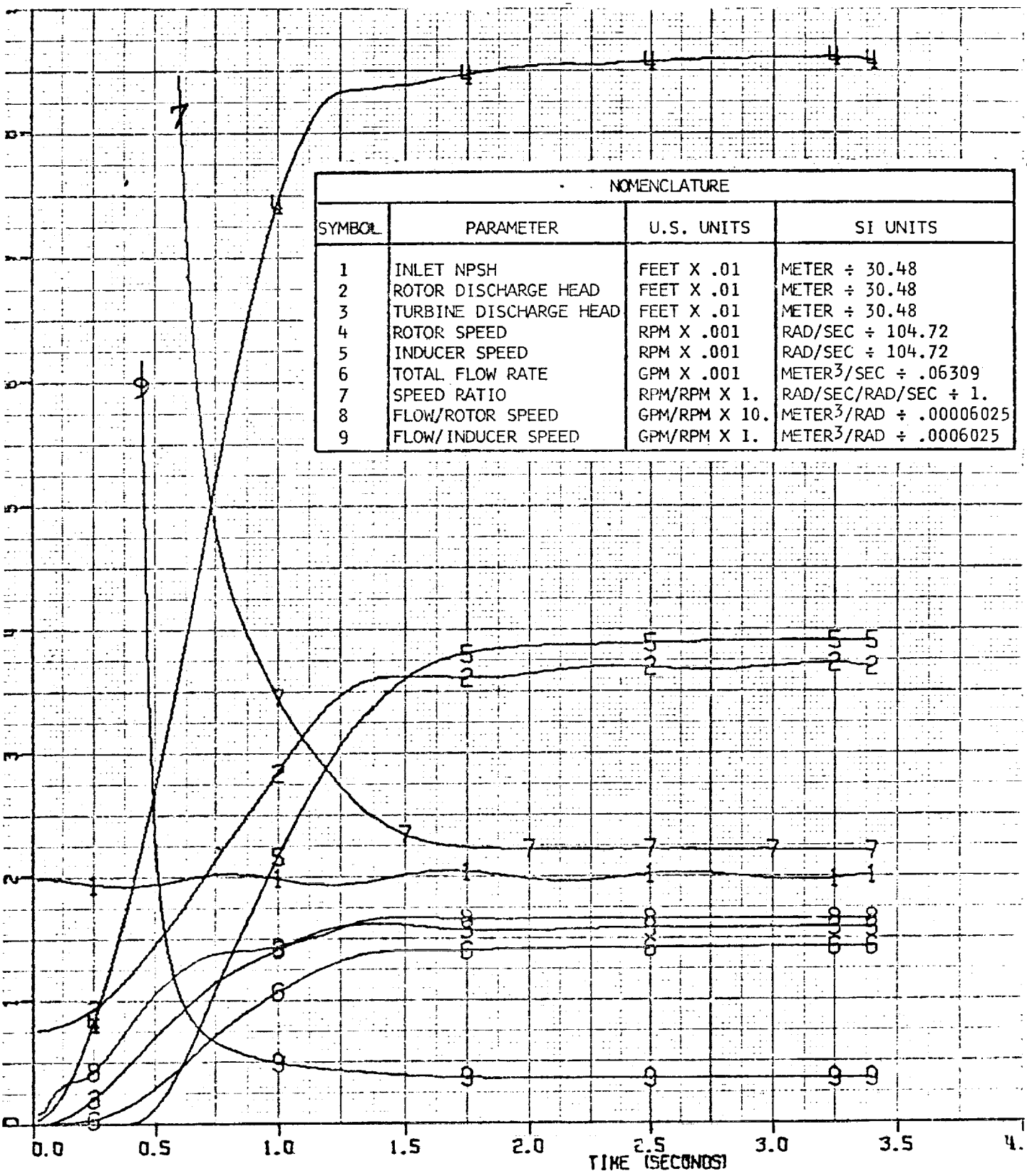

Figure 59. - Conventional Inducer, 1.5 sec Start Transient at 100% φ (Non-Cavitating)

speed leads the flow, which is caused by fluid inertia in the entire flow loop system. The fluid inertia in the flow loop is most likely more than would be found in a rocket engine. Curve 9 shows that the flow is being 'pulled' through the inducer because the speed ratio is greater than the steady-state value.

The discharge heads, Curves 2 and 3, are consistant with the speed and flow at any given point. This indicates that a start transient model can use a quasi steady-state technique as described in Ref 3.

Figures 60 through 62 show the conventional inducer during cavitating start transients at different flows and times. For the 3-sec starts, the rotor has reached 100% speed before the inducer starts to rotate. The flow rate is almost zero until this time. This means that the rotor is completely cavitated out (maximum speed with near zero inlet head) and one could expect that flow would not start. Apparently there is enough fluid shear drag between the rotor and the inducer - hydraulic turbine that rotation is initiated. When the inducer does rotate and generates NPSH for the rotor, rotor begins to generate head which, in turn, initiates flow.

The NPSH shown on Figure 61 is reduced to 4.5 ft (1.7 m) at 5.25 sec. This is equivalent to a boost pump suction specific speed of 85,000 (31.0) which approaches the maximum capability of 92,000 (33.6) as discussed in the previous section. As indicated by Figure 58, this would be at considerable head loss but recovery was possible, as can be seen by Figure 61, Curve 3.

A typical shutdown is shown in Figure 63. This particular shutdown occurred at nearly constant specific speed, as indicated in Curve 8. The inducer speed returns to zero faster than the rotor, causing both the speed ratio and the flow/speed parameter, Curves 7 and 9, respectively, to go to an infinite value.

2. Hubless Inducer

The boost pump, with the 45° hubless inducer, transient non-cavitating performance at the design flow coefficient is shown in Figure 64. The inlet NPSH was set high enough to preclude cavitation (see Curve 1). There is little or no difference between the non-cavitating transient performance of the boost pump with the hubless inducer and that of the conventional inducer. Since the shroud drag torque was approximately 40% of the total torque delivered by the hydraulic turbine, the effect of difference in inducer torques was minimized. Locked speed ratio therefore occurred in the same time regardless of inducer configuration.

Figures 65 through 67 show the cavitating transient performance of the hubless inducer at different flow coefficients and elapsed times. The inlet NPSH had to be increased from 10 ft (3.05 m), the minimum value used on the conventional inducer, to 26 ft (7.95 m) at design flow and 16 ft (4.88 m) at 80% flow because the hubless inducer would not start at the lower NPSH value.

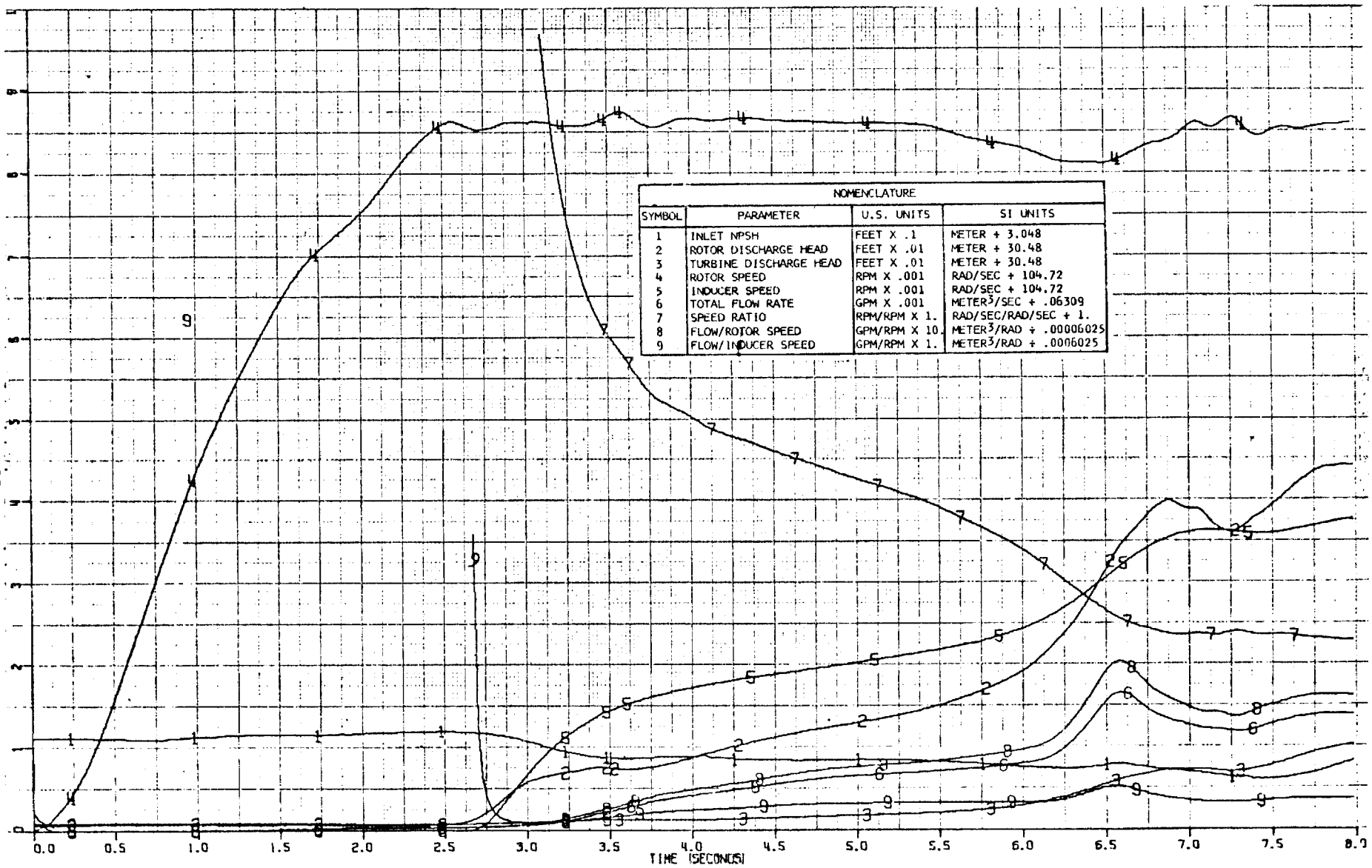

Figure 60

Conventional Inducer, 2.5 sec Start Transient at 100% φ (Cavitating)

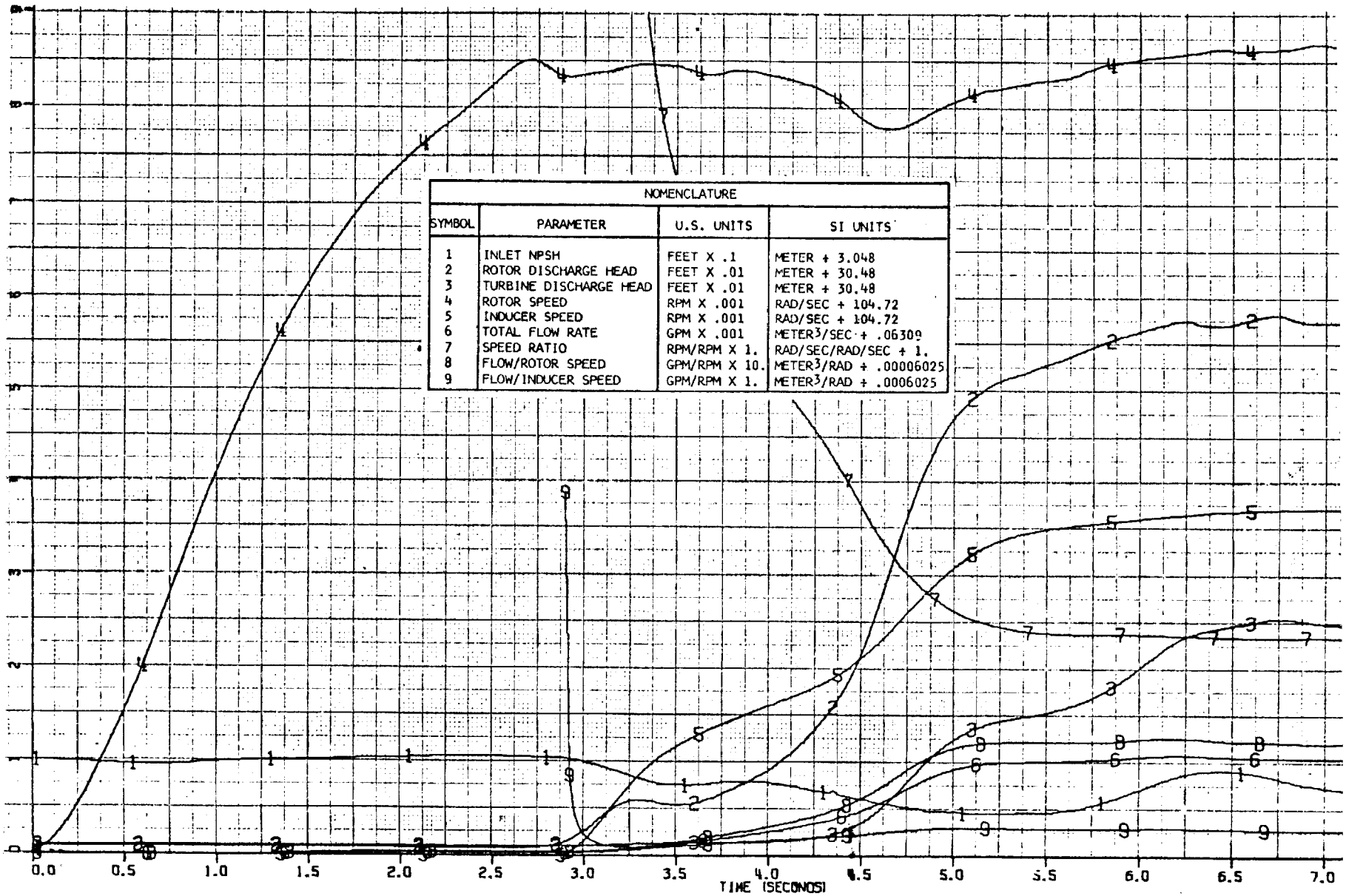

Figure 61

Conventional Inducer, 3 sec Start Transient at 80% φ (Cavitating)

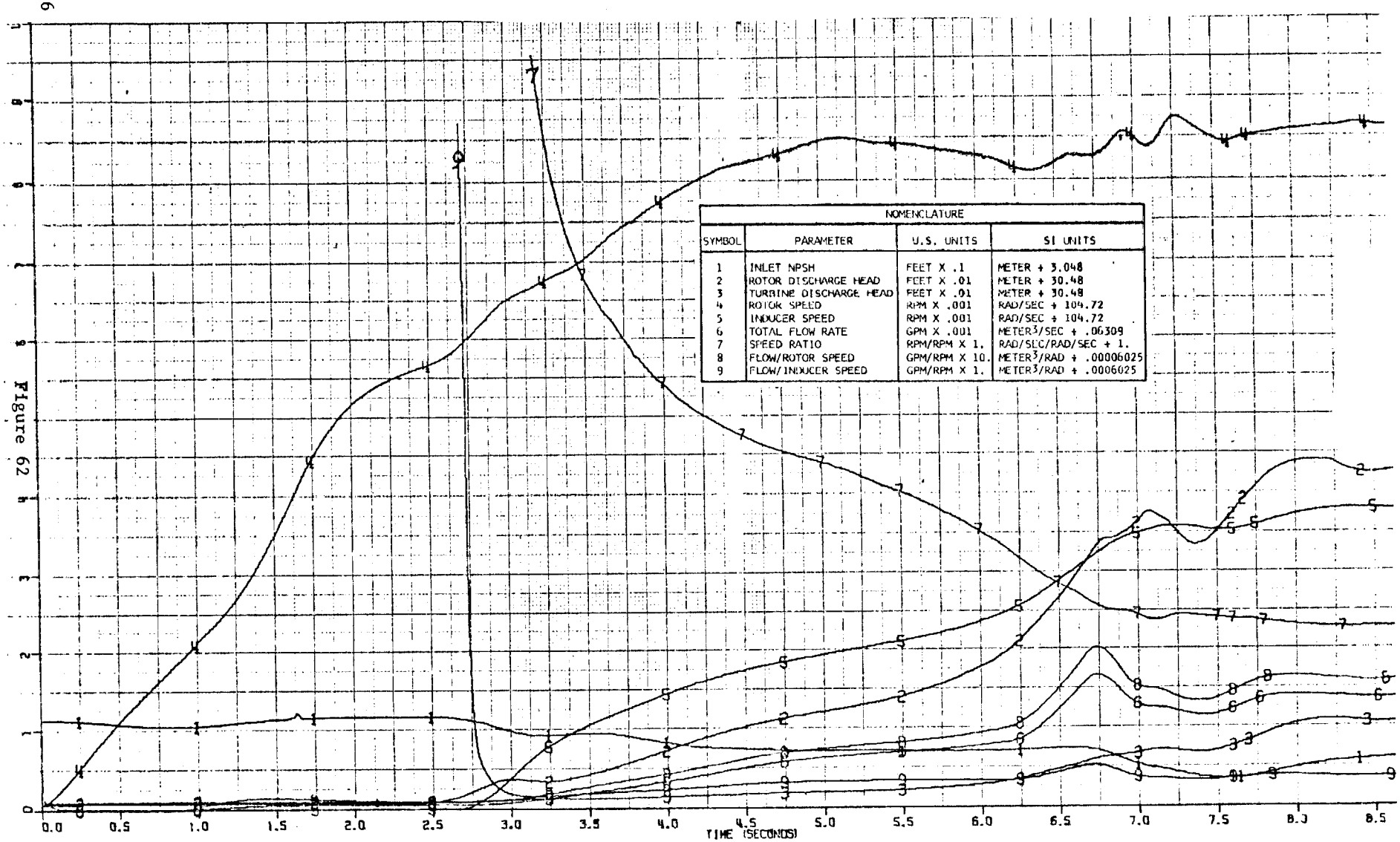

Figure 62

Conventional Inducer, 5 sec Start Transient at 80% φ (Cavitating)

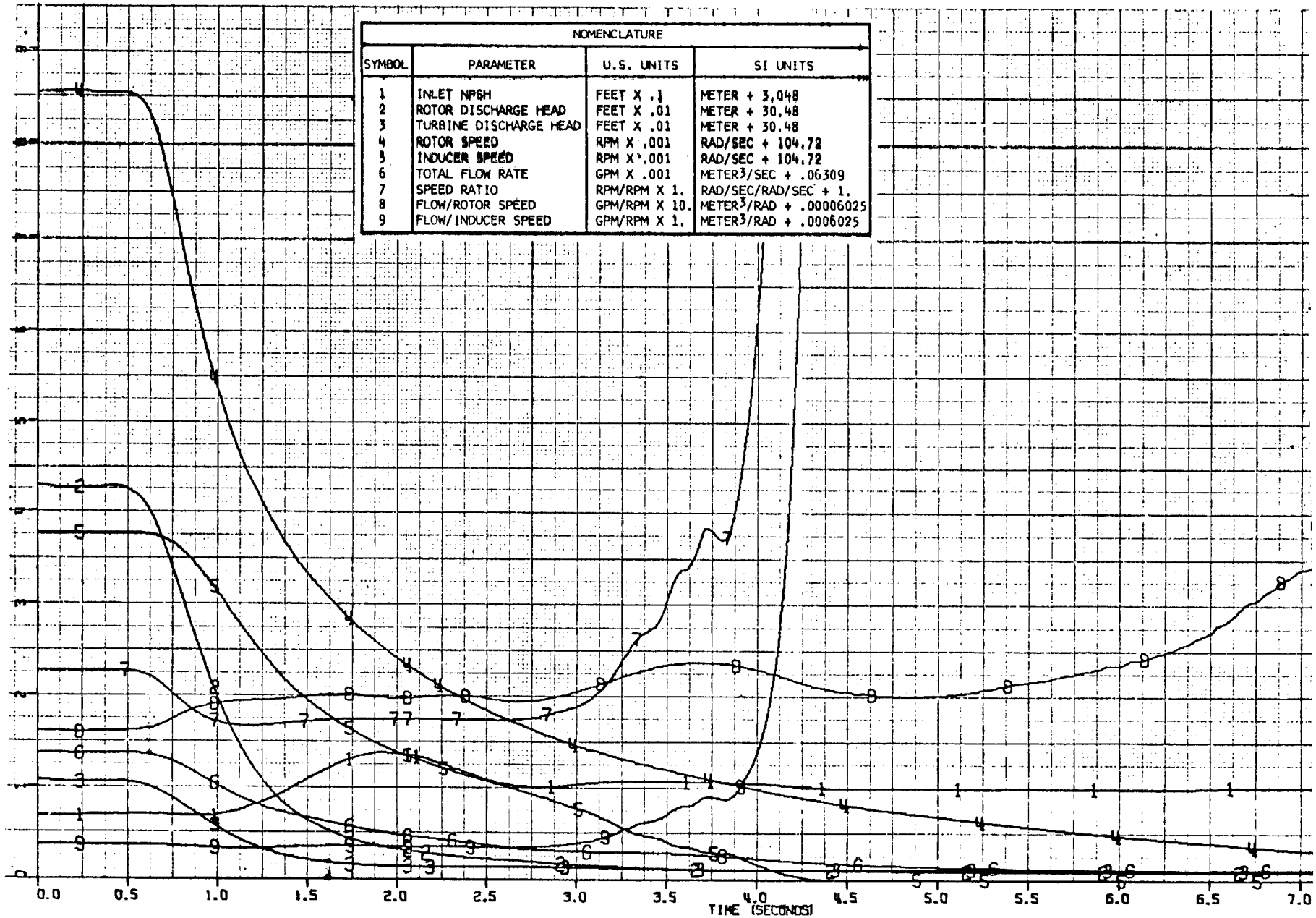

Figure 63

Conventional Inducer, Shutdown Transient at 100% φ (Cavitating)

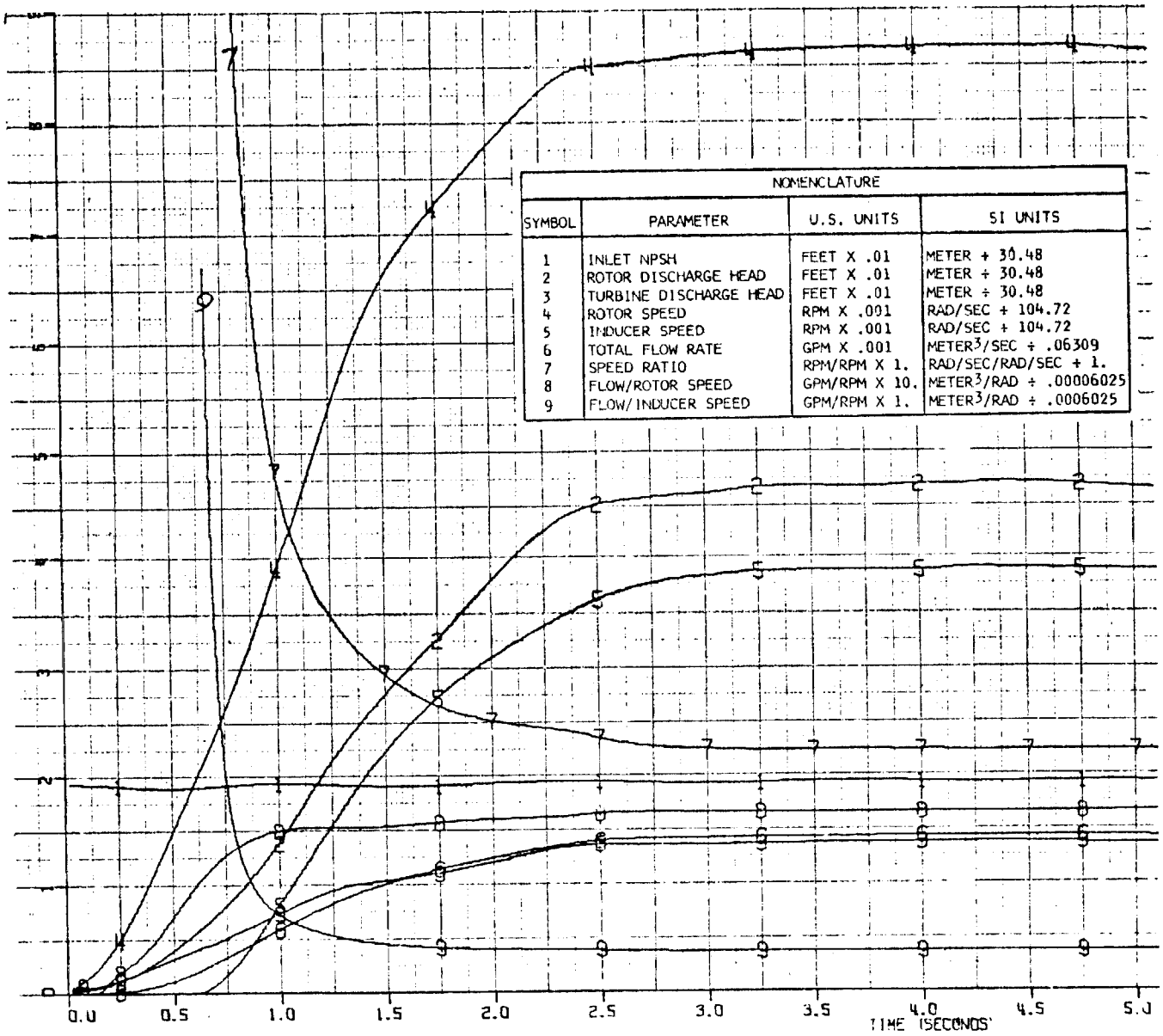

Figure 64

Hubless Inducer (45°), 2.5 sec Start Transient at 100% φ (Non-Cavitating)

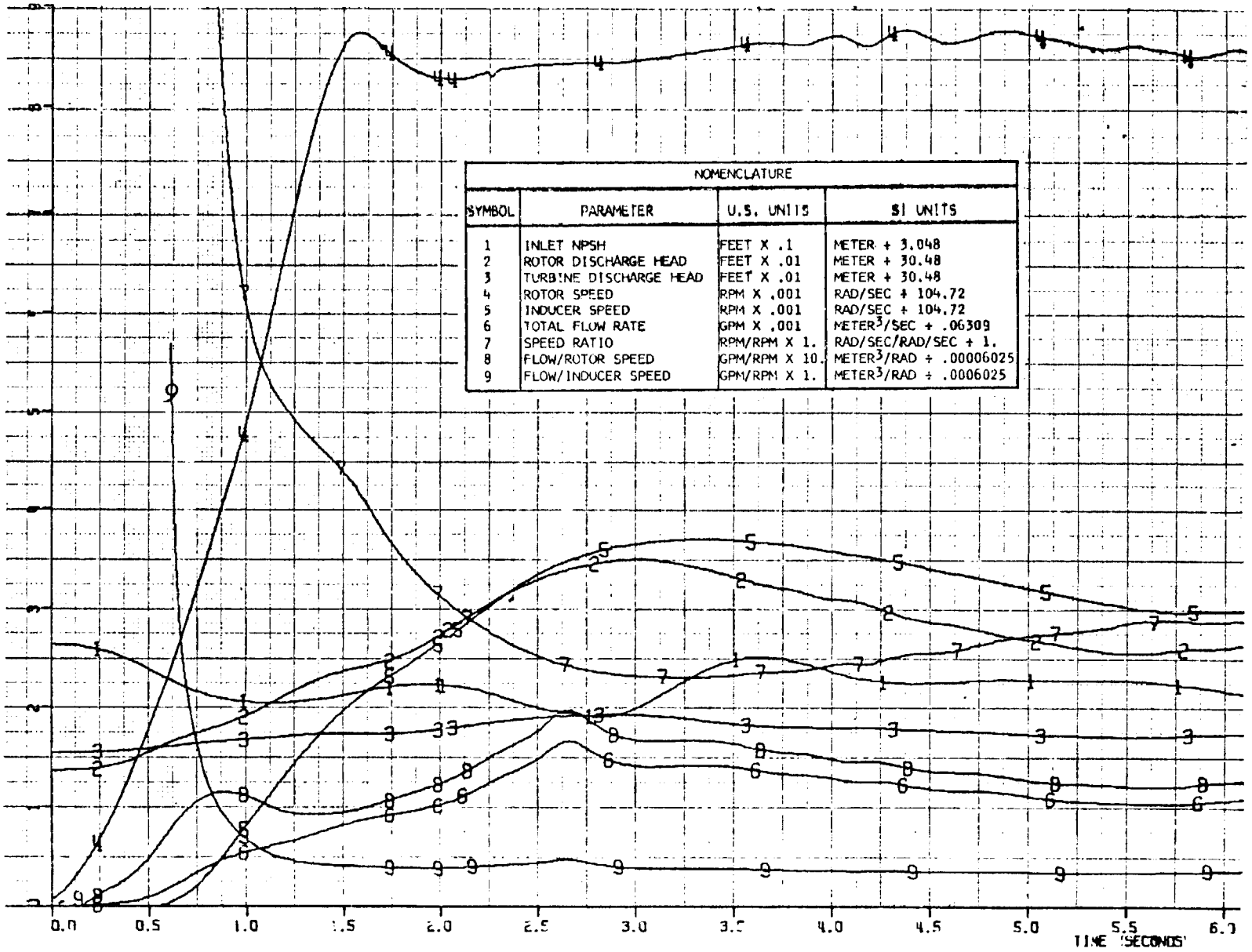

Figure 65

Hubless Inducer (45°), 1.5 sec Start Transient at 100% Φ (Cavitating)

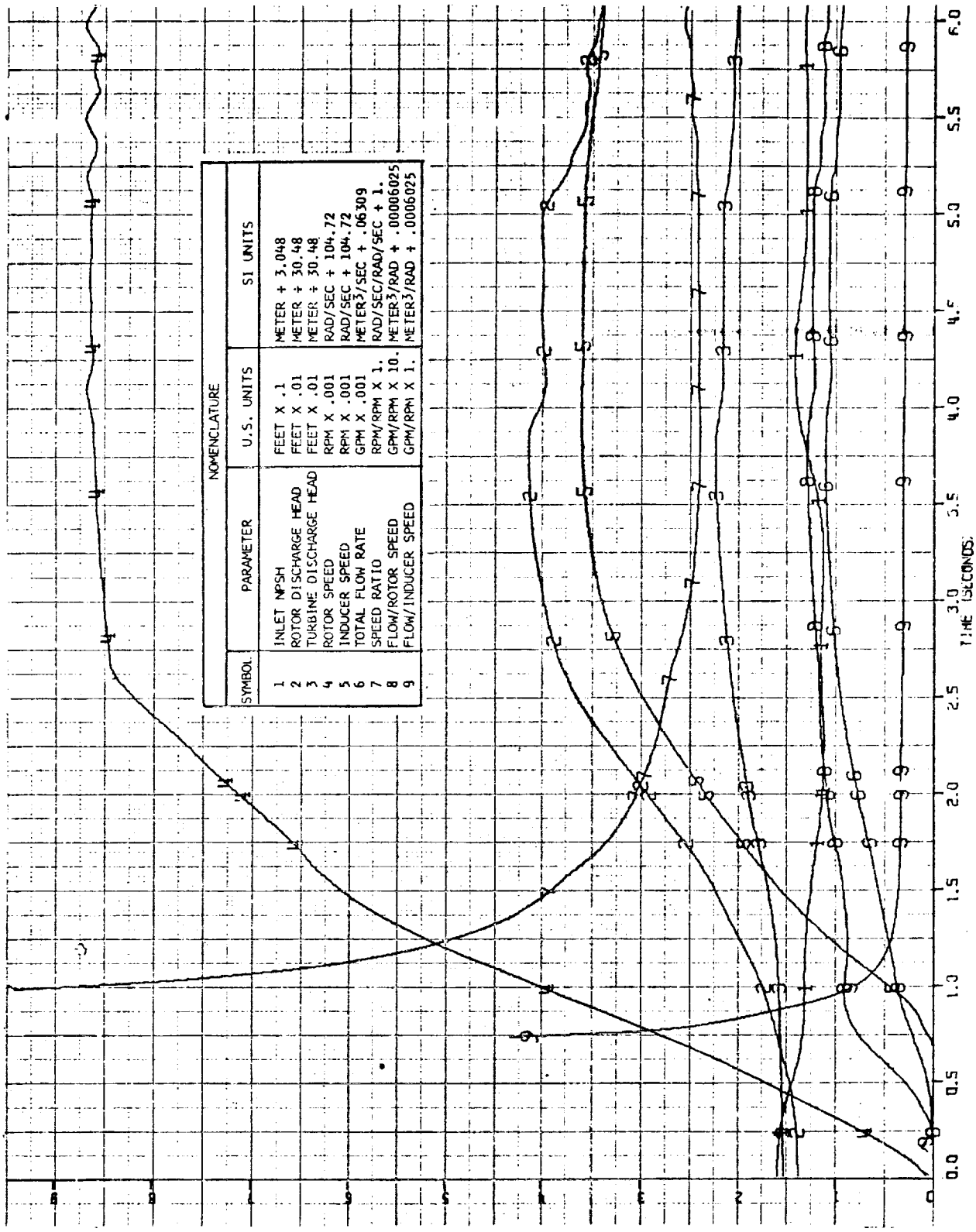

Hubless Inducer (45°), 3 sec Start Transient at 80% Φ (Cavitating)

Figure 66

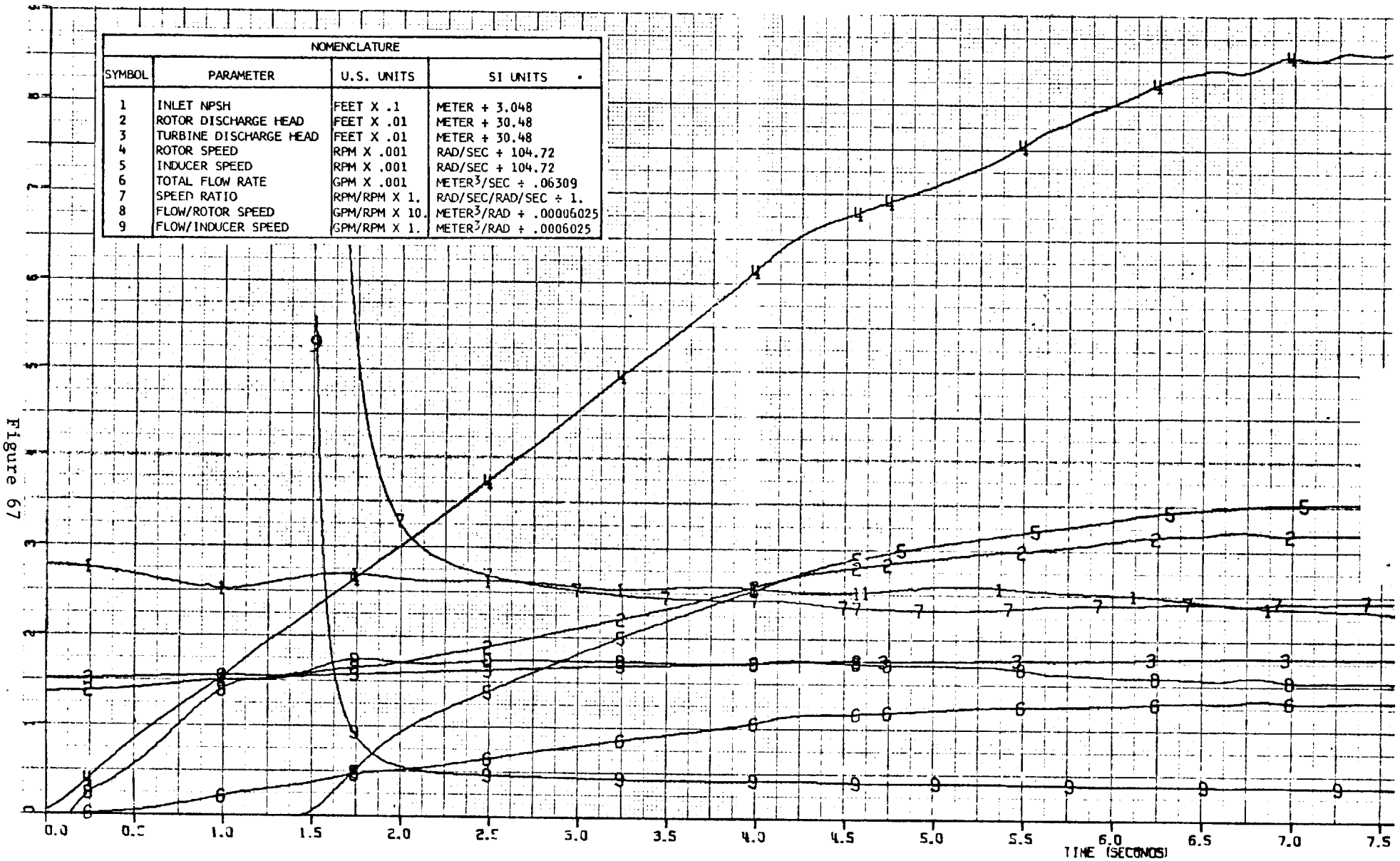

Figure 67

Hubless Inducer (45°), 6 sec Start Transient at 100% φ (Cavitating)

This was caused by the decrease in head produced by the hubless inducer compared to the conventional. This has the effect of decreasing the available NPSH to the rotor causing complete cavitation breakdown and consequently zero delivered head.

3. High Frequency

A comparison of the boost pump suction and discharge pressure oscillations with the conventional and with the 45° hubless inducer during transient operation is shown on Figure 68. The 45° hubless inducer had the highest peak-to-peak pressure oscillations during steady-state operation (Section VII.B.3.b.). In most cases there appeared to be some resonance between 1 and 3 seconds. This could have been caused by 'ringing' of the flow loop. All frequencies with significant peak-to-peak pressure magnitude were between 5 and 30 Hertz with 20 being the predominant frequency. In all cases except one, hubless inducer discharge pressure at 80% flow coefficient, peak-to-peak pressure returned to the minimal steady-state value after 4 seconds. The suction peak-to-peak oscillations in transient are approximately three times those measured in steady-state (see Figure 55 for comparison). The discharge peak-to-peak pressure oscillations, however, are approximately the same during transient and steady-state (see Figure 56 for comparison).

D. MODIFIED ROTOR

Upon completion of the contract-required test program, the rotor was modified in an attempt to improve its cavitation performance. The modification consisted of reducing the maximum blade thickness by approximately one-half at mid cord from hub to tip on the suction side. From mid cord to 20% and 80% cord the material removal was reduced to zero. Since the blade was a double circular arc with little camber, the radius of curvature on the pressure side was extremely large, consequently the modification had the effect of making suction and pressure surfaces parallel from 20% cord to 80% cord. In addition the leading edge was reduced from 0.030 in. (0.00076 m) to 0.007 in. (0.00018 m). The thickness increased from the leading edge linearly to the 20% cord station.

Figure 69 shows the head coefficient and efficiency vs. flow coefficient for the maximum test speed. The head coefficient is less than the design but 16% higher than the original head coefficient. The efficiency appears to peak at a higher than design flow coefficient and is 13 percentage points less than design and 7 percentage points less than the origianl. Stall is not evident down to 70% flow coefficient. The original rotor stalled at approximately 85% flow coefficient. At 120% flow coefficient the modified rotor has a 23% higher head coefficient, indicating that decreasing the thickness kept the rotor from choking at the higher flow.

The modified rotor head coefficient at four radial stations vs. flow coefficient is shown in Figure 70. This should be compared to Figure 42, which is the same data for the original rotor. The stall at the hub in the

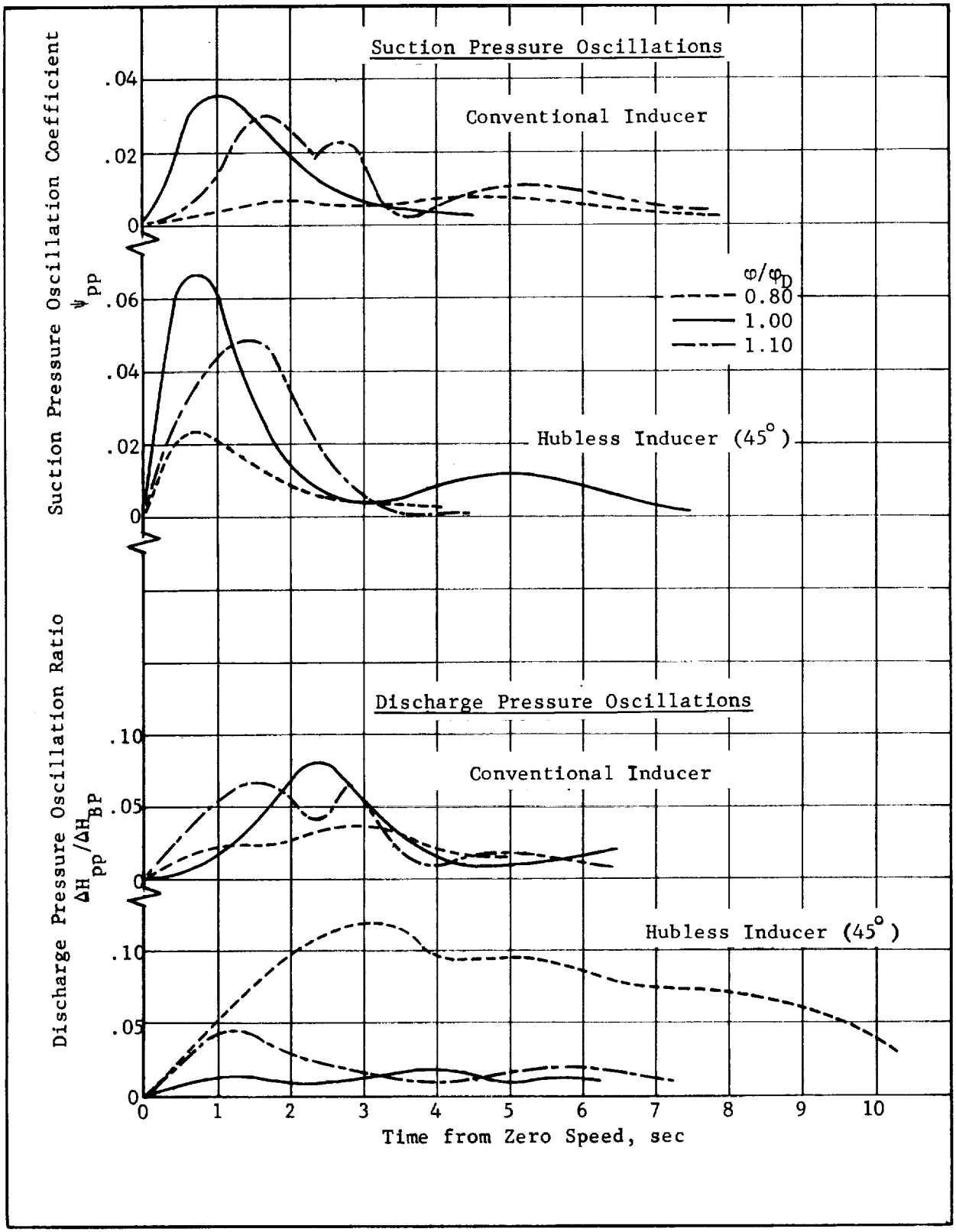

Figure 68. - Boost Pump (with Conventional Inducer), Transient Suction and Discharge Pressure Oscillations vs. Time (Cavitating)

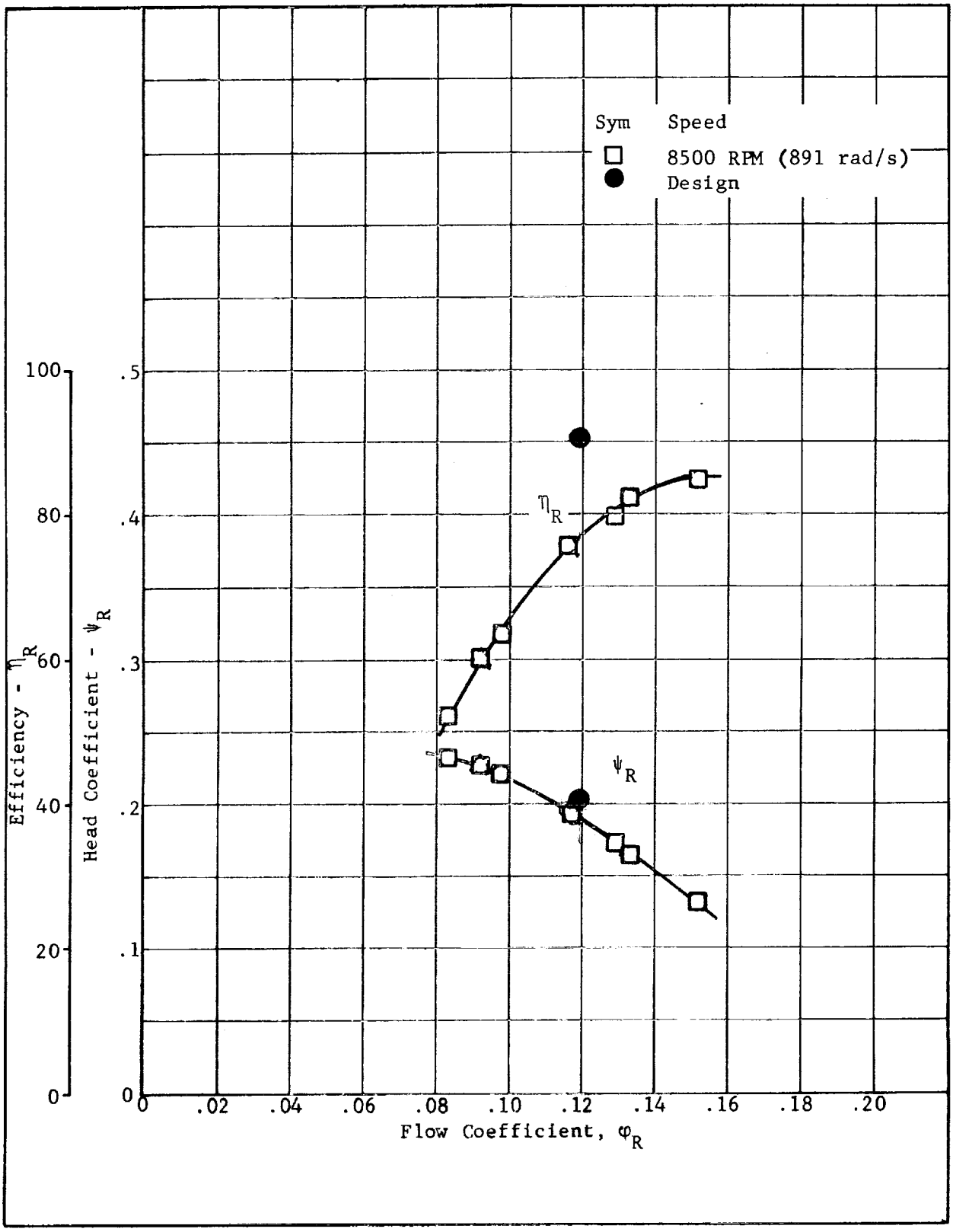

Figure 69. - Modified Rotor, Head Coefficient and Efficiency vs. Flow Coefficient (Non-Cavitating)

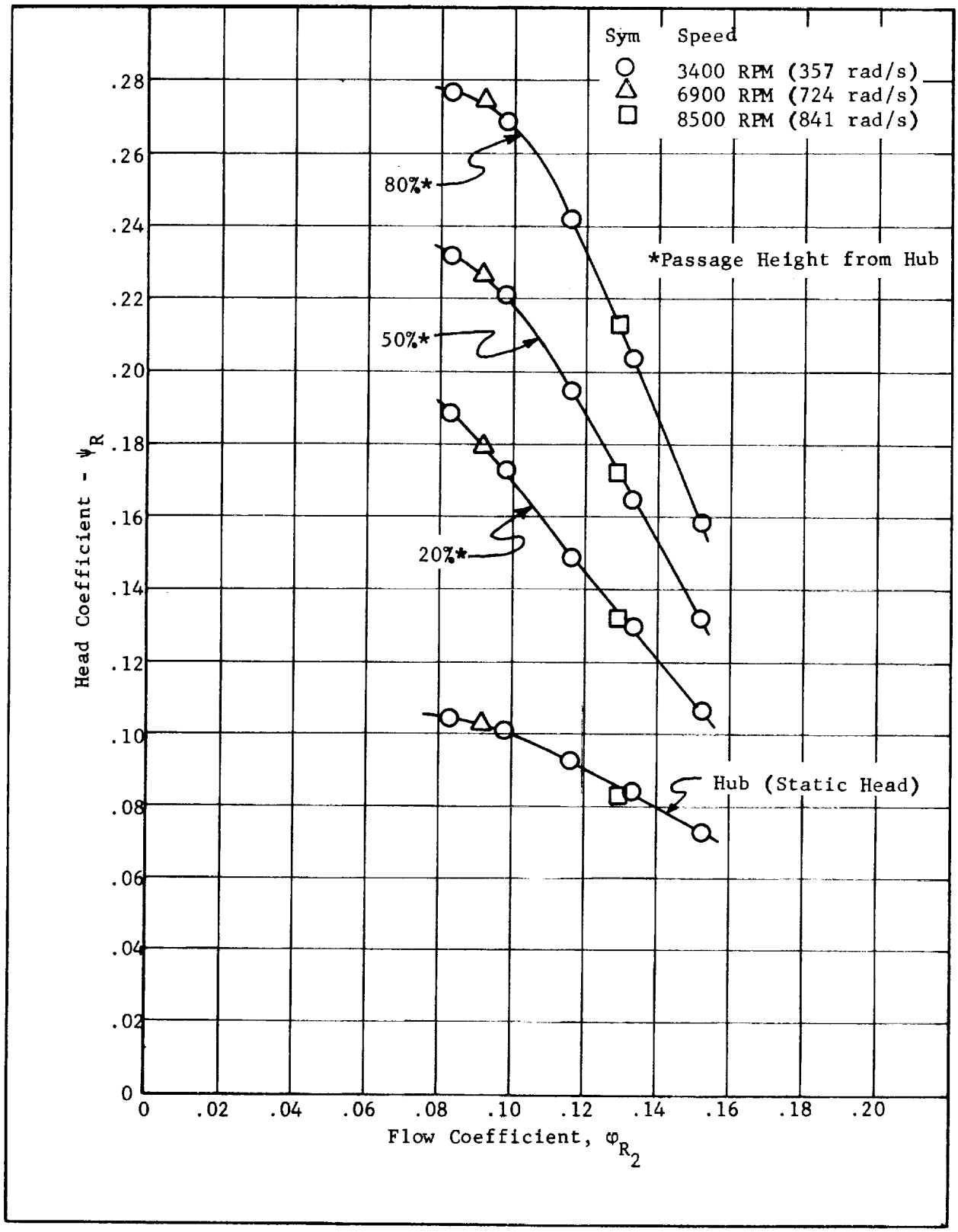

Figure 70. - Modified Rotor, Head Coefficients vs. Flow Coefficient at Four Radial Measuring Stations (Non-Cavitating)

original rotor is completely absent in the modified rotor. The head coefficient is higher at each radial station over the entire flow range for the modified rotor.

To determine what the expected or predicted performance of the modified rotor would be, the design analysis method discussed previously was used with the new deviation angles produced by the change in thickness-to-cord ratio. The results of this prediction can be seen in Figure 71 where the test data is overlaid on the design-predicted values. The mass average of the design-predicted value is the same as was shown on Figure 69.

The suction performance of the modified rotor is shown in Figure 72. There is no significant difference in performance between the modified and the original rotor (Figure 57). The 80% flow is somewhat less, while the 110% flow is slightly better. Since the head coefficient of the modified rotor was higher at a given flow coefficient, the blade loading would likewise be higher. In general, the more highly loaded blades will have lower cavitation performance, as was shown in Ref 3. This could account for the unchanged suction performance; that is, any gain realized by sharpening the lead edge was offset by the higher blade loading.

VIII. CONCLUSIONS

1. The hubless inducer concept allows the inlet blade tip angle to be increased from the present manufacturing limit of 83° to 86°. This is accomplished by attaching the blade to a shroud after machining the fluid passages. After attachment the hub is removed and blade leading edge is faired to the desired sharpness.

2. The suction performance of a hubless inducer is limited to that value predicted by Ref 12 for the corresponding inlet blade tip angle. That is, larger blade angles have smaller flow coefficients which, in turn, produce the highest suction specific speed performance.

3. The head coefficient of a hubless inducer is lower than that of a conventional inducer with the same discharge flow coefficient and blade angle. A hubless inducer therefore must be used in an application requiring low head rise inducer, or a downstream stage must be used to produce additional head.

4. Hubless inducers mechanically couple best in shroud driven applications, i.e., with a shrouded pump impeller or a hydraulic turbine driven inducer concept similar to Figure 2.

5. The design method used to predict inducer, rotor, and hydraulic turbine head performance at design flow proved to be very accurate. This accuracy is shown by Figures 31, 34, 41, 44, 45, 47, 69, and 71.

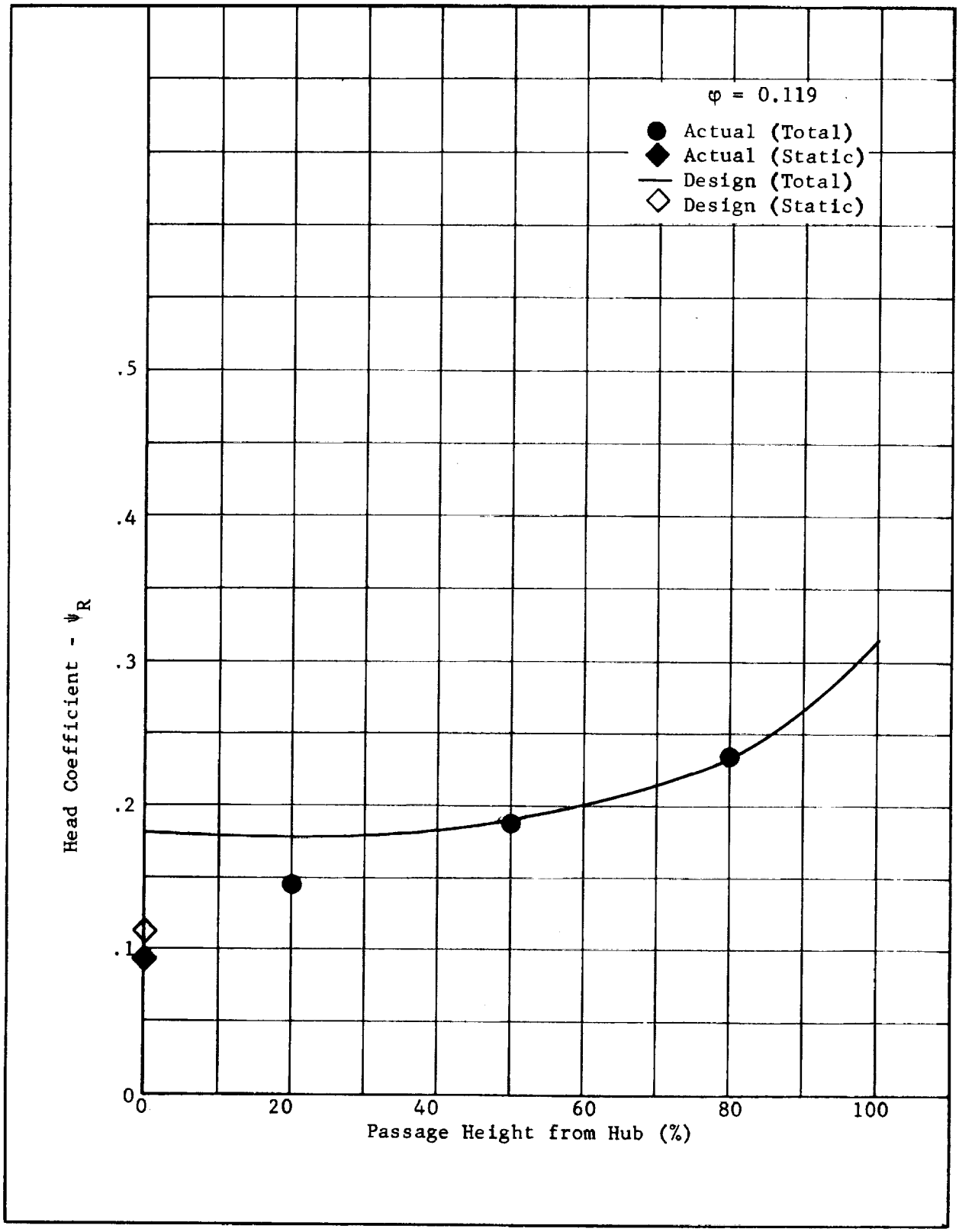

Figure 71. - Modified Rotor, Radial Head Coefficient Distribution at Design Flow Coefficient (Non-Cavitating)

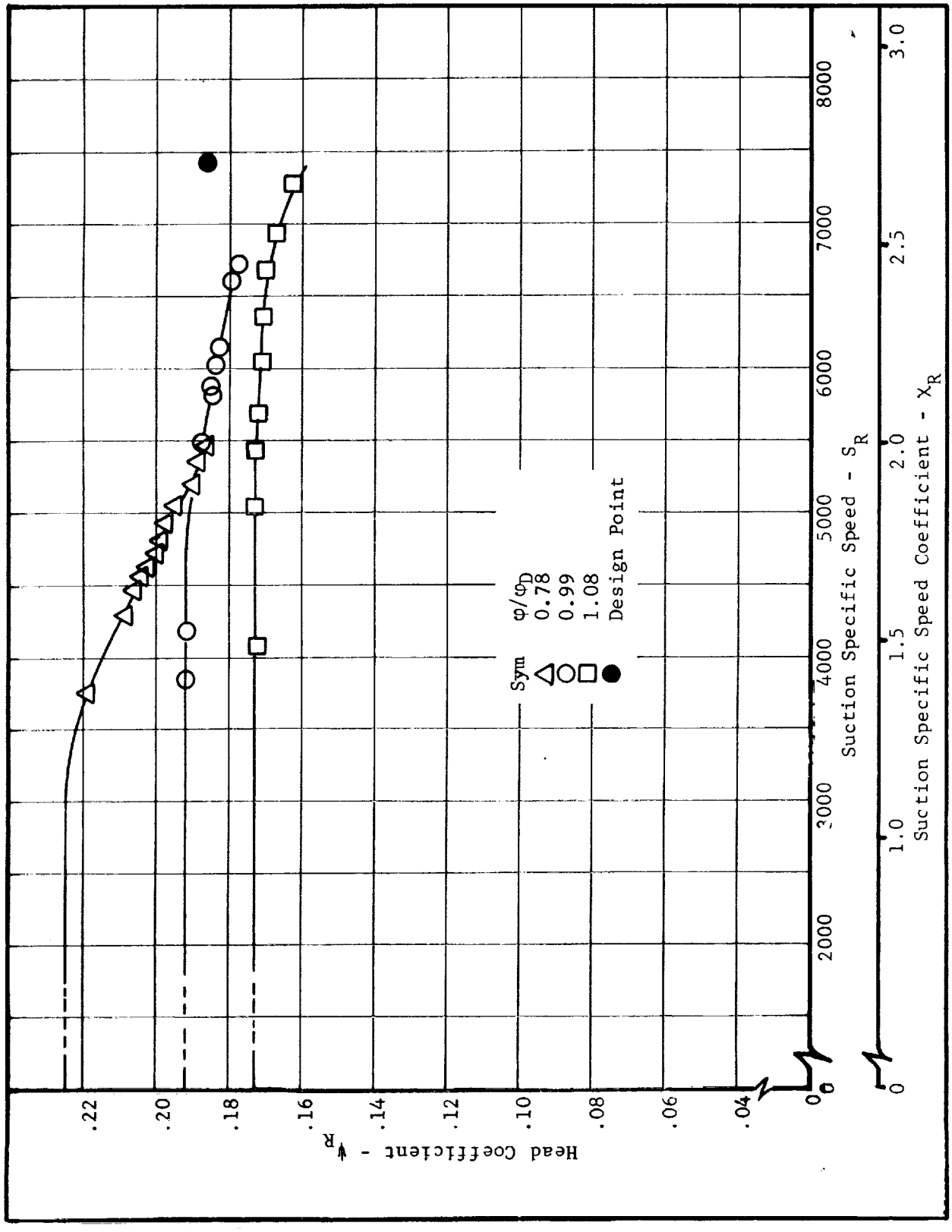

Modified Rotor, Head Coefficients vs. Suction Specific Speed (Cavitating)

Figure 72

6. The full flow hydraulic turbine driven inducer boost pump in the configuration shown in Figure 2 has the following characteristics:

- Maximum speed ratio of 2.5 limited by the cavitation performance of the rotor.
- The speed ratio has nearly the same value as the design from 0 to 120% of the design flow coefficient.
- The boost pump has the capability of start transient times less than 1 second.
- Successful start transients can be realized even through a high degree of rotor cavitation exists at some point during the transient. These transients, however, require a longer elapsed time.

7. Rotor cavitation performance appears to be somewhat a function of hub/tip diameter ratio as shown by Figure 73. If this indication is correct, cavitation performance is limited and can be improved to the required 7420 (2.7) suction specific speed only by decreasing the hub/tip diameter ratio. This of course affects the complete design of the boost pump and may impose other restrictions.

8. Blade row head rise performance across the discharge passage can be successfully measured by the use of fixed-position Kiel probes. Care must be taken to set probes so that the required flow range can be met.

9. Shroud drag calculated by standard disk friction procedures was in error by 25% to 40%. This could be partially caused by larger than normal clearances or by pumping action through the radial thrust bearings.

10. Full flow hydraulic turbine driven inducer boost pumps similar to the concept shown in Figure 74 are not speed ratio limited at 2.5 but can be designed for speed ratios as high as 4. The disadvantages are a high speed shroud coupling and return flow into the inlet of the high speed inducer. All hydraulic components are within the state-of-the-art.

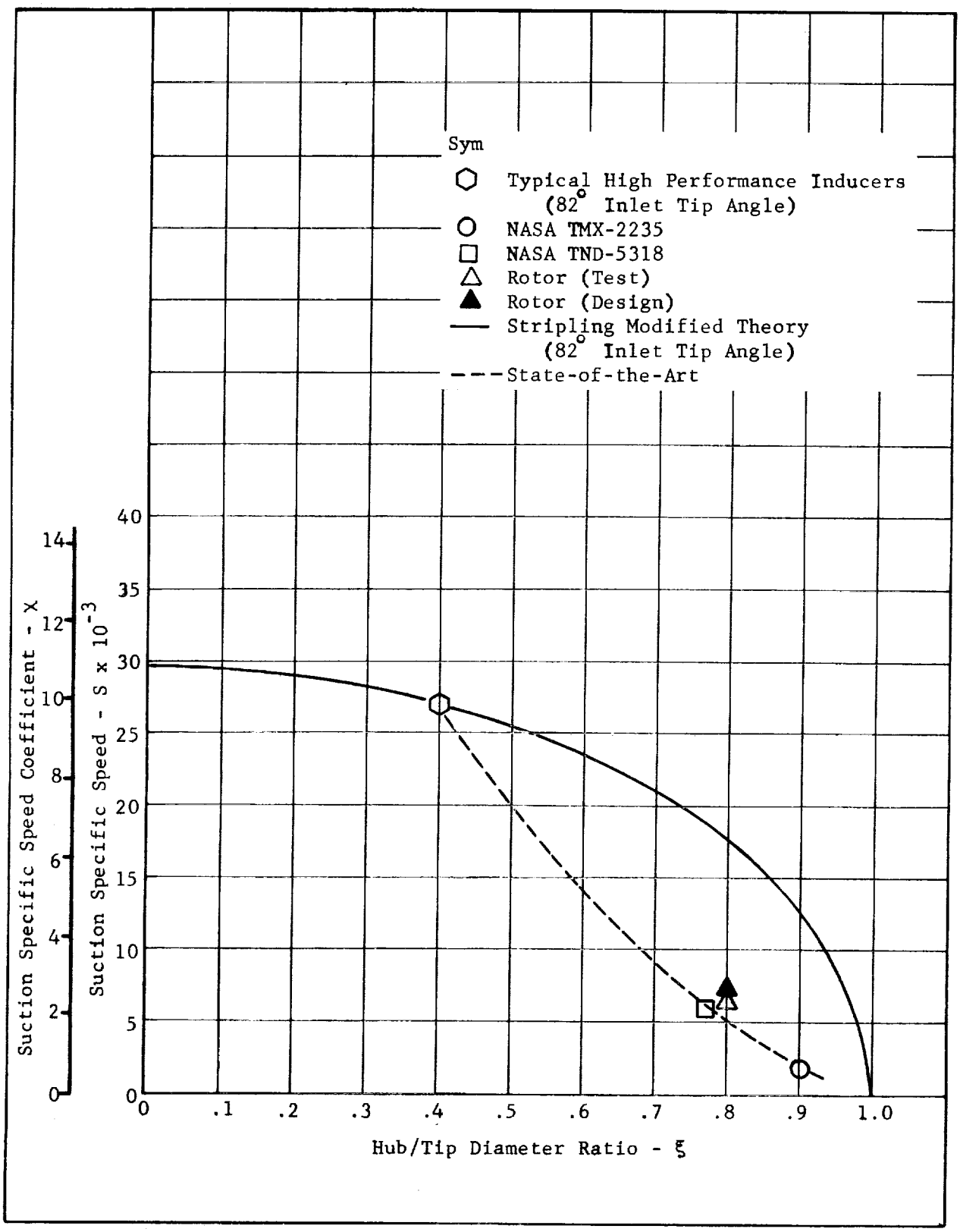

Figure 73. - Suction Specific Speed (at 3% Head Loss) vs. Hub/Tip Diameter Ratio

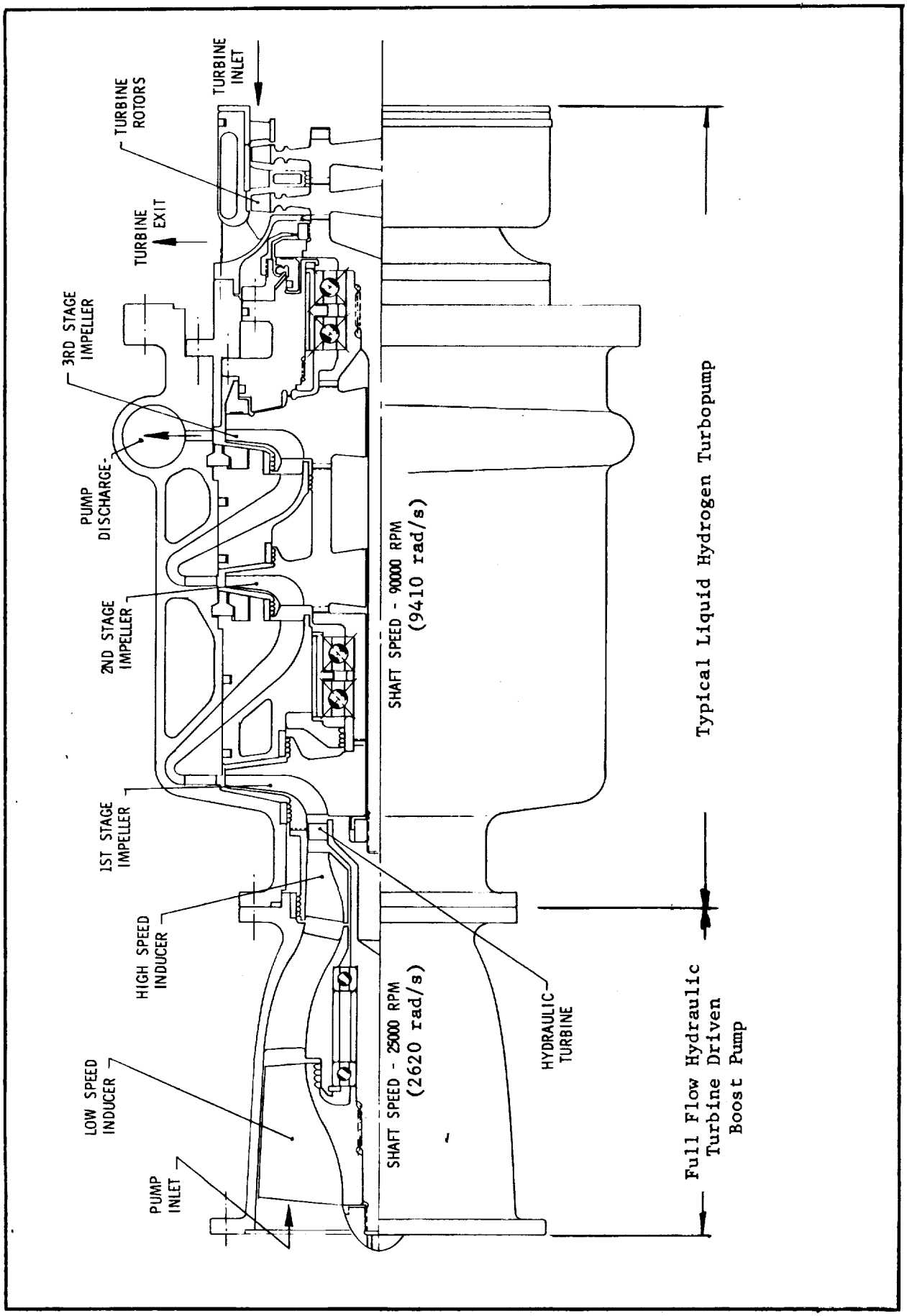

Figure 74

Full Flow Hydraulic Turbine Driven Inducer Boost Pump and a Typical Hydrogen Main Pump

APPENDIX A

SYMBOLS

APPENDIX A

Symbols

D	blade diffusion factor
g	acceleration due to gravity, 32.17 ft/sec^2 (9.8 m/s^2)
H	total head, ft (m)
ΔH	blade head rise, ft (m)
i	incidence angle, deg
K	cavitation number
N	rotating speed, RPM (rad/s)
NPSH	net positive suction head, ft (m)
Q	flow rate, gal/min (m^3/s)
R	radius, ft (m)
S	suction specific speed, RPM (gpm)$^{1/2}$/(ft)$^{3/4}$
SR	speed ratio
U	blade velocity, ft/sec (m/s)
V	fluid velocity, ft/sec (m/s)
α	blade setting angle with respect to axial direction, deg
β	blade angle with respect to axial direction, deg
β^*	fluid angle with respect to axial direction, deg
δ	deviation angle, deg
η	efficiency
ξ	hub/tip radius ratio
σ	blade solidity, ratio of blade cord length to blade tangential spacing
τ	cavitation parameter
ϕ	flow coefficient
Φ	blade camber angle, deg
χ	suction specific speed coefficient
ψ	head coefficient
ψ^*	head coefficient ideal
$\bar{\omega}$	loss coefficient

Subscripts

BP	boost pump (inducer inlet to hydraulic turbine exit)
D	design point
h	hub
I	inducer
IC	conventional inducer (forward section)
IH	hubless inducer (forward section)
IT	transition inducer (aft section)
m	mean
pp	peak-to-peak pressure oscillations
R	rotor
t	tip
T	turbine
θ	tangential direction
Z	axial direction
1	inlet
2	outlet

Superscripts

$'$	relative to rotor

APPENDIX B

EQUATIONS

APPENDIX B

Equations

Diffusion Factor

$$D = 1 - \frac{V_2'}{V_1'} + \frac{R_2 V_{\theta 2} - R_1 V_{\theta 1}}{(R_2+R_1)\ \sigma\ V_1'}$$

Incidence Angle

$$i = \beta_1^* - \beta_1$$

Cavitation Number

$$K = \frac{NPSH \cdot 2g}{(V_1')^2} - \left[\frac{V_{Z1}}{V_1'}\right]^2$$

Speed Ratio

$$SR = N_R/N_I$$

Deviation Angle

$$\delta = \beta_2^* - \beta_2$$

Efficiency

$$\eta = \frac{\psi}{\psi^*}$$

Cavitation Parameter

$$\tau = \frac{NPSH \cdot 2g}{(U_t)^2}$$

Suction Specific Speed

$$S = N\ (Q)^{1/2}/(NPSH)^{3/4}$$

Flow Coefficient

$$\phi = \frac{V_Z}{U_t}$$

Camber Angle

$$\Phi = \beta_1 - \beta_2$$

Head Coefficient

$$\psi = \frac{\Delta H \cdot g}{(U_t)^2}$$

Head Coefficient Ideal

$$\psi^* = \frac{V_\theta}{U_t}$$

Loss Coefficient

$$\bar{\omega} = \frac{2\,(\psi^{*}-\psi)\,(U)^{2}}{(V_1')^{2}}$$

Head Rise

$$\Delta H = H_2 - H_1$$

Hub Tip Diameter Ratio

$$\xi = R_h/R_t$$

Suction Specific Speed

$$\chi = N\,(Q)^{1/2}/(NPSH\cdot g)^{3/4} \quad \text{(unitless)}$$

APPENDIX C

DRAWINGS

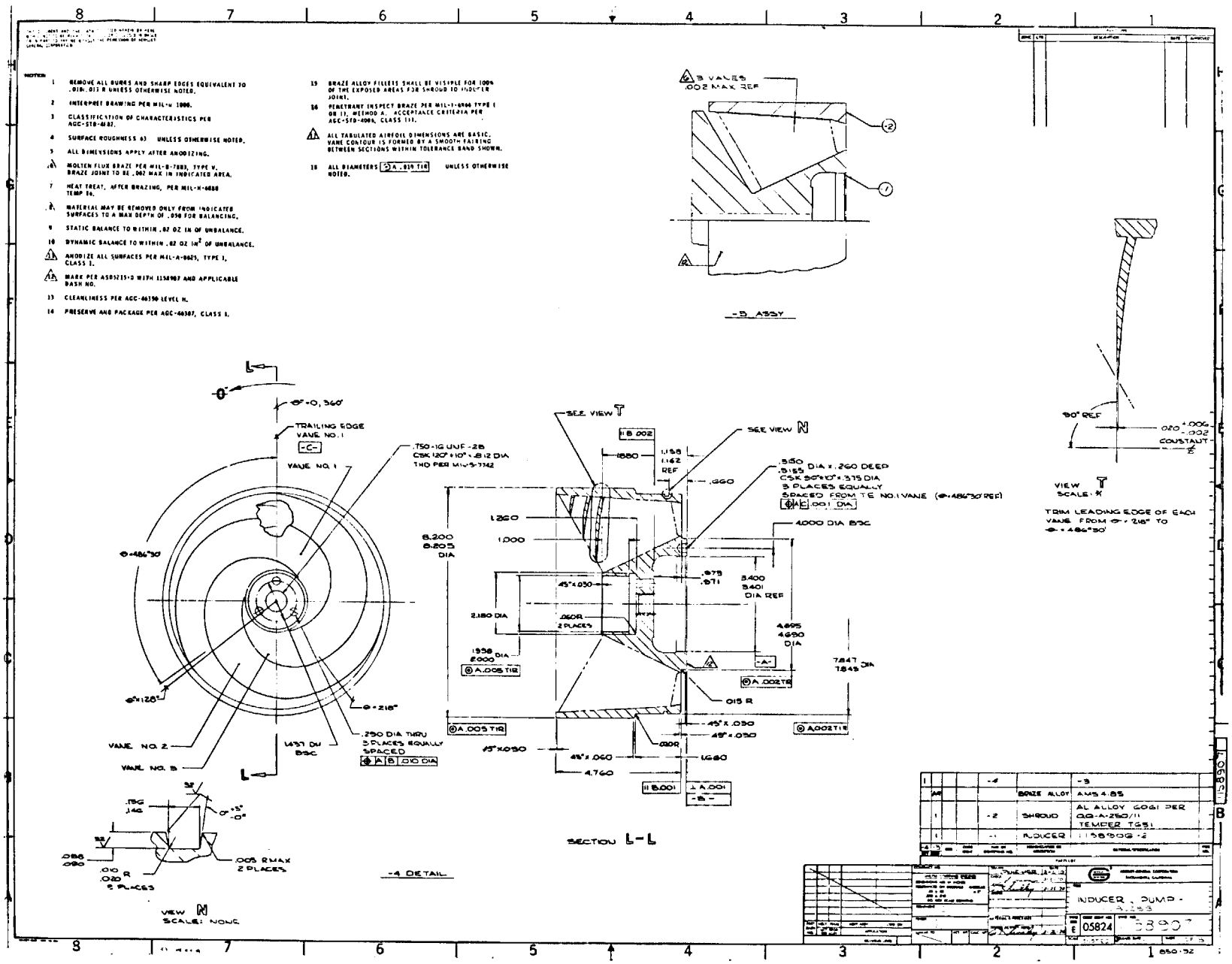
NOTES:
1 REMOVE ALL BURRS AND SHARP EDGES EQUIVALENT TO .018 R, .012 R UNLESS OTHERWISE NOTED.
2 INTERPRET DRAWING PER MIL-STD 100B.
3 CLASSIFICATION OF CHARACTERISTICS PER AGC-STD-4102.
4 SURFACE ROUGHNESS 63 UNLESS OTHERWISE NOTED.
5 ALL DIMENSIONS APPLY AFTER ANODIZING.
6 MOLTEN FLUX BRAZE PER MIL-B-7883, TYPE V. BRAZE JOINT TO BE .002 MAX IN INDICATED AREA.
7 HEAT TREAT, AFTER BRAZING, PER MIL-H-6088 TEMP 16.
8 MATERIAL MAY BE REMOVED ONLY FROM INDICATED SURFACES TO A MAX DEPTH OF .030 FOR BALANCING.
9 STATIC BALANCE TO WITHIN .02 OZ IN OF UNBALANCE.
10 DYNAMIC BALANCE TO WITHIN .02 OZ IN² OF UNBALANCE.
11 ANODIZE ALL SURFACES PER MIL-A-8625, TYPE I, CLASS 1.
12 MARK PER AS05215-D WITH 1158987 AND APPLICABLE DASH NO.
13 CLEANLINESS PER AGC-46150 LEVEL H.
14 PRESERVE AND PACKAGE PER AGC-46307, CLASS 1.
15 BRAZE ALLOY FILLETS SHALL BE VISIBLE FOR 100% OF THE EXPOSED AREAS FOR SHROUD TO INDUCER JOINT.
16 PENETRANT INSPECT BRAZE PER MIL-I-6866 TYPE I OR II, METHOD A. ACCEPTANCE CRITERIA PER AGC-STD-4066, CLASS 1 (1).
17 ALL TABULATED AIRFOIL DIMENSIONS ARE BASIC. VANE CONTOUR IS FORMED BY A SMOOTH FAIRING BETWEEN SECTIONS WITHIN TOLERANCE BAND SHOWN.
18 ALL DIAMETERS ⌀A .010 TIR UNLESS OTHERWISE NOTED.
3 VANES .002 MAX REF
-3 ASSY
TRAILING EDGE VANE NO. 1
-C-
VANE NO. 1
.750-16 UNF-2B CSK 120° ±10° x .812 DIA THD PER MIL-S-7742
SEE VIEW T
SEE VIEW N
.550 DIA x .260 DEEP .585 CSK 80°±10° x .375 DIA 3 PLACES EQUALLY SPACED FROM TE NO. 1 VANE (⌀=486°30' REF)
⌀A⌀E .001 DIA
4.000 DIA BSC
.290 DIA THRU 3 PLACES EQUALLY SPACED
⌀A⌀B⌀C .010 DIA
VANE NO. 2
VANE NO. 3
1.437 DIA BSC
SECTION L-L
-4 DETAIL
VIEW N SCALE: NONE
VIEW T SCALE: X
TRIM LEADING EDGE OF EACH VANE FROM ⌀=218° TO ⌀=486°30'
.020 +.006 -.002 COUSTAUT
90° REF
BRAZE ALLOY AMS 4185
SHROUD AL ALLOY 6061 PER QQ-A-250/11 TEMPER T651
INDUCER 1158900-2
INDUCER, PUMP
SIZE E
05824
1158907

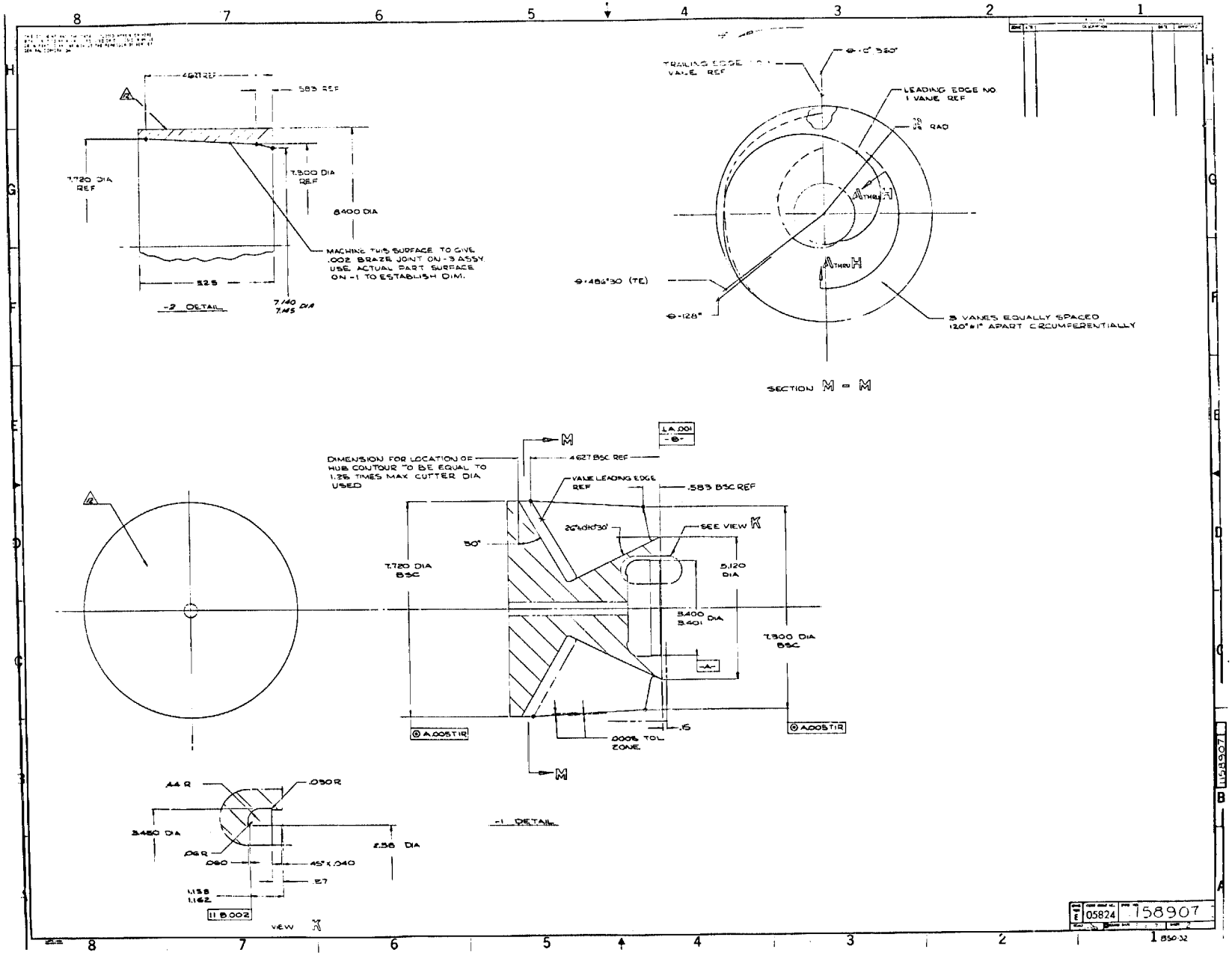
.583 REF
7.720 DIA REF
7.300 DIA REF
8.400 DIA
MACHINE THIS SURFACE TO GIVE .002 BRAZE JOINT ON -3 ASSY. USE ACTUAL PART SURFACE ON -1 TO ESTABLISH DIM.
-2 DETAIL
7.140 7.145 DIA
TRAILING EDGE NO 1 VANE REF
LEADING EDGE NO 1 VANE REF
.250 RAD
Φ.486"30 (TE)
Φ.128"
5 VANES EQUALLY SPACED 120°±1° APART CIRCUMFERENTIALLY
SECTION M - M
DIMENSION FOR LOCATION OF HUB CONTOUR "O" BE EQUAL TO 1.25 TIMES MAX CUTTER DIA USED
4.627 BSC REF
VANE LEADING EDGE REF
.583 BSC REF
SEE VIEW K
30°
7.720 DIA BSC
5.120 DIA
8.400 DIA 8.401
7.300 DIA BSC
.15
.0005 TOL ZONE
A.005 TIR
LA.001 -B-
.44 R
.050 R
3.460 DIA
.062 R
.060
45° x .040
2.56 DIA
.157
M38 1.162
11 B.002
VIEW K
-1 DETAIL

158907

⚠ SECTION A-A THRU H-H COORDINATES FOR RADIAL SECTIONS NEGLECTING FILLET RADII AT VANE ROOT AND HUB INTERSECTION

ℓ	SECTION A-A R = 1.550		SECTION B-B R = 1.950		SECTION C-C R = 2.310		SECTION D-D R = 2.500		SECTION E-E R = 2.560		SECTION F-F R = 3.420		SECTION G-G R = 3.650		SECTION H-H R = 3.660	
	XP	XS	XP	XS	XP	XS	XP	XS	XP	XS	XP	XS	XP	XS	XP	XS
0							.379	.413	.445	.483	.515	.555	.653	.693	.583	.623
8					.500	.540	.519 ±.004	.571 ±.004	.548 ±.004	.589 ±.004	.618 ±.004	.658 ±.004	.675 ±.004	.708 ±.004	.648 ±.004	.729 ±.004
18					.690 ±.004	.710 ±.004	.701	.824	.728	.844	.734	.858	.735	.845	.736	.814
28					.872	.992	.872	1.032	.870	1.028	.886	1.009	.843	.993	.826	.977
38					1.030	1.191	1.027	1.181	1.011	1.165	.974	1.129	.952	1.104	.923	1.074
48					1.180	1.341	1.174	1.334	1.144	1.298	1.095	1.248	1.061	1.213	1.024	1.173
58			1.330	1.492	1.321	1.481	1.313	1.472	1.269	1.423	1.210	1.363	1.170	1.322	1.131	1.282
68			1.478	1.640	1.459	1.618	1.441	1.600	1.389	1.541	1.325	1.476	1.279	1.431	1.236	1.387
78			1.628	1.770	1.579	1.738	1.560	1.718	1.502	1.655	1.435	1.586	1.386	1.538	1.341	1.492
88			1.776	1.887	1.694	1.853	1.674	1.832	1.612	1.765	1.540	1.693	1.490	1.642	1.443	1.594
98			1.940	2.001	1.806	1.964	1.784	1.941	1.720	1.873	1.646	1.799	1.594	1.746	1.545	1.696
108			1.948	2.108	1.915	2.073	.891	2.047	1.828	1.981	1.751	1.904	1.698	1.850	1.647	1.798
118	2.064	2.226	2.050	2.210	2.024	2.181	1.997	2.153	1.939	2.057	1.856	2.009	1.802	1.954	1.749	1.900
128	2.170	2.330	2.152	2.311	2.126	2.282	2.102	2.258	2.039	2.191	1.961	2.113	1.906	2.056	1.851	2.002
138	2.272	2.432	2.252	2.411	2.226	2.382	2.204 ±.003	2.360 ±.007	2.141 ±.003	2.293 ±.007	2.063 ±.003	2.215 ±.007	2.004 ±.003	2.158 ±.007	1.938 ±.003	2.106 ±.007
148	2.370	2.530	2.350	2.508 ±.003	2.324 ±.003	2.480 ±.007	2.302 ±.003	2.457 ±.007	2.239 ±.003	2.391 ±.007	2.161 ±.003	2.313 ±.007	2.104 ±.003	2.256 ±.007	2.051 ±.007	2.202 ±.008
158	2.465 ±.003	2.624 ±.007	2.445 ±.003	2.603 ±.007	2.419 ±.007	2.575 ±.003	2.397 ±.007	2.552 ±.003	2.336 ±.007	2.484 ±.003	2.256 ±.007	2.408 ±.008	2.199 ±.003	2.351 ±.003	2.146	2.297
168	2.558 ±.007	2.717 ±.003	2.538 ±.007	2.695	2.512	2.667	2.490	2.645	2.427	2.579	2.349	2.501	2.292	2.444	2.239	2.390
178	2.649	2.808	2.629	2.786	2.603	2.758	2.581	2.735	2.518	2.670	2.440	2.592	2.383	2.535	2.330	2.481
188	2.738	2.896	2.718	2.874	2.692	2.847	2.670	2.826	2.607	2.759	2.529	2.681	2.472	2.623	2.419	2.569
198	2.825	2.983	2.805	2.961	2.779	2.934	2.757	2.911	2.694	2.846	2.616	2.768	2.559	2.710	2.506	2.656
208	2.910	3.068	2.890	3.045	2.864	3.018	2.842	2.996	2.779	2.931	2.701	2.853	2.644	2.795	2.591	2.741
218	2.994	3.151	2.974	3.128	2.948	3.102	2.926	3.079	2.863	3.015	2.785	2.937	2.728	2.879	2.675	2.825
228	3.077	3.234	3.057	3.209	3.031	3.185	3.009	3.162	2.946	3.098	2.868	3.020	2.811	2.962	2.758	2.908
238	3.159	3.315	3.138	3.289	3.112	3.265	3.090	3.243	3.027	3.179	2.949	3.101	2.892	3.043	2.839	2.989
248	3.237	3.394	3.217	3.368	3.191	3.344	3.169	3.322	3.106	3.258	3.028	3.180	2.971	3.122	2.918	3.068
258			3.295	3.446	3.269	3.422	3.247	3.400	3.184	3.336	3.106	3.258	3.049	3.200	2.996	3.146
268			3.372	3.523	3.346	3.499	3.324	3.477	3.261	3.413	3.183	3.335	3.126	3.277	3.073	3.223
278			3.448	3.599	3.422	3.575	3.400	3.553	3.337	3.487	3.259	3.411	3.202	3.353	3.149	3.299
288					3.496	3.651	3.476	3.628	3.413	3.565	3.335	3.487	3.278	3.429	3.225	3.375
298					3.569	3.726	3.551	3.703	3.488	3.640	3.410	3.562	3.353	3.504	3.300	3.450
308					3.648	3.801	3.626	3.778	3.563	3.715	3.485	3.637	3.428	3.579	3.375	3.525
318							3.700	3.852	3.637	3.789	3.559	3.711	3.502	3.653	3.449	3.599
328							3.773	3.925	3.710	3.862	3.632	3.784	3.575	3.726	3.522	3.672
338									3.783	3.935	3.705	3.857	3.648	3.799	3.595	3.745
348									3.855	4.007	3.777	3.929	3.720	3.871	3.667	3.817
358									3.926	4.078	3.848	4.000	3.791	3.942	3.738	3.888
368									3.996	4.137	3.918	4.059	3.861	4.001	3.808	3.948
378									4.065	4.193	3.981	4.117	3.930	4.060	3.877	4.007
388											4.055	4.175	3.998	4.118	3.945	4.065
398											4.122	4.232	4.065	4.175	4.012	4.122
408											4.181	4.287	4.130	4.230	4.078	4.178
418											4.235	4.342	4.195	4.285	4.143	4.233
428											4.314	4.396	4.259	4.339	4.208	4.288
438													4.323	4.393	4.272	4.342
448													4.386	4.446	4.336	4.396
458													4.449	4.499	4.399	4.449
468															4.462	4.512
478															4.524	4.574
488.30															4.577	4.627

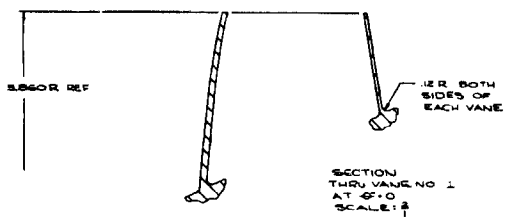

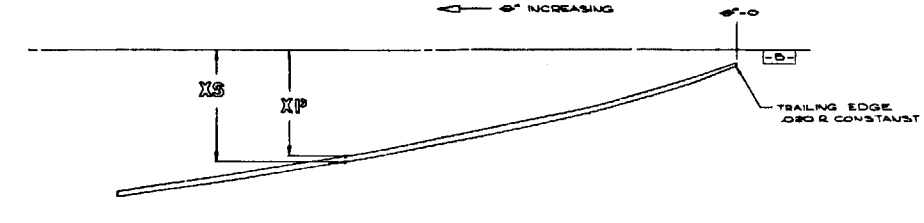

SCHEMATIC VANE DEVELOPMENT

SIZE	CAGE CODE NO.	DWG NO.
E	05824	55907

NOTES:
1. REMOVE ALL BURRS & SHARP EDGES EQUIVALENT TO .005-.015 R UNLESS OTHERWISE NOTED.
2. INTERPRET DRAWING PER MIL-D-1000.
3. CLASSIFICATION OF CHARACTERISTICS PER AGC-STD-49B2
4. ALL FILLET RADII TO BE .030 UNLESS OTHERWISE NOTED
5. ALL DIAMETERS Ⓐ A .001 Ⓢ UNLESS OTHERWISE NOTED
6. ALL TABULATED AIRFOIL DIMENSIONS ARE BASIC. VANE CONTOUR IS FORMED BY A SMOOTH FAIRING BETWEEN AIRFOIL SECTIONS WITHIN TOLERANCE BAND SHOWN.
7. SURFACE ROUGHNESS 63 UNLESS OTHERWISE NOTED
8. PENETRANT INSPECT PER AGC-STD-4B16 TYPE II ACCEPTANCE CRITERIA PER AGC-STD-4006 CLASS II.
9. CLEANLINESS PER AGC-46950, LEVEL H.
10. PRESERVE AND PACKAGE PER AGC-46987, CLASS 1.

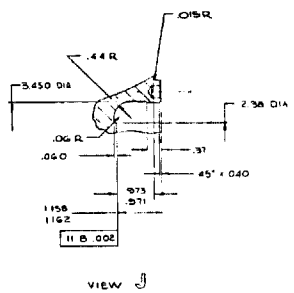

VIEW J

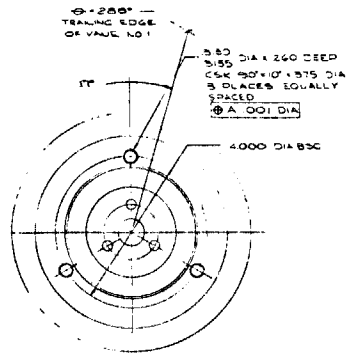

VIEW K = K ROTATED 55° CCW

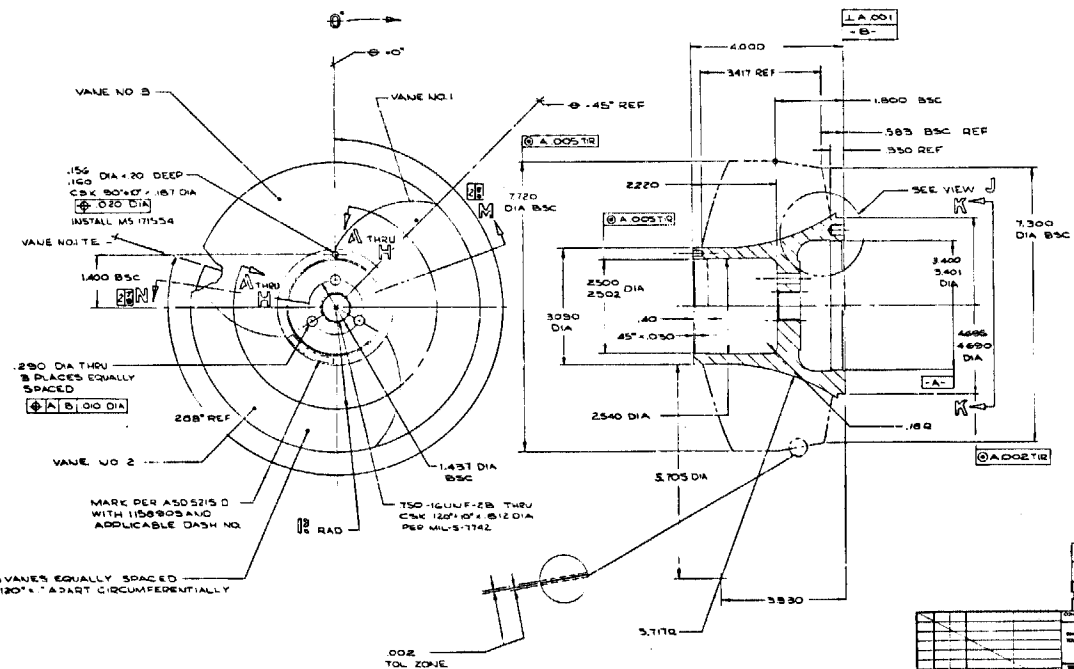

1	MS 171554	PU SPRING	
1	-1	1538906-1	

REDUCER, DUCT

SIZE E	05824	1538905

SCALE 1/2 SHEET 1 OF 2

⚠ SECTION A-A THRU H-H CO ORDINATES FOR RADIAL SECTIONS NEGLECTING FILLET RAD AT VANE ROOT & HUB INTERSECTION

θ°	SECTION A-A R = 1.545				SECTION B-B R = 1.930				SECTION C-C R = 2.310				SECTION D-D R = 2.500				SECTION E-E R = 2.950				SECTION F-F R = 3.420				SECTION G-G R = 3.650				SECTION H-H R = 3.860			
	X		Y		X		Y		X		Y		X		Y		X		Y		X		Y		X		Y		X		Y	
0°	3.768		3.788																													
10°	3.669		3.728	±.002	3.445	±.002	3.685	±.002																								
20°	3.568	±.002	3.673		3.546		3.616		3.516		3.561	±.002	3.498	±.002	3.538	±.002		±.002		±.002		±.002		±.002		±.002		±.002		±.002		±.002
30°	3.469		3.611		3.446		3.556		3.417		3.497		3.398		3.478		3.344		3.375													
40°	3.370		3.560		3.346		3.496		3.318		3.438		3.298		3.418		3.244		3.309		3.172		3.207		3.122		3.152					
50°	3.270	+.000	3.500		3.247		3.427		3.218		3.373		3.199		3.359		3.145		3.240		3.073		3.143		3.022		3.089		2.962		3.002	
60°	3.170	-.008	3.436		3.148		3.348		3.118		3.298		3.100		3.293		3.046		3.176		2.974		3.075		2.922		3.022		2.842		2.932	
70°	3.071		3.337		3.048		3.282		3.019		3.229		3.000		3.195		2.946		3.107		2.874		3.003		2.823		2.937		2.765		2.865	
80°	2.972		3.238	+.008	2.948		3.182		2.920		3.129		2.900		3.095		2.846		3.007		2.774		2.903		2.724		2.838		2.664		2.765	
90°	2.872		3.138	-.000	2.849		3.083		2.820		3.029		2.801		2.994		2.747		2.908		2.675		2.804		2.624		2.738		2.564		2.665	
100°	2.772		3.098		2.750	+.000	2.984	+.008	2.720	+.000	2.929	+.008	2.702	+.002	2.895	+.006	2.648	±.004	2.809	±.004	2.576	±.004	2.705	±.004	2.524	±.004	2.638	±.004	2.464	±.004	2.545	±.004
110°					2.650	-.008	2.884	-.000	2.621	-.008	2.830	-.000	2.602	-.006	2.795	-.002	2.548		2.709		2.476		2.605		2.424		2.538		2.365		2.446	
120°					2.550		2.784		2.522		2.731		2.502		2.695		2.448		2.609		2.374		2.505		2.320		2.434		2.264		2.345	
130°					2.450		2.684		2.422		2.631		2.402		2.595		2.346		2.507		2.272		2.401		2.216		2.330		2.161		2.242	
140°					2.350		2.584		2.323		2.532		2.302		2.495		2.244		2.405		2.169		2.298		2.112		2.226		2.057		2.158	
150°					2.250		2.484		2.224		2.433		2.202		2.395		2.142		2.303		2.065		2.194		2.008		2.122		1.955		2.054	
160°					2.150		2.385		2.124		2.333		2.102		2.296		2.039		2.200		1.961		2.090		1.904		2.018		1.851		1.952	
170°					2.050		2.286		2.024		2.233		1.997		2.192		1.934		2.096		1.855		1.985		1.800		1.914		1.749		1.850	
180°					1.948		2.185		1.915		2.125		1.891		2.084		1.828		1.990		1.751		1.880		1.696		1.810		1.647		1.748	
190°					1.842		2.081		1.806		2.016		1.784		1.981		1.720		1.885		1.646		1.775		1.594		1.708		1.545		1.646	
200°					1.726		1.967		1.694		1.905		1.674		1.872		1.612		1.775		1.540		1.669		1.490		1.604		1.448		1.544	
210°					1.608		1.851		1.519		1.792		1.560		1.759		1.502		1.666		1.433		1.562		1.386		1.500		1.341		1.442	
220°					1.478		1.723		1.454		1.669		1.434		1.634		1.388		1.562		1.328		1.462		1.279		1.393		1.236		1.337	
230°					1.330		1.577		1.321		1.538		1.315		1.514		1.269		1.434		1.210		1.339		1.170		1.284		1.131		1.232	
240°									1.180		1.399		1.174		1.375		1.144		1.309		1.095		1.224		1.061		1.175		1.026		1.127	
250°									1.030		1.253		1.027		1.230		1.010		1.176		.976		1.105		.952		1.066		.925		1.024	
260°									.872		1.067		.872		1.067		.870		1.036		.856		.985		.843		.957		.826		.927	
270°									.690		.815		.701		.821		.724		.844		.734		.844		.735		.900		.736		.846	
280°									.500		.540		.519		.599		.568		.648		.612		.692		.625		.705		.648		.728	
288°													.375		.413		.443		.485		.515		.555		.553		.593		.585		.623	

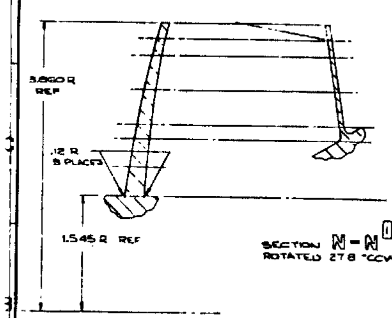

SECTION N-N THRU VANE NO.1 ROTATED 27.8 °CCW

SECTION M-M THRU VANE NO.1 ROTATED 70 °CCW

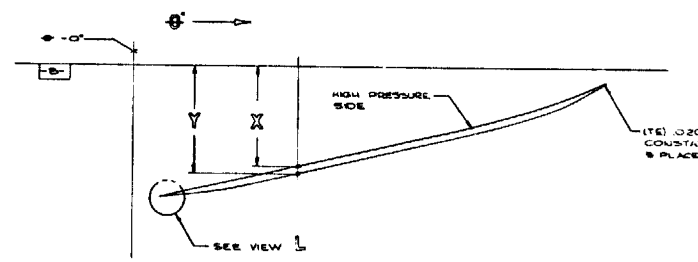

SCHEMATIC VANE DEVELOPMENT

VIEW L SCALE: NONE 3 PLACES

E 05824

NOTES

1. REMOVE ALL BURRS AND SHARP EDGES EQUIVALENT TO .005-.015 R UNLESS OTHERWISE NOTED.
2. INTERPRET DRAWING PER MIL-D-1000.
3. CLASSIFICATION OF CHARACTERISTICS PER AGC-STD-6882
4. SURFACE ROUGHNESS 63 UNLESS OTHERWISE NOTED.
5. ALL DIMENSIONS APPLY AFTER ANODIZING.
6. MOLTEN FLUX BRAZE PER MIL-B-7383, TYPE T. BRAZE JOINT TO BE .002 MAX IN INDICATED AREA.
7. HEAT TREAT, AFTER BRAZING, PER MIL-H-6088 TEMP T6.
8. MATERIAL MAY BE REMOVED ONLY FROM INDICATED SURFACES TO A MAX DEPTH OF .050 FOR BALANCING.
9. STATIC BALANCE TO WITHIN .02 OZ IN OF UNBALANCE.
10. DYNAMIC BALANCE TO WITHIN .02 OZ IN^2 OF UNBALANCE.
11. ANODIZE ALL SURFACES OF -3 PER MIL-A-8625 TYPE I, CLASS 1.
12. MARK PER ASD5215-D WITH LISMR13 AND APPLICABLE DASH NO.
13. CLEANLINESS PER AGC-66350 LEVEL H.
14. PRESERVE AND PACKAGE PER AGC-66387, CLASS 1.
15. BRAZE ALLOY FILLETS SHALL BE VISIBLE FOR 100% OF THE EXPOSED AREAS FOR SHROUD TO ROTOR JOINT.
16. PENETRANT INSPECT BRAZE PER MIL-I-6866 TYPE I OR II, METHOD A, ACCEPTANCE CRITERIA PER AGC-STD-6006, CLASS LEI.
17. ALL TABULATED AIRFOIL DIMENSIONS ARE BASIC. VANE CONTOUR IS FORMED BY A SMOOTH FAIRING BETWEEN SECTIONS WITHIN TOLERANCE BAND SHOWN.

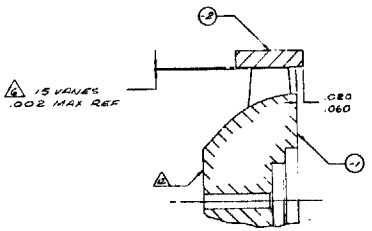

-3 ASSY
SCALE: NONE

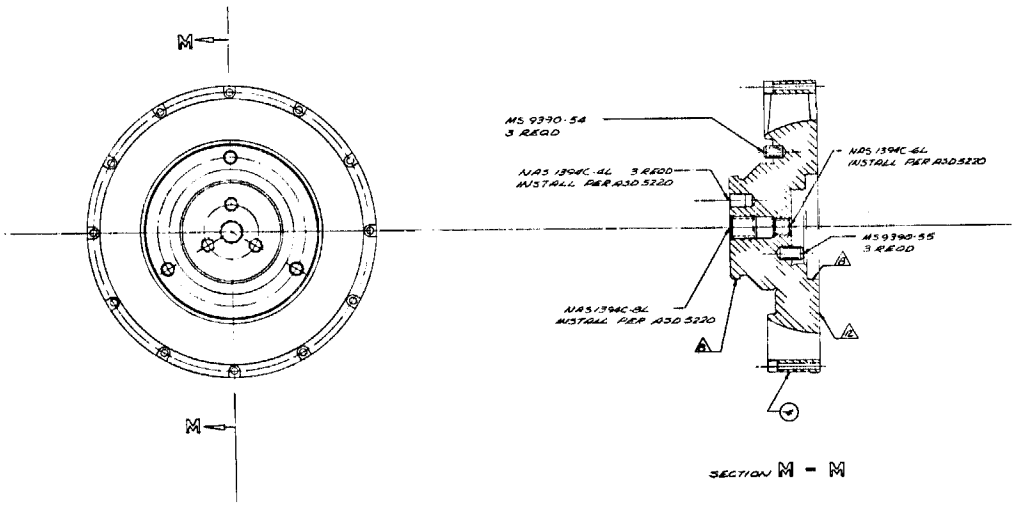

SECTION M - M

-9 ASSY

5		MS9390-55	DOWEL PIN	
3		MS9390-54	DOWEL PIN	
1		NAS1396C-6L	INSERT	
1		NAS1396C-8L	INSERT	
3		NAS1396C	INSERT	
1		-4	ROTOR	-3
AR			BRAZE ALLOY	AMS 4185
1		-2	SHROUD	AL ALLOY 6061 PER QQ-A-250/11 TEMPER T651
1		-1	ROTOR	1158906-3

		ROTOR, PUMP TRANSITION	
	E	05824	1158913

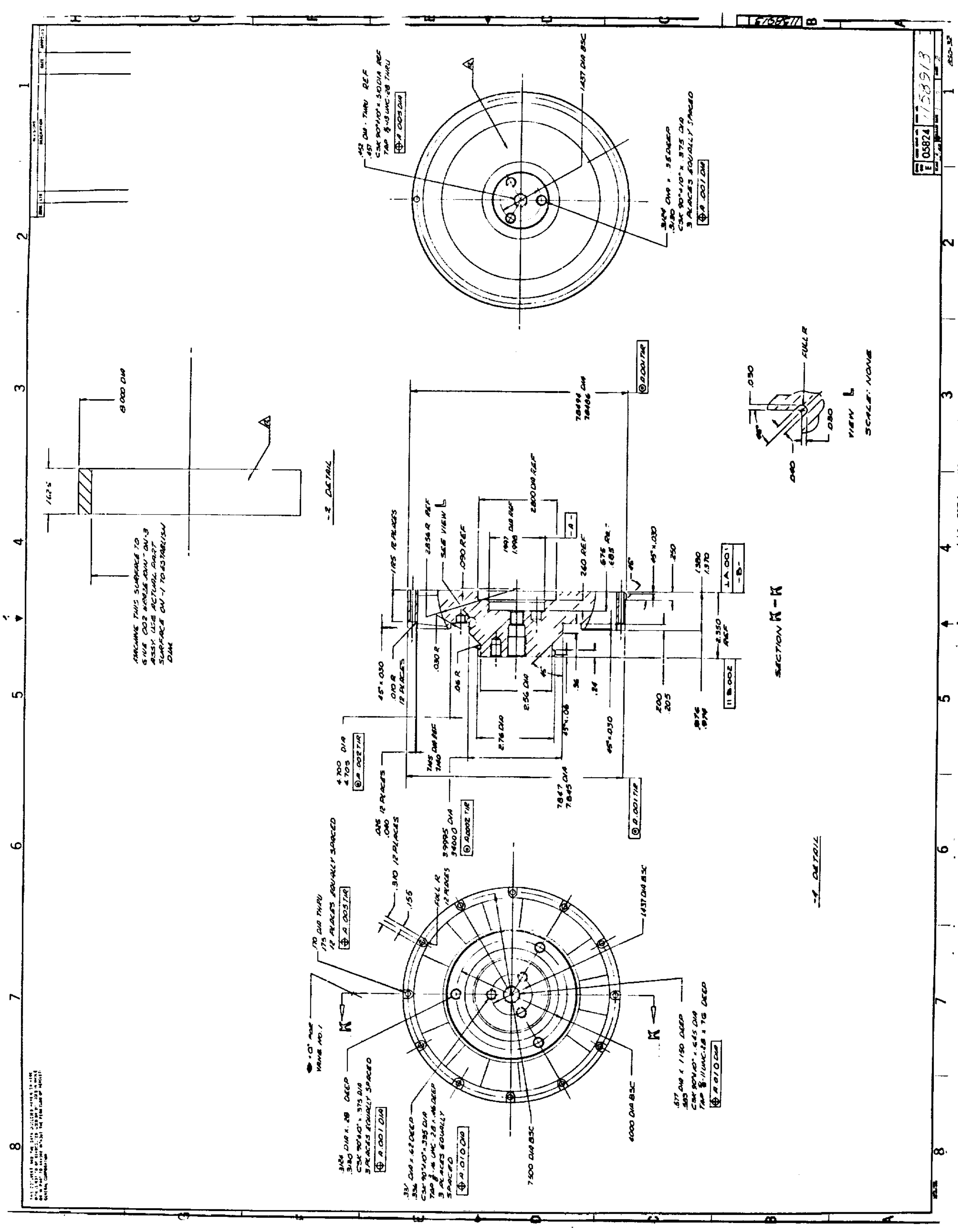
SECTION K-K
VIEW L
SCALE: NONE
-1 DETAIL
-2 DETAIL

△ SECTION A-A THRU H-H COORDINATES ARE RADIAL SECTIONS NEGLECTING FILLET RAD AT VANE POST & TIME INTERSECTION

θ	SECTION A-A R-2.620 XP	SECTION A-A R-2.620 XS	SECTION B-B R-2.830 XP	SECTION B-B R-2.830 XS	SECTION C-C R-3.000 XP	SECTION C-C R-3.000 XS	SECTION D-D R-3.140 XP	SECTION D-D R-3.140 XS	SECTION E-E R-3.280 XP	SECTION E-E R-3.280 XS	SECTION F-F R-3.430 XP	SECTION F-F R-3.430 XS	SECTION G-G R-3.570 XP	SECTION G-G R-3.570 XS
+22°														
+20°	.163 +.005	.200 +.005												
+18°	.226 +.005	.291 +.005	.232 +.000 -.005	.282 +.000 -.005	.242 +.005 -.000	.282 +.005 -.000	.335 +.000 -.005	.242 +.000 -.005	.277 +.005 -.000	.325 +.005 -.000	.233 +.005 -.000	.267 +.000 -.005	.243 +.000 -.005	.297 +.005 -.000
+16°	.288	.377	.294	.370	.302	.370	.328	.356	.340	.416	.303	.370	.322	.406
+14°	.350	.459	.355	.453	.367	.453	.398	.482	.402	.501	.371	.464		
+12°	.412	.536	.414	.530	.420	.530	.468	.522	.464	.581	.437	.552	.397	.507
+10°	.471	.608	.472	.603	.477	.603	.476	.597	.525	.655	.502	.632	.470	.601
+8°	.529	.676	.530	.672	.534	.672	.532	.667	.580	.724	.566	.709	.542	.687
+6°	.585	.740	.586	.736	.589	.736	.588	.732	.637	.787	.628	.778	.613	.765
+4°	.641	.800	.642	.796	.643	.795	.642	.792	.698	.846	.690	.843	.682	.838
+2°	.696	.856	.696	.852	.695	.850	.696	.849	.748	.900	.749	.903	.749	.906
0°	.750 +.000 -.010	.909 +.010 -.000	.748 +.000 -.010	.905 +.010 -.000	.747 +.000 -.010	.902 +.010 -.000	.748 +.000 -.010	.900 +.010 -.000	.749 +.000 -.010	.900 +.010 -.000	.749 +.000 -.010	.903 +.010 -.000	.749 +.000 -.010	.906 +.010 -.000
-2°	.802	.959	.800	.953	.798	.951	.800	.949	.801	.951	.801	.958	.814	.967
-4°	.854	1.005	.852	.999	.849	.996	.851	.994	.854	.997	.849	1.007	.878	1.022
-6°	.905	1.049	.902	1.042	.899	1.038	.901	1.035	.905	1.040	.919	1.052	.940	1.073
-8°	.956	1.090	.951	1.082	.948	1.076	.949	1.073	.956	1.079	.973	1.094	1.000	1.119
-10°	1.008	1.128	.999	1.118	.995	1.110	.996	1.107	1.005	1.114	1.026	1.131	1.039	1.161
-12°	1.051	1.163	1.046	1.152	1.041	1.142	1.042	1.138	1.052	1.145	1.071 +.000 -.005	1.164 +.005 -.000	1.117 +.000 -.005	1.198 +.005 -.000
-14°	1.098	1.195	1.092	1.189	1.087	1.172	1.088 +.000 -.005	1.167 +.005 -.000	1.099 +.001 -.005	1.173 +.005 -.000	1.128	1.193	1.173	1.250
-16°	1.144	1.226	1.137	1.211 +.005 -.000	1.132 +.000 -.005	1.190 +.005 -.000	1.132	1.193	1.145	1.197	1.178	1.220	1.227	1.258
-18°	1.188 +.000 -.005	1.259 +.005 -.000	1.182 +.000 -.005	1.236	1.176	1.222	1.175	1.215	1.190	1.219				
-20°	1.232	1.279	1.227	1.260	1.219	1.262								
-22°	1.275	1.301												
LE θLE	-22.732		-21.369		-20.586		-19.592		-18.770		-17.857		-16.956	
LE XLE	1.300		1.264		1.236		1.219		1.218		1.231		1.262	
TE θTE	+20.782		+19.369		+19.022		+18.344		+17.568		+16.651		+15.667	
TE XTE	.146		.186		.219		.256		.257		.221		.186	

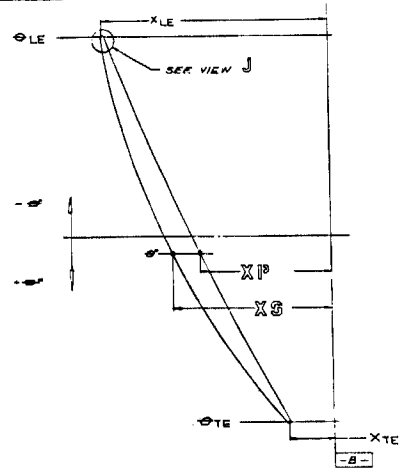

SCHEMATIC VANE DEVELOPMENT

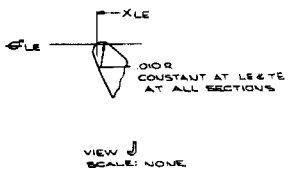

VIEW J
SCALE: NONE

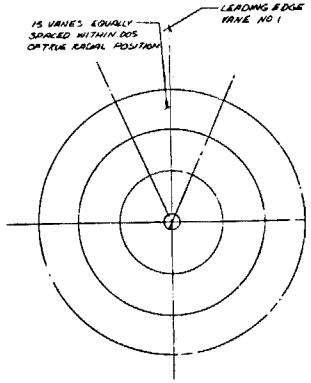

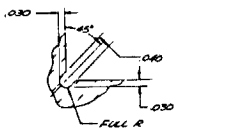

VIEW H
SCALE: NONE

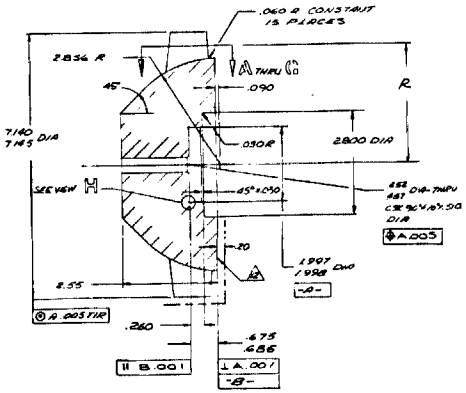

DETAIL

E 05824 52915

850-32

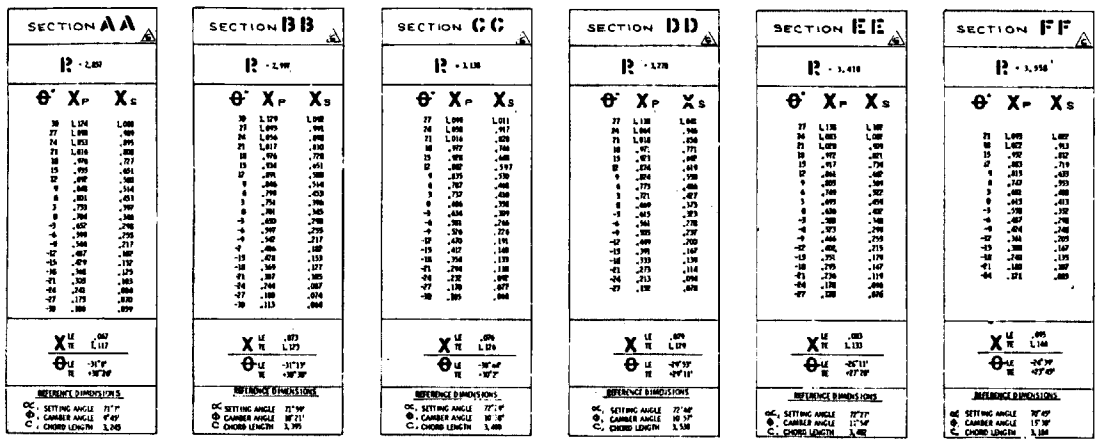

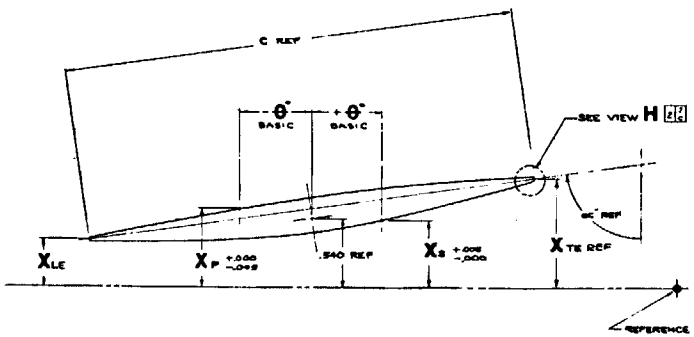

SECTION AA THRU FF

SCALE: NONE

11 VANES EQUALLY SPACED

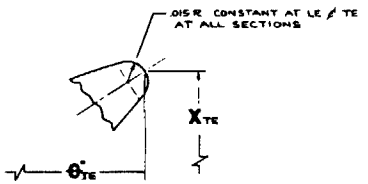

VIEW H

SCALE: NONE

SIZE F	05824	1160008

SSC 321

NOTES:

1. REMOVE ALL BURRS AND SHARP EDGES.
2. INTERPRET DRAWING PER MIL-STD-100 AND MIL-D-1000 FORM 2.
3. CLASSIFICATION OF CHARACTERISTICS PER AGC-STD-4002.
4. SURFACE ROUGHNESS 63 UNLESS OTHERWISE NOTED, -2 ONLY.
5. ALL DIA TO BE ⌖ .001 M A B UNLESS OTHERWISE NOTED.
6. ALL TABULATED AIRFOIL DIMENSIONS ARE TOLERANCED AS NOTED. VANE CONTOUR IS FORMED BY A SMOOTH FAIRING BETWEEN AIRFOIL SECTIONS WITHIN TOLERANCE SPECIFIED.
7. PENETRANT INSPECT PER MIL-I-6866, TYPE I, METHOD A. ACCEPTANCE CRITERIA PER AGC-STD-4006, CLASS II.
8. STATIC BALANCE TO WITHIN .020 OZ IN. OF UNBALANCE.
9. DYNAMIC BALANCE TO WITHIN .020 OZ IN^2 OF UNBALANCE.
10. MATERIAL MAY BE REMOVED ONLY FROM INDICATED AREAS FOR BALANCING.
11. CLEANLINESS PER AGC-66350, LEVEL N.
12. PRESERVE AND PACKAGE PER AGC-66307, CLASS E.
13. FORGING SHALL ALLOW FOR .25 MIN CLEANUP ON ALL SURFACES.
14. ANODIZE ALL SURFACES OF -2 PART PER MIL-A-8625, TYPE I, CLASS 1.
15. ULTRASONIC INSPECT PER AGC-STD 4019. ACCEPTANCE CRITERIA PER AGC-STL-4006 CLASS II.
16. SURFACE ROUGHNESS 125 -1 ONLY.
17. MARK FORGING PER AS9215-C WITH FORG 1160008-1, FORGE SHOP SYMBOL, AND QUALITY ACCEPTANCE STAMPS.

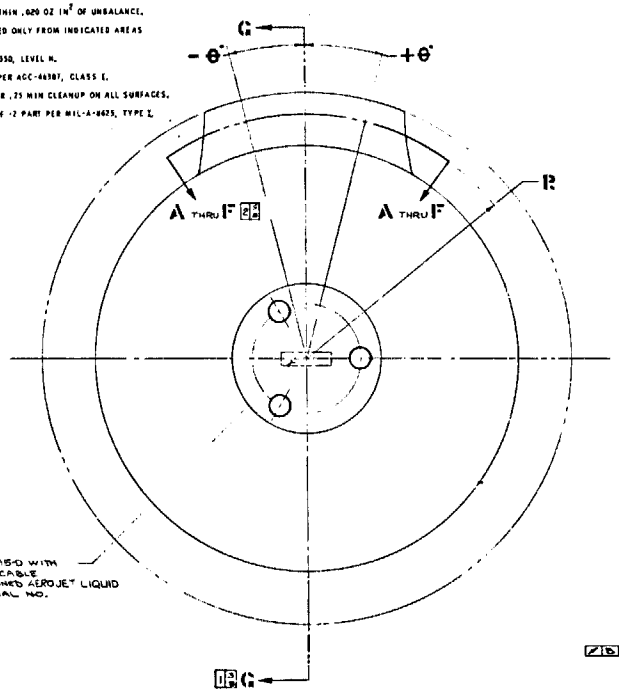

MARK PER ASD 52150 WITH 1160008 IF APPLICABLE DASH NO. & ASSIGNED AEROJET LIQUID ROCKET CO. SERIAL NO.

DIRECTION OF ROTATION

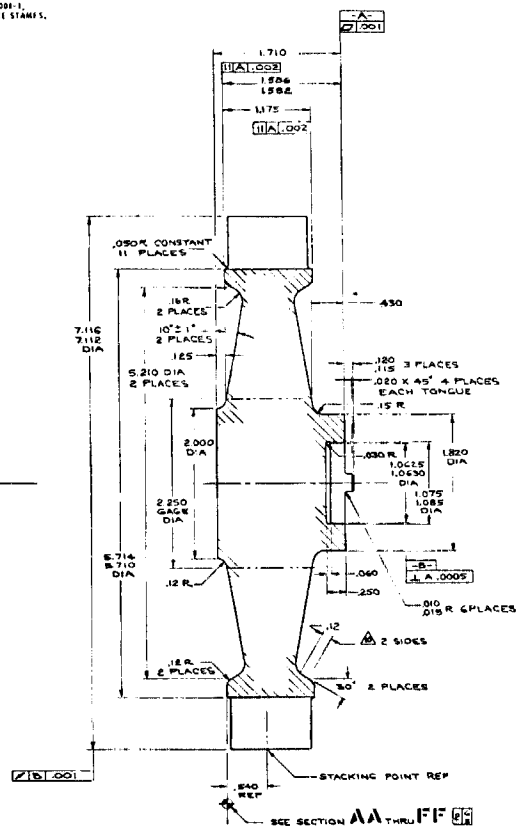

SECTION GG

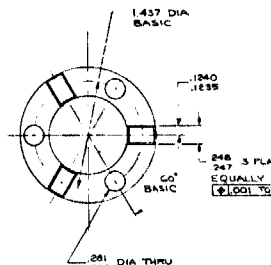

-2	MAKE FROM -1 FORGING	
-1	FORGING	AL ALLOY 7075 MIL-A-22771 TYPE 7075-T652

DRAWN	L.J. BRERETON
TITLE	PUMP ROTOR, HIGH SPEED
SIZE	E
CAGE CODE	05824
DRAWING NO.	1160008

1160008

950-32 1

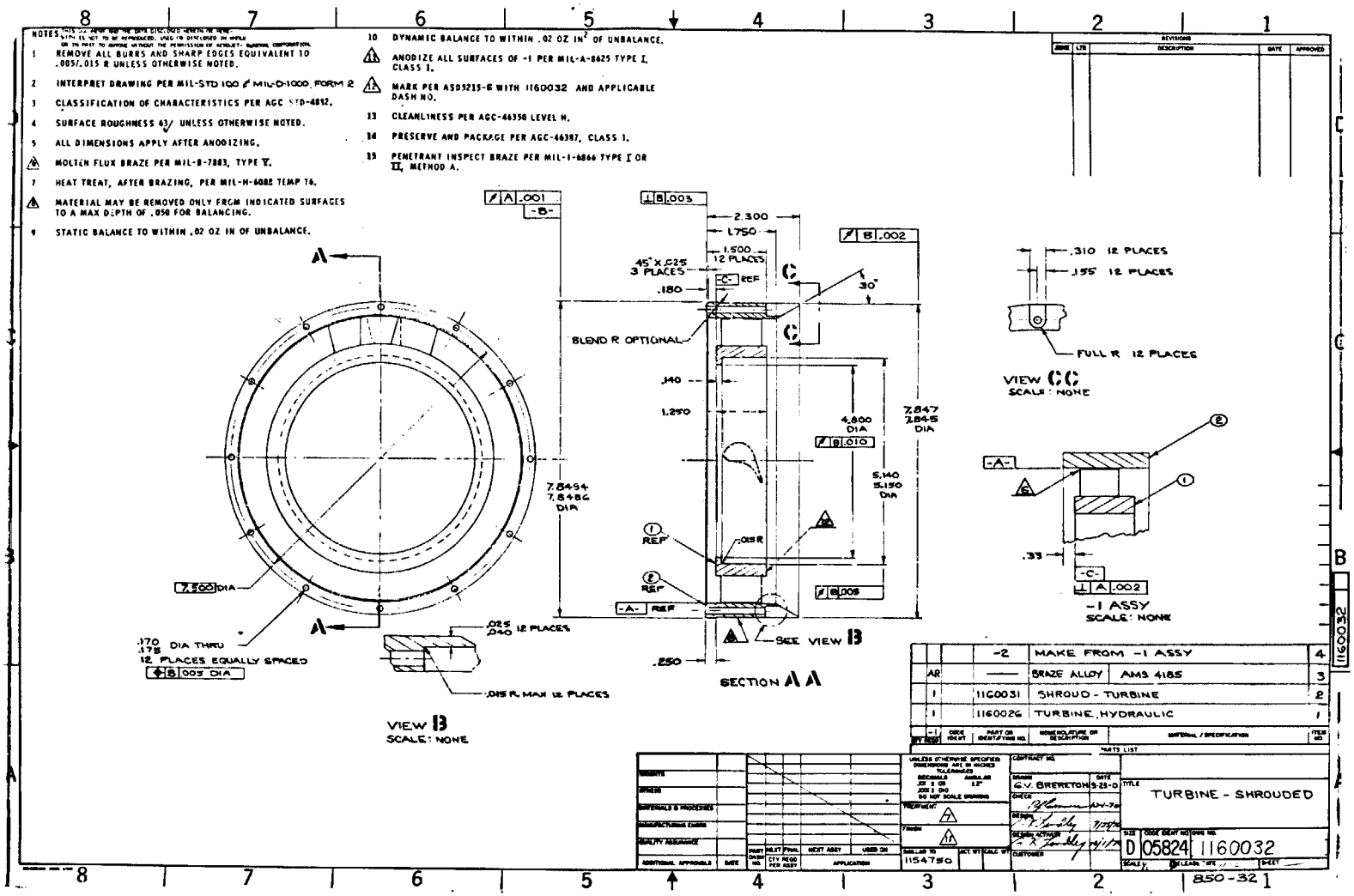
NOTES
1 REMOVE ALL BURRS AND SHARP EDGES EQUIVALENT TO .005/.015 R UNLESS OTHERWISE NOTED.
2 INTERPRET DRAWING PER MIL-STD 100 & MIL-D-1000, FORM 2
3 CLASSIFICATION OF CHARACTERISTICS PER AGC STD-4812.
4 SURFACE ROUGHNESS 63 UNLESS OTHERWISE NOTED.
5 ALL DIMENSIONS APPLY AFTER ANODIZING.
6 MOLTEN FLUX BRAZE PER MIL-B-7883, TYPE Y.
7 HEAT TREAT, AFTER BRAZING, PER MIL-H-6088 TEMP T6.
8 MATERIAL MAY BE REMOVED ONLY FROM INDICATED SURFACES TO A MAX DEPTH OF .050 FOR BALANCING.
9 STATIC BALANCE TO WITHIN .02 OZ IN OF UNBALANCE.
10 DYNAMIC BALANCE TO WITHIN .02 OZ IN² OF UNBALANCE.
11 ANODIZE ALL SURFACES OF -1 PER MIL-A-8625 TYPE I, CLASS 1.
12 MARK PER ASD5215-E WITH 1160032 AND APPLICABLE DASH NO.
13 CLEANLINESS PER AGC-46350 LEVEL H.
14 PRESERVE AND PACKAGE PER AGC-46387, CLASS 1.
15 PENETRANT INSPECT BRAZE PER MIL-I-6866 TYPE I OR II, METHOD A.
REVISIONS
ZONE LTR DESCRIPTION DATE APPROVED
A .001 -B-
B .003
2.300
1.750
1.500 12 PLACES
45° X .025 3 PLACES
C REF
.180
30°
B .002
BLEND R OPTIONAL
.140
1.250
4.600 DIA
B .010
7.847 7.845 DIA
5.140 5.150 DIA
7.849 7.848 DIA
1 REF
2 REF
-A- REF
.015 R
B .005
7.500 DIA
.170 .175 DIA THRU 12 PLACES EQUALLY SPACED
B .005 DIA
.025 .040 12 PLACES
.015 R MAX 12 PLACES
.250
SECTION A-A
SEE VIEW B
VIEW B
SCALE: NONE
.310 12 PLACES
.155 12 PLACES
FULL R 12 PLACES
VIEW C-C
SCALE: NONE
-A-
-C-
A .002
.33
-1 ASSY
SCALE: NONE
-2 MAKE FROM -1 ASSY 4
AR — BRAZE ALLOY AMS 4185 3
1 1160031 SHROUD - TURBINE 2
1 1160026 TURBINE, HYDRAULIC 1
PARTS LIST
CONTRACT NO.
DRAWN G.V. BRERETON 5-23-0
CHECK
DESIGN
DESIGN ACTIVITY
CUSTOMER
TITLE TURBINE - SHROUDED
SIZE D
CODE IDENT NO. 05824
DWG NO. 1160032
SCALE
RELEASE DATE
SHEET
1154750
850-32
1160032

DISTRIBUTION LIST

	Copies
National Aeronautics and Space Administration Lewis Research Center 21000 Brookpark Road Cleveland, Ohio 44135	
Attention: Contracting Officer. MS 500-313	1
Project Manager , MS 5-9	15
Technical Report Control Office, MS 5-5	1
Technology Utilization Office, MS 3-16	1
AFSC Liaison Office, MS 4-1	2
Library	2
I.A. Johnsen , MS 500-205	1
Fluid Systems Components Division, MS 5-3	3
W. R. Britsch, MS 5-9	1
National Aeronautics and Space Administration Washington, D.C. 20546	
Attention: Code MT	1
RPX	2
RPL	2
SV	1
Scientific and Technical Information Facility P.O. Box 33 College Park, Maryland 20740	
Attention: NASA Representative Code CRT	6
National Aeronautics and Space Administration Ames Research Center Moffett Field, California 94035	
Attention: Library	1
C. A. Syvertson	1
National Aeronautics and Space Administration Flight Research Center P.O. Box 273 Edwards, California 93523	
Attention: Library	1
National Technical Information Service Springfield, Virginia 22151	20

DISTRIBUTION LIST (cont.)

	Copies
National Aeronautics and Space Administration Goddard Space Flight Center Greenbelt, Maryland 20771	
Attention: Library	1
National Aeronautics and Space Administration John F. Kennedy Space Center Cocoa Beach, Florida 32931	
Attention: Library	1
National Aeronautics and Space Administration Langley Research Center Langley Station Hampton, Virginia 23365	
Attention: Library	1
National Aeronautics and Space Administration Manned Spacecraft Center Houston, Texas 77001	
Attention: Library	1
National Aeronautics and Space Administration George C. Marshall Space Flight Center Huntsville, Alabama 35812	
Attention: Library	1
Keith Chandler, R-P & VE-PA	1
Loren Gross, R-P & VE-PAC	1
Jet Propulsion Laboratory 4800 Oak Grove Drive Pasadena, California 91103	
Attention: Library	1
Henry Burlage	1
Office of the Director of Defense Research & Engineering Washington, D.C. 20301	
Attention: Office of Assistant Director	1

REFERENCES

1. Sabiers, R.L., Stek, J.B., Boost Pumps Design Criteria Monograph, Contract NAS 3-11176, AGC 9400-8 (Conf.), February 1968

2. Jekat, W.A., The Worthington Inducer, NAS 8-2680, February 1964

3. Farquhar, J., Lindley, B.K., McKinney, E.B., Olson, G.K., Buckman, P.S., Inducer Dynamics Full-Flow, Full-Admission Hydraulic Turbine Drive, NASA CR-72566, August 1969

4. Farquhar, J. and Lindley, B.K., Hydraulic Design of the M-1 Liquid Hydrogen Turbopump, NASA CR-54822, 15 July 1966

5. Farquhar, J., Viteri, F., Axial Flow Pumps, Design Criteria Monograph, Contract NAS 3-10293, AGC 9400-6 Rev. 1, July 1968

6. Taylor, W.E., Murrin, T.A., Colombo, R.M., Systematic Two-Dimensional Cascade Testing Vol. 1 - Double Circular-Arc Hydrofoils, NASA CR-72498, December 1969

7. Cunnan, W.S., Kovich, G., Reemsnyder, D.C., Effect of Fluid Temperature on the Cavitation Performance of a High Hub-Tip Ratio Axial Flow Pump in Water to 250°F (394 K), NASA TN D-5318, July 1969

8. Crouse, J.E., Soltis, R.F., and Montgomery, J.C., Investigation of the Performance of an Axial Flow-Pump Stage Designed by the Blade Element Theory, NASA TN D-1109, December 1966

9. Crouse, J.E. and Sandercock, D.M., Design and Over-all Performance of an Axial-Flow Pump Rotor with a Blade Tip Diffusion Factor of 0.43, NASA TN D-2295, May 1964

10. Miller, M.J. and Crouse, J.E., Design and Over-all Performance of an Axial-Flow Pump Rotor with a Blade Tip Diffusion Factor of 0.66, NASA TN D-3024, September 1965

11. Crouse, J.E., and Sandercock, D.M., Blade Element Performance of Two-Stage Axial-Flow Pump with Tandem-Row Inlet Stage, NASA TN-3962, May 1967

12. Stripling, L.B., "Cavitation in Turbopumps - Part 2," Trans. ASME, Journal of Basic Engineering, Vol. 84, 1962, pp. 339-350

13. Jakobsen, J.K., Design Criteria Monograph Pump Inducers, Rocketdyne Report R-7422, NAS 3-11180, March 1968

References (cont.)

14. Crouse, J.F., Sandercock, D.M., Design and Overall Performance of a Two-Stage Axial-Flow Pump with a Tandem-Row Inlet Stage, NASA TN D-2874, June 1965

15. Moore, R.D., Meng, P.K., Effect of Blade Leading Edge Thickness on Cavitation Performance of 80.6° Helical Inducer in Hydrogen, NASA TN D-6855, June 1970

16. Anderson, D.A., Soltis, R.F., and Sandercock, D.M., Performance of 84° Flat-Plate Helical Inducer and Comparison with Performance of Similar 78° and 80.6° Inducers, NASA TN D-2553, December 1964

17. Sandercock, D.M., Soltis, R.F., and Anderson, D.A., Investigation of the Performance of a 78° Flat-Plate Helical Inducer, NASA TN D-1170, March 1962

18. Sandercock, D.M., Soltis, R.F., and Anderson, D.A., Cavitation and Non-Cavitation Performance of an 80.6° Flat-Plate Helical Inducer at Three Rotational Speeds, NASA TN D-1439, November 1962.

19. Miller, M.J., Sandercock, D.M., Blade Element Performance of Axial-Flow Pump Rotor with Tip Diffusion Factor of 0.66, NASA TN D-3602, September 1962

20. Vavra, M.H., Investigation of Axial Stage, ASME 68-FE-51, Presented at Fluids Engineering Conference, Philadelphia, Pa., May 6-9, 1968

21. Kovich, G., Comparison of Predicted and Experimental Cavitation Performance of 84° Helical Inducer in Water and Hydrogen, NASA TN D-7016, December 1970

22. Urasek, D.C., Design and Performance of a 0.9-Hub-Tip-Ratio Axial-Flow Pump Rotor with Blade-Tip Diffusion Factor of 0.63, NASA TMX-2235, March 1971

DISTRIBUTION LIST

		Copies
National Aeronautics and Space Administration Lewis Research Center 21000 Brookpark Road Cleveland, Ohio 44135		
Attention:	Contracting Officer, MS 500-313	1
	Project Manager , MS 5-9	15
	Technical Report Control Office, MS 5-5	1
	Technology Utilization Office, MS 3-16	1
	AFSC Liaison Office, MS 4-1	2
	Library	2
	I.A. Johnsen , MS 500-205	1
	Fluid Systems Components Division, MS 5-3	3
	W. R. Britsch, MS 5-9	1
National Aeronautics and Space Administration Washington, D.C. 20546		
Attention:	Code MT	1
	RPX	2
	RPL	2
	SV	1
Scientific and Technical Information Facility P.O. Box 33 College Park, Maryland 20740		
Attention:	NASA Representative Code CRT	6
National Aeronautics and Space Administration Ames Research Center Moffett Field, California 94035		
Attention:	Library	1
	C. A. Syvertson	1
National Aeronautics and Space Administration Flight Research Center P.O. Box 273 Edwards, California 93523		
Attention:	Library	1
National Technical Information Service Springfield, Virginia 22151		20

DISTRIBUTION LIST (cont.)

	Copies
National Aeronautics and Space Administration Goddard Space Flight Center Greenbelt, Maryland 20771	
Attention: Library	1
National Aeronautics and Space Administration John F. Kennedy Space Center Cocoa Beach, Florida 32931	
Attention: Library	1
National Aeronautics and Space Administration Langley Research Center Langley Station Hampton, Virginia 23365	
Attention: Library	1
National Aeronautics and Space Administration Manned Spacecraft Center Houston, Texas 77001	
Attention: Library	1
National Aeronautics and Space Administration George C. Marshall Space Flight Center Huntsville, Alabama 35812	
Attention: Library	1
Keith Chandler, R-P & VE-PA	1
Loren Gross, R-P & VE-PAC	1
Jet Propulsion Laboratory 4800 Oak Grove Drive Pasadena, California 91103	
Attention: Library	1
Henry Burlage	1
Office of the Director of Defense Research & Engineering Washington, D.C. 20301	
Attention: Office of Assistant Director	1

DISTRIBUTION LIST (cont.)

	Copies
Defense Documentation Center Cameron Station Alexandria, Virginia 22314	1
RTD(RTNP) Bolling Air Force Base Washington, D.C. 20332	1
Arnold Engineering Development Center Air Force Systems Command Tullahoma, Tennessee 37389	
Attention: AEOIM	1
Advanced Research Projects Agency Washington, D.C. 20525	
Attention: D. E. Mock	1
Aeronautical Systems Division Air Force Systems Command Wright-Patterson Air Force Base, Dayton, Ohio 45433	
Attention: D. L. Schmidt, Code ASRCNC-2	1
Air Force Missile Test Center Patrick Air Force Base, Florida 32925	
Attention: L. J. Ullian	1
Air Force Systems Command (SCLT/Capt. S. W. Bowen) Andrews Air Force Base Washington, D.C. 20332	1
Air Force Rocket Propulsion Laboratory (RPR) Edwards, California 93523	1
Air Force FTC (FTAT-2) Edwards Air Force Base, California 93523	1

DISTRIBUTION LIST (cont.)

	Copies
Air Force Office of Scientific Research Washington, D.C. 20333	
Attention: SREP, Dr. J. F. Masi	1
Office of Research Analyses (OAR) Holloman Air Force Base, New Mexico 88330	
Attention: RRRT	1
Major R. E. Brocken, Code MDGRT	1
Commanding Officer U.S. Army Research Office (Durham) Box CM, Duke Station Durham, North Carolina 27706	1
U.S. Army Missile Command Redstone Scientific Information Center Redstone Arsenal, Alabama 35808	
Attention: Chief, Document Section	1
Dr. W. Wharton	1
Bureau of Naval Weapons Department of the Navy Washington, D.C. 20360	
Attention: J. Kay, Code RTMS-41	1
Commander U.S. Naval Missile Center Point Mugu, California 93041	
Attention: Technical Library	1
Commander U.S. Naval Ordnance Test Station China Lake, California 93557	
Attention: Code 45	1
Code 753	1

DISTRIBUTION LIST (cont.)

	Copies
Commanding Officer Office of Naval Research 1030 E. Green Street Pasadena, California 91101	1
Director (Code 6180) U.S. Naval Research Laboratory Washington, D.C. 20390 Attention: H. W. Carhart	1
Picatinny Arsenal Dover, New Jersey 07801 Attention: I. Forsten, Chief Liquid Propulsion Laboratory	1
Air Force Aero Propulsion Laboratory Research & Technology Division Air Force Systems Command United States Air Force Wright-Patterson AFB, Ohio 45433 Attention: APRP (C. M. Donaldson)	1
Aerojet-General Corporation P.O. Box 296 Azusa, California 91703 Attention: Librarian	1
Aerojet-General Corporation 11711 South Woodruff Avenue Downey, California 90241 Attention: F. M. West, Chief Librarian	1
Aerojet-General Corporation P.O. Box 1947 Sacramento, California 95809 Attention: Technical Library 2484-2015A	1

DISTRIBUTION LIST (cont.)

	Copies
Aeronutronic Division of Philco Corporation Ford Road Newport Beach, California 92600	
Attention: Dr. L. H. Linder, Manager	1
Technical Information Department	1
Aerospace Corporation P.O. Box 95085 Los Angeles, California 90045	
Attention: Library-Documents	1
Arthur D. Little, Inc. Acorn Park Cambridge, Massachusetts 02140	
Attention: A. C. Tobey	1
ARO, Incorporated Arnold Engineering Development Center Arnold AF Station, Tennessee 37389	
Attention: Dr. B. H. Goethert Chief Scientist	1
Battelle Memorial Institute 505 King Avenue Columbus, Ohio 43201	
Attention: Report Library, Room 6A	1
Bell Aerosystems, Inc. Box 1 Buffalo, New York 14205	
Attention: Library	1
The Boeing Company Aero Space Division P.O. Box 3707 Seattle, Washington 98124	
Attention: Ruth E. Peerenboom (1190)	1

DISTRIBUTION LIST (cont.)

	Copies
Chemical Propulsion Information Agency Applied Physics Laboratory 8621 Georgia Avenue Silver Spring, Maryland 20910	1
Chrysler Corporation Space Division New Orleans, Louisiana 70150	
Attention: Librarian	1
Curtiss-Wright Corporation Wright Aeronautical Division Woodridge, New Jersey 07075	
Attention: G. Kelley	1
University of Denver Denver Research Institute P.O. Box 10127 Denver, Colorado 80210	
Attention: Security Office	1
Douglas Aircraft Company, Inc. Santa Monica Division 3000 Ocean Park Blvd. Santa Monica, California 90405	
Attention: Library	1
Fairchild Stratos Corporation Aircraft Missiles Division Hagerstown, Maryland 20740	
Attention: J. S. Kerr	1
General Dynamics/Astronautics P.O. Box 1128 San Diego, California 92112	
Attention: Library & Information Services (128-00)	1

DISTRIBUTION LIST (cont.)

	Copies
Convair Division General Dynamics Corporation P.O. Box 1128 San Diego, California 92112 Attention: Mr. W. Fenning Centaur Resident Project Office	1
General Electric Company Flight Propulsion Lab. Department Cincinnati, Ohio 45215 Attention: D. Suichu	1
Grumman Aircraft Engineering Corporation Bethpage, Long Island New York 11714 Attention: Joseph Gavin	1
IIT Research Institute Technology Center Chicago, Illinois 60616 Attention: Library	1
Kidde Aero Space Division Walter Kidde & Company, Inc. 675 Main Street Belleville, New Jersey 07109 Attention: R. J. Hanville, Director of Research Engineering	1
Lockheed Missiles & Space Company P.O. Box 504 Sunnyvale, California 94088 Attention: Technical Information Center	1
Lockheed Propulsion Company P.O. Box 111 Redlands, California 92374 Attention: Miss Belle Berlad, Librarian	

DISTRIBUTION LIST (cont.)

	Copies
Lockheed Missiles & Space Company Propulsion Engineering Division (D. 55-11) 1111 Lockheed Way Sunnyvale, California 94087	1
Marquardt Corporation 16555 Saticoy Street Box 2013 - South Annex Van Nuys, California 91404	
Attention: Librarian	1
Purdue University Lafayette, Indiana 47907	
Attention: Technical Librarian	1
Rocketdyne, A Division of North American Rockwell Corporation 6633 Canoga Avenue Canoga Park, California 91304	
Attention: Library, Department 596-306	1
J.A. King , Dept. 596-115	1
Stanford Research Institute 333 Ravenswood Avenue Menlo Park, California 94025	
Attention: Thor Smith	1
TRW Systems, Incorporated One Space Park Redondo Beach, California 90200	
Attention: G. W. Elverum	1
STL Tech. Lib. Doc. Acquisitions	1
TRW, Incorporated TAPCO Division 23555 Euclid Avenue Cleveland, Ohio 44117	
Attention: P. T. Angell	1

DISTRIBUTION LIST (cont.)

	Copies
United Aircraft Corporation Corporation Library 400 Main Street East Hartford, Connecticut 06118	
Attention: Library	1
Frank Owen	1
W. E. Taylor	1
United Aircraft Corporation Pratt and Whitney Division Florida Research and Development Center P.O. Box 2691 West Palm Beach, Florida 33402	
Attention: Library	1
California Institute of Technology Pasadena, California 91109	
Attention: Dr. A. Acosta	1
Prof. M. S. Plesset	1
The Pennsylvania State University Ordnance Research Laboratory P.O. Box 30 State College, Pennsylvania 16801	
Attention: Prof. G. F. Wislicenus	1
Dr. J. W. Holl	1
Hydronautics, Incorporated Pendell School Road Howard County Laurel, Maryland 20810	
Attention: Dr. Philip Eisenberg	1

DISTRIBUTION LIST (cont.)

	Copies
Pesco Products 24700 N. Miles Road Bedford, Ohio 44014 Attention: Mr. J. F. DiStefano	1
TRW Systems, Incorporated Bldg. 01, Room 1070F One Space Park Redondo Beach, California 90278	1